Instituto Universitário de Ciências Psicológicas, Sociais e da Vida

Oceanographic Insights from Apex Predators: the MAANTA NAUTILOS Tag for Dissolved Oxygen Monitoring

Orientadores da Dissertação:
Doutor Jorge Miguel Rodrigues Fontes (externo)
Prof. Doutor Paulo Catry (interno)

Professor do Seminário de Dissertação:
Prof. Doutor Emanuel Gonçalves

Dissertação submetida como requisito parcial para a obtenção do grau de:

MESTRE EM BIOLOGIA MARINHA E CONSERVAÇÃO

2025

Dissertação de Mestrado realizada sob a orientação do Doutor Jorge Miguel Rodrigues Fontes e do Professor Paulo Catry, apresentada no ISPA – Instituto Universitário para obtenção de grau de Mestre na especialidade de Biologia Marinha e Conservação

Acknowledgments

Primeiramente agradecer ao Dr. Jorge Fontes pela oportunidade e toda a confiança que depositou em mim durante este ano. Desde os serões existenciais para resolver problemas ao trabalho de campo em Santa Maria onde recolhemos os últimos dados, já calibrados, para demonstrar que todo o esforço dos últimos anos foi recompensado! Igualmente ao Dr. Bruno Macena que foi incansável desde a formação de vários softwares, à parte analítica e revisão da tese, sem dúvida sem ele não seria possível nada deste trabalho.

Ao Dr. Paulo Catry que desde as aulas se demonstrou um professor apaixonado na pedagogia e na conservação das tartarugas marinhas e "dos seus albatrozes". Deu-me uma visão mais alargada do mundo fascinante das aves e que um biólogo é 4x4, sucede em qualquer intempérie.

Agradecer ao instituto OKEANOS pela disponibilidade em acolher-me e a toda a equipa ECODIVE em especial ao Bruno Saraiva. Com esta tese foi também possível fazer um intercâmbio no CIBIO, agradeço ao Dr. Nuno Queiroz e à sua equipa, em especial ao Ivo da Costa e Tiago Cidade pela ajuda a analisar os dados.

Nada disto teria sido possível sem o projeto NAUTILOS, que promoveu o desenvolvimento desta tag não invasiva de baixo custo que está na vanguarda do estudo dos efeitos da desoxigenação. Sem esquecer a CEiiA e especialmente à Catarina Lemos, obrigada por toda a ajuda!

Esta epopeia foi sempre acompanhada de perto pela minha mãe, irmã e todas as pessoas que fizeram desta ilha casa, Obrigada.

As ilhas de bruma são escola para quem se atreve ao desassossego do verão e se consola com o nevoeiro que não tarda a deitar-se sobre o Pico.

Resumo

A desoxigenação dos oceanos tem vindo a intensificar-se globalmente, mas os seus efeitos sobre predadores de topo, como os elasmobrânquios, permanecem pouco compreendidos. No âmbito do projeto NAUTILOS (*New Approach to Underwater Technologies for Innovative, Low-cost Ocean Observation*), foi desenvolvida e validada a MAANTA tag — a primeira ferramenta de biotelemetria não invasiva, capaz de registar dados de alta resolução de oxigénio dissolvido, temperatura e comportamento.

Validações abrangentes em laboratório e *in situ*, incluindo comparações com perfis simultâneos de CTD (condutividade, temperatura e profundidade) e dados modelados do CMEMS, confirmaram a precisão das medições, embora se recomende a calibração regular pós-utilização para aumentar a precisão dos sensores.

O caso de estudo da aplicação da MAANTA tag na jamanta-chilena (*Mobula tarapacana*) forneceu a primeira caracterização *in situ* do comportamento de mergulho da espécie em relação ao oxigénio dissolvido. Os resultados indicaram que a jamanta chilena ocupa águas bem oxigenadas (210–230 μmol/L), apresenta ampla tolerância térmica (9–24 °C) e apresenta uma tendência de aumento da velocidade vertical em águas mais frias e ricas em oxigénio, de acordo com os padrões de migração vertical circadianos. O animais marcados atingiram velocidades de descida até 5,41 m/s, destacando-se entre os organismos marinhos com velocidades verticais mais elevadas já registadas.

Estes resultados demonstram a eficácia da MAANTA tag na monitorização simultânea de parâmetros comportamentais e variáveis ambientais essenciais, fornecendo novos contributos sobre a ecologia térmica e de oxigénio da jamanta chilena e contribuindo para conservação desta espécie criticamente ameaçada num oceano em progressiva desoxigenação

Palavras-chave: Oxigénio dissolvido; Biotelemetria; Jamanta Chilena

Abstract

Ocean deoxygenation is intensifying globally, yet its effects on apex predators such as elasmobranchs remain poorly understood. Within the framework of the NAUTILOS project (*New Approach to Underwater Technologies for Innovative, Low-cost Ocean Observation*), we developed and validated the MAANTA tag—a non-invasive biologging tool that records high-resolution dissolved oxygen (DO), temperature, and fine-scale movement data.

Extensive laboratory and *in situ* tests, including comparisons with calibrated conductivity–temperature–depth (CTD) instruments and modelled environmental data from CMEMS, confirmed the tag's accuracy, although regular post-deployment calibration remains essential to minimize sensor drift.

Deployment on the Chilean devil ray (*Mobula tarapacana*) provided the first *in situ* characterization of its diving behaviour in relation to DO. The species occupied well-oxygenated waters (210–230 µmol/L), tolerated a broad temperature range (9–24 °C), and showed increased vertical activity in cooler, oxygen-rich waters, consistent with diel vertical migration. Descent speeds reached up to 5.41 m/s—among the fastest recorded in marine animals.

These findings demonstrate the MAANTA tag's effectiveness for simultaneous behavioural and environmental monitoring, offering novel insights into the oxygen and thermal ecology of the Chilean devil ray supporting the conservation of this critically endangered species in an increasingly deoxygenated ocean.

Keywords: Dissolved oxygen; Biologging; Chilean devil ray

Table of contents

List of figures

Chapter I: Performance Assessment and Validation of the MAANTA tag

Anexes

List of Tables

Chapter I

Chapter I: Performance Assessment and Validation of the MAANTA Tag

1. Introduction

Dissolved oxygen (DO) is essential for the survival and fitness of aerobic organisms (Breitburg et al., 2018; Petsch et al., 2003), serving as the primary electron acceptor in cellular respiration and enabling efficient energy production (Semenza, 2007). Nevertheless, oxygen concentrations in the marine environment have been declining — a phenomenon known as ocean deoxygenation (Limburg et a., 2020). Global projections indicate a further reduction of 1–7% by 2100 (Breitburg et al., 2018; Schmidtko et al., 2017). This decline is largely driven by ocean warming, as excess heat reduces oxygen solubility (Ito et al., 2017), and by the expansion of oxygen minimum zones (OMZs) in eastern boundary upwelling systems, where oxygen is consumed through the respiration and decomposition of organic matter (Davila et al., 2023; Levin et al., 2018). Oxygen concentrations in these OMZs can fall below 20 µmol/L (Levin, 2018), compared to normoxic levels of 200–320 µmol/L (Schmidtko et al., 2017).

Elasmobranchs — sharks, skates, and rays — represent over 1,000 extant species (Guinot & Cavin, 2016) and play vital ecological roles as apex and mesopredators, shaping trophic dynamics, nutrient cycling, and overall ecosystem balance (Hammerschlag et al., 2011). Their biological traits, including slow growth, late maturity, and low fecundity, make them highly vulnerable to anthropogenic stressors, particularly overexploitation (Adams et al., 2018; Cortes et al., 2010; Queiroz et al., 2019). As ocean deoxygenation progresses, understanding how it affects elasmobranch physiology, behaviour and habitat use becomes critical for developing effective conservation strategies (Vedor et al., 2021; Watanabe & Papastamatiou, 2023).

Despite their ecological importance, the physiological and behavioural responses of elasmobranchs to declining oxygen levels remain poorly understood (Watanabe & Payne, 2023). Most oxygen demand estimates derive from laboratory respirometry experiments (Lawson et al., 2019; Carlson & Parsons, 2001), which often focus on small-bodied species and may not reflect natural conditions. Species-specific responses vary: highly mobile pelagic sharks tend to avoid hypoxic zones (Waller et al., 2024), while benthic species such as skates rely on compensatory physiological mechanisms to withstand low

oxygen (Wearmouth et al., 2014; Jensen et al., 1993). Behaviourally, migratory elasmobranchs are expected to avoid areas below their optimal oxygen thresholds (Vedor et al., 2021), whereas less active species may exhibit oxyconforming responses (Musa et al., 2020). Ecologically, deoxygenation can lead to habitat compression, forcing species into oxygen-rich surface layers and intensifying competition and exposure to fisheries (Prince et al., 2010; Vedor et al., 2021). Prolonged hypoxia may increase mortality risk in low-mobility species (Wearmouth et al., 2014) and shift community composition toward more hypoxia-tolerant taxa (Crear et al., 2020). Such long-term shifts may alter trophic interactions and threaten overall ecosystem stability (Waller et al., 2024).

Recent advances in biologging technologies have revolutionized marine ecology by enabling fine-scale analysis of animal movement and behaviour (Hussey et al., 2015; Hays et al., 2016). The integration of environmental sensors into animal-borne tags allows the measuring of key Essential Ocean Variables (EOVs), effectively transforming marine organisms into **"**animal oceanographers**"** by opportunistically collecting *in situ* environmental data. (Harcourt et al., 2019). These biologging approaches have provided valuable insights into undersampled regions such as the Southern Ocean, improving model accuracy and understanding of environmental variability (Guinet et al., 2013; Roquet et al., 2013).

Nonetheless, few biologging studies have focused on the measurement of DO concentrations *in situ* using free-ranging animals (Bailleul et al., 2015; Coffey & Holland, 2015; Da costa et al., 2024; Priede et al., 1988; Svendsen et al., 2006). Most research instead relies on modelled datasets such as the Copernicus Marine Environment Monitoring Service (CMEMS) or the World Ocean Atlas (WOA). These models predict DO distributions using satellite-derived inputs and assimilate multi-source oceanographic data, which vary in quality, resolution, and spatial coverage, often leading to coarse outputs with inherent uncertainties (Grégoire et al., 2021). Consequently, model-based estimates may overlook fine-scale behavioural or physiological responses (Hussey et al., 2015).

To address this limitation, the NAUTILOS project (New Approach to Underwater Technologies for Innovative, Low-cost Ocean observation) was established. This project aims to bridge gaps in marine observation and modelling by developing a new generation of cost-effective sensors and samplers of essential ocean variables (EOVs). By integrating

these technologies into existing observing platforms and deploying them across European seas, NAUTILOS seeks to enhance spatial and temporal data coverage, complement current monitoring systems, and democratize access to ocean observation (for more information: www.nautilos-h2020.eu). Within this framework, the MAANTA tag was developed — a state-of-the-art, multisensor, animal-borne towed tag equipped with a fiber-optic dissolved oxygen sensor, inspired by the concept of the iPilot and Gpilot non-invasive towed tags (Fontes et al., 2022). The device also records temperature, pressure, and tri-axial acceleration, gyroscope and magnetometer, providing a detailed three-dimensional view of animal movement and associated environmental conditions. In the scope of the NAUTILOS project, the MAANTA tag prototype was experimentally deployed across five elasmobranch species with contrasting ecologies: the bluntnose sixgill (*Hexanchus griseus* Bonnaterre, 1788), shortfin mako (*Isurus oxyrinchus* Rafinesque, 1810), whale (*Rhincodon typus* Smith, 1828), and blue (*Prionace glauca* Linnaeus, 1758) sharks and Chilean devil ray (*Mobula tarapacana* Philippi, 1892).

Here, we present the development and validation of the MAANTA tag prototype, evaluating its performance through laboratory calibrations against calibrated reference sensors, field comparisons with Conductivity, Temperature, and Depth (CTD) measurements, and post-deployment data analyses (i.e., case studies) with modeled environmental data.

2. Materials and methods

2.1 Tag specifications

The MAANTA multisensor tag (Fig. 1a, b) weighs 1.1 kg and measures 375 × 120 × 155 mm. All sensors are housed within pressure-resistant containers mounted on a positively buoyant syntactic foam torpedo shaped float, allowing operation at depths of up to 1000 m. The additional hydrodynamic force (drag) exerted on the tagged animals was evaluated through computational fluid dynamics (CFD) (Maillard et al., 2025; McKnight et al., 2024) with a maximum allowable drag increase of +5% for tag-t-body-mass ratio (Casper et al., 2009) established for safe deployment.

The tag package integrates both environmental and motion sensors. The environmental module includes a Keller 4 LD temperature and pressure sensor (Keller, Switzerland), which operates within a temperature range of –10 to 80 °C (±2 °C) and pressure range up

to 200 bar (±0.03 bar). The 4 LD series employ Keller's chip-in-oil technology, combining a pressure-measuring cell with digital temperature compensation, sampling at 0.5 m/s intervals. Dissolved oxygen (DO) measurements are obtained using a PICO-O2-SUB fiber-optic oxygen sensor (PyroScience GmbH, Germany), which utilizes REDFLASH® technology. This system employs red-light excitation of an oxygen-sensitive indicator, producing analyte-dependent luminescence in the near-infrared (NIR) range. The LED and photodiode assembly excite and detect luminescence via an optical fiber that connects the sensing tip to the oxygen meter. Because the luminescence of REDFLASH indicators is temperature-dependent, oxygen readings are automatically compensated for temperature variations. Oxygen concentrations are recorded every 10 s across a range of 0–720 µmol/L (±0.3 µmol/L).

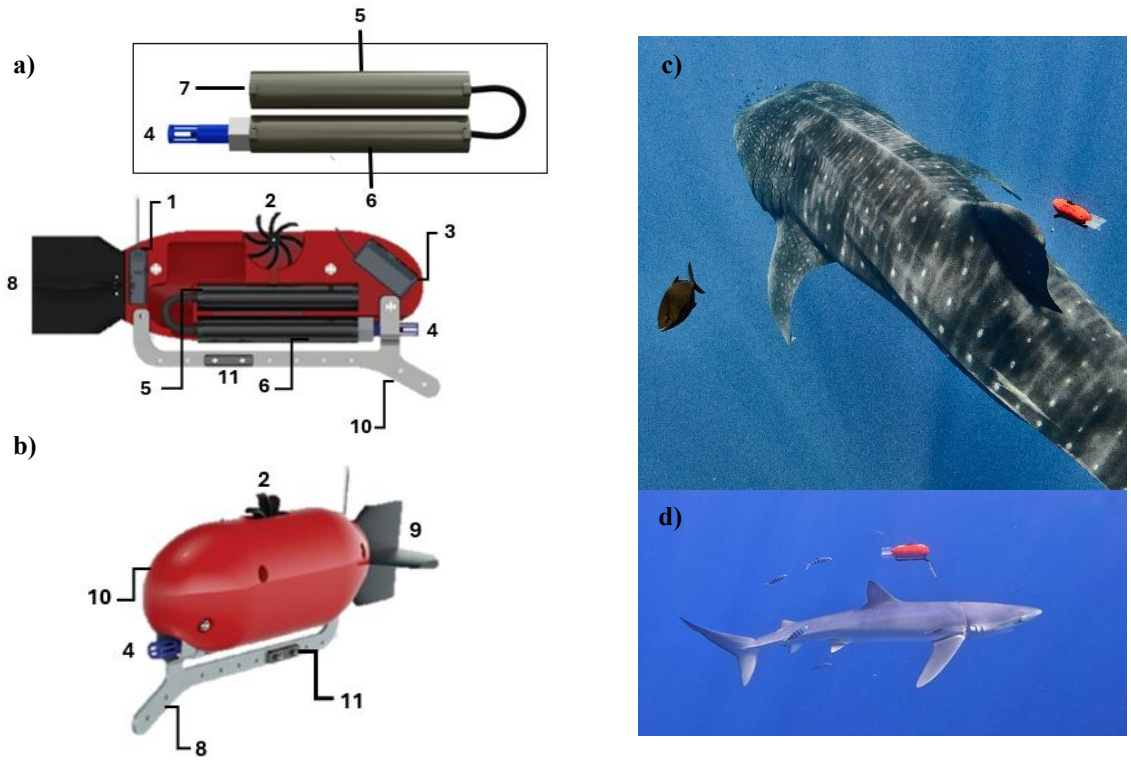

Figure 1. Schematic diagram of the MAANTA tag showing **(a)** interior view, **(b)** exterior view, **(c)** attached on a whale shark (Rhincodon typus) (Photo: Fred Buyle), and **(d)** attached on a blue shark (Prionace glauca) (Photo: DOP-OKEANOS-UAc). **1** — ATS VHF radio transmitter F1835B; **2** — magnetic paddle wheel; **3** — wildlife computer SPOT 363 A transmitter; **4** —PICO-O2-SUB fiber-optic oxygen cap; **5** — LITE electronics container; **6** — LITE oxygen sensor container; **7** — Keller 4 LD pressure temperature sensor; **8** — tow connection; **9** — stabilizing fins; **10** — floater; **11** — Ballast weight

The motion sensor suite includes a tri-axial accelerometer (1–50 Hz sampling frequency) to capture fine-scale body movements, a paddle wheel with eight magnets, with sequential inverse polarity, for velocity measurements, and both a tri-axial magnetometer and gyroscope to determine spatial orientation.

The electronic container, LITE (Fig. 1a-5), contains the inertial measurement unit (IMU), micro-SD memory card, pressure and temperature sensor, lithium battery and common control board (PCB). The LITE oxygen sensor container (Fig 1a-6) is housed separately in a dedicated container that holds all optical components for the DO sensor, including the fiber optic end cap. Both containers are made from aluminium (AL 7075-T6), connected by a cable and sealed using WetLink penetrators rated to 1000 m, tightened with a torque wrench to the correct pressure of 1 N. Cable insertion and sealing were completed using an auxiliary tool designed to prevent leakage (see Annex II, Fig. 2a–c).

Tag attachment was achieved using a body harness loop (Figure 1c, d; see Fontes et al., 2022 for details), with designs adapted to each species' anatomy and ecology. For blue and mako sharks, a 160 cm, 1.40 mm monofilament threaded through 50 cm of 3 mm silicone tubing was positioned around the pectoral fins to prevent abrasion, with one end connected to a galvanic timed release (GTR; International Fishing Devices Inc., Jupiter, Florida) and the other secured through the end a rubber piece. The GTR, composed of dissimilar metals, corroded predictably in seawater, ensuring timed detachment. Bluntnose sixgill sharks were fitted with an 8 mm bungee harness adjusted to individual girth and joined by a GTR, with an 80 mm, 1.40 mm monofilament connecting the tag to a 12 mm metal ring and 150 g of lead added to counter tag buoyancy. For whale sharks, a 180 cm, 8 mm bungee harness was placed around the dorsal fin, while Chilean devil rays were fitted with a 140 cm, 8 mm bungee positioned posterior to the cephalic fins and anterior to the pectoral fins, with the tag attached via an 80 cm tether to a 10 mm metal ring.

2.2 Study area

The Azores Archipelago, composed of nine volcanic islands, is located along the Mid-Atlantic Ridge at the convergence of the American, Eurasian, and African tectonic plates (Fernandes et al., 2006). Its Exclusive Economic Zone (EEZ) spans approximately 930,687 km² (Directorate General for Natural Resources, Safety, and Maritime Services [DGRM], n.d.). Situated 1,400–2,000 km from continental Europe and North America, the islands are surrounded by deep ocean waters exceeding 1,500 m (Afonso et al., 2020; Santos et al., 1995). The region experiences a mix of subtropical and temperate oceanic conditions, with mean sea surface temperatures ranging from 22–24°C in summer and autumn to 17–18°C in winter and spring (Caldeira & Reis, 2017). Oceanographically, the

Azores are influenced by the Azores Current, its associated eddies, and the Gulf Stream (Santos et al., 1995; Caldeira & Reis, 2017). The complex bathymetry, shaped by numerous seamounts and ridges, enhances local productivity and biodiversity compared to the surrounding open ocean, attracting a wide range of migratory marine megafauna (Afonso et al., 2020)

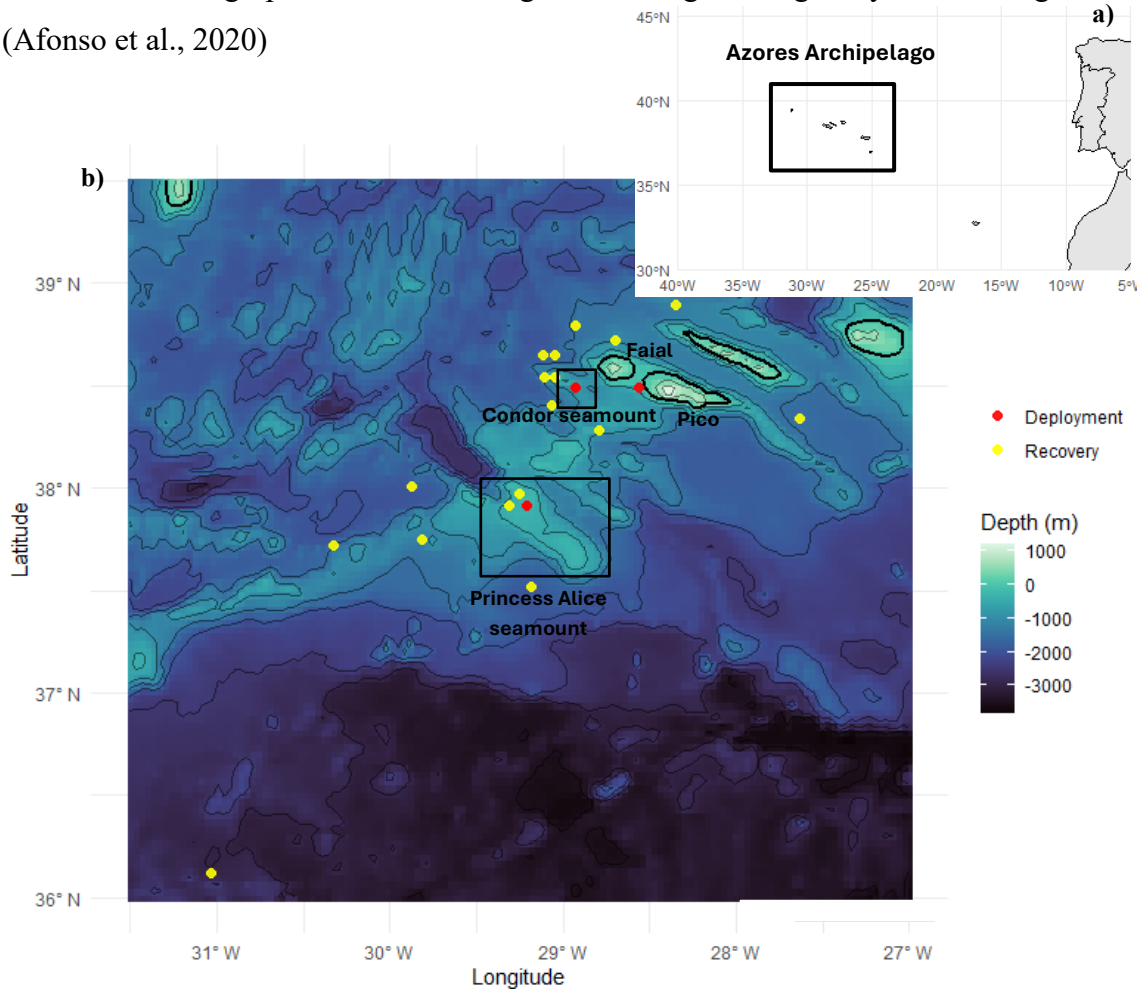

Figure 2. (a) Azores Archipelago relative to mainland Portugal **(b)** Geographical location of the Central Group of the Azores Archipelago and adjacent seamounts showing tag deployment sites (red circles) and recovery locations (yellow circles).

2.3 Field deployments

Trials were conducted between April and September of 2024 in the channel between Faial and Pico Island, Princess Alice and Condor bank, in the central group of the Azores Archipelago, Portugal. A total of 17 elasmobranchs (one bluntnose sixgill shark, one mako shark, four Chilean devil rays, four whale sharks and seven blue sharks) were tagged (Fig. 2b).

Blue sharks were attracted with bait made from a mixture of grinded sardine (*Sardina pilchardus*) and skipjack tuna (*Katsuwonus pelamis*). The lasso technique (i.e., harness) was used for tagging free swimming blue sharks, deployed by a freediver with a harness

loop (Fontes et al., 2022). Once a shark was sighted, a U-shaped frame was used to hold the harness loop open, allowing easier positioning over the shark's head while minimizing bite risk of the freediver. The freediver guided the harness onto the animal using the frame, and once the loop passed over the head and was retained in front of the pectoral fins, the diver adjusted the harness to fit the shark's girth and secure the deployment.

The bluntnose sixgill and shortfin mako sharks were captured using rod-and-reel fishing methods. The first tagged blue shark was initially caught in the same way, after which the non-invasive lasso technique was employed (i.e. harness). Once the shark had taken the bait, it was placed parallel to the vessel with the head facing the bow to promote water flow over the gills. The hook was secured to the bow of the vessel, and a rope was tied around the shark's tail and secured to the stern of the vessel to restrict the shark's movement and prevent injury. After the animal was safely restrained, tonic immobility was induced to facilitate handling and minimize stress during the tagging procedure. Once the individual was totally secured, the harness was inserted. In contrast, the natural aggregation behaviour of mobulas and whale sharks made it possible to opportunistically deploy the tag while freediving without the use of bait or invasive methods.

Tag recovery occurred once the galvanic timed release (GTR) corroded, detaching the positively buoyant tag, which then floated to the surface. A secondary safety GTR, set with an extra day of duration, was added between the tether and tag to ensure release in case of entanglement. GTR timing (24–48 h) was selected based on water temperature and salinity, which affect corrosion rate. Tags were located using ARGOS satellite coordinates for general positioning and VHF telemetry for active tracking. Upon recovery, data were downloaded via the MAANTA app (see Section 2.6), and the tags were recharged and reprogrammed for subsequent deployments.

2.4 Animal ethical approval

These procedures received approval and authorization from the Azorean Directorate of Sea Affairs of the Autonomous Region of the Azores under the permits AMP/2017/013, AMP/2018/015, ELMAS-DRA/2019/05204 and ELMAS-DRAM/2021/06. Operations were conducted or supervised by trained personnel of the Institute of Marine Sciences - OKEANOS.

2.6 MAANTA APP

The data is stored in an 8GB micro-SD card with storage for 500 days of logged data and an 18350 Li-ion Battery (1400 mAh) with autonomy for up to 1 week, depending on the duty-cycle program. The MANNTA app was developed to manage data access, mission configuration, and keep track of the data recovered, without connecting the device. Additionally, the app supports firmware updates and calibrates both the accelerometer and gyroscope.

2.7 Oxygen sensor calibration

The calibration of the PICO-O2-SUB dissolved oxygen sensor (PyroScience, GmbH) was carried out using a two-point calibration procedure following the manufacturer's instructions. The lower calibration point (0% oxygen) was established with an anoxic solution prepared by dissolving O2 calibration capsules (PyroScience) in 50ml of distilled water. The upper calibration (100% air-saturation) was prepared using an air-saturated saline solution (35.5 ppm salinity) at ambient atmospheric pressure, closely matching environmental conditions. Live measurements were monitored using the Pyro Developer Tool software and the Pyro Workbench.

2.8 Oxygen and temperature sensors data validation

2.8.1 *In situ* vs modelled data

To validate the *in situ* dissolved oxygen (DO) concentrations, oxygen data from the LITE devices were compared with the CMEMS Global Ocean Biogeochemistry Analysis and Forecast product (https://doi.org/10.48670/moi-00015), while temperature values were validated against the corresponding CMEMS dataset (https://doi.org/10.48670/moi-00016). The Global Ocean Biogeochemistry Analysis and Forecast product, used here to obtain DO estimates, is based on the biogeochemical PISCES-v2 model, which simulates lower trophic levels of marine ecosystems and associated biogeochemical cycles across a range of spatial and temporal scales (Aumont et al., 2015). For this comparison, daily mean average of the *in situ* DO and temperature were paired with modelled profiles extracted from the corresponding modelled profiles extracted from the same grid cell (0.25° × 0.25° resolution) and day, based on each tag's tagging/pop-off location.

2.8.2 Calibrated PreSens® multi-parameter

To validate the PICO-O2-SUB and Keller 4 LD temperature sensor readings were compared with a calibrated PreSens® multi-parameter sensor. Both sensors were immersed in air-saturated deionized water (Annex III: Fig. 1a), starting at 100% oxygen saturation and gradually reduced to approximately 0% by bubbling nitrogen.

2.8.3 Conductivity, Temperature and Depth- CTD (AML-6 LGR)

To validate and assess the accuracy of the PICO-O2-SUB dissolved oxygen sensor (PyroScience, GmbH) and the Keller 4 LD temperature and pressure sensor (Keller, Switzerland) under *in situ* conditions, deployments were conducted with a CTD (AML-6 LGR). These deployments were carried out at various phases of the tagging operations. The sensors were integrated into the CTD setup both with and without the foam housing to evaluate any potential influence on sensor readings (Annex III; Fig. 1b).

2.9 Statistical analysis

Statistical analyses were conducted in R version 4.3.2 (R Core Team, 2024). The distribution of the data was first assessed using the Shapiro–Wilk test for normality, and homogeneity of variances was evaluated with Levene's test. As the data deviated from a normal distribution ($p < 0.05$), non-parametric methods were applied.

2.9.1 *In situ*–Model Comparison of Dissolved Oxygen and Temperature Profiles

Tag (*in situ*) and modelled oxygen and temperature data (Copernicus) were first filtered for outliers based on LOESS residuals (±1 SD). Both datasets were smoothed with LOESS, aggregated into 10 m depth bins, and summarized as mean ± SD at bin midpoints. Modelled oxygen values were extracted for the same depth bins and compared to tag data using Spearman's rank correlation.

2.9.2 Calibrated PreSens® multi-parameter comparison

Comparisons were carried out in laboratory conditions. Dissolved oxygen (DO) and temperature data from PICO-O2-SUB sensor and PreSens® sensors deviated from normality ($p < 0.05$). Differences between sensors were evaluated with the Kruskal–Wallis test, followed by pairwise Wilcoxon rank-sum tests with Benjamini–Hochberg correction. Mean differences (± SD) were also calculated to assess offset.

2.9.3 CTD (AML-6 LGR)

Drops of CTD and LITE sensor data were carried out in the sea. The comparison was done using the Wilcoxon signed-rank test. To test for variability by sampling phase (ascent vs. descent), Mann–Whitney U tests were applied. Differences between fully assembled and LITE-only configurations were analyzed with the Kruskal–Wallis test and Dunn's post hoc comparisons (adjusted p-values). Results are reported as means ± SD, with significance at $p < 0.05$.

3. Results

3.1 *In situ*- Model Comparison of Dissolved Oxygen and Temperature Profiles

A total of 17 elasmobranchs were tagged with the multisensor MAANTA tag (Table I). Tag deployment durations ranged from a minimum of 5 minutes to a maximum of 46 hours. Four LITE units were used (IDs: **6b306470**, 6143647e, 6142647b, and **6142647f**); however, two of them flooded (in bold) during the initial testing and deployment procedures.

All tagged blue sharks were males and all whale sharks were females. Two mobulas were sexed, one male and one female, the sex of the two remaining mobulas was undetermined.

Table I. Summary metadata of the tagged elasmobranchs, showing individual data and mean ± SD values of the deployment duration.

Shark ID	Tag ID	Species	Sex	Tagging date	Pop-up date	Deployment duration (h)
ALB_01	LITE6b306470	*H. griseus*	F	30-04-2024	01-05-2024	23.50
MAK_01	LITE 6b306470	*I. oxyrhincus*	M	26-06-2024	27-06-2024	30.42
PIN_01	LITE 6142647b	*R. typus*	F	16-08-2024	16-08-2024	00.05
PIN_02	LITE 6143647e	*R. typus*	F	19-08-2024	19-08-2024	03.38
PIN_03	LITE 6142647b	*R. typus*	F	19-08-2024	20-08-2024	26.32
PIN_04	LITE 6143647e	*R. typus*	F	21-08-2024	22-08-2024	18.11
JAM_01	LITE 6143647e	*M. tarapacana*	-	12-08-2024	13-08-2024	31.23
JAM_02	LITE 6142647b	*M. tarapacana*	-	12-08-2024	13-08-2024	15.36
JAM_03	LITE 6142647b	*M. tarapacana*	F	25-08-2024	27-08-2024	46.53
JAM_04	LITE 6143647e	*M. tarapacana*	M	28-08-2024	29-08-2024	31.17
BLU_01	LITE 6142647f	*P. glauca*	M	27-06-2024	28-06-2024	20.46
BLU_02	LITE 6142647b	*P. glauca*	M	09-09-2024	09-09-2024	01.27
BLU_03	LITE 6143647e	*P. glauca*	M	09-09-2024	09-09-2024	00.08
BLU_04	LITE 6143647e	*P. glauca*	M	09-09-2024	09-09-2024	00.09
BLU_05	LITE 6142647b	*P. glauca*	M	11-09-2024	12-09-2024	24.17
BLU_06	LITE 6143647e	*P. glauca*	M	11-09-2024	12-09-2024	16.26
BLU_07	LITE 6143647e	*P. glauca*	M	19-09-2024	20-09-2024	25.05
					Mean (s.d.)	**18.44 (± 13.63)**

From each species, one representative dataset was selected for detailed analysis based on stronger correlations with modelled data, while very short deployments (<1 h) were excluded (see Annex IV; Table I, II for correlation results across all IDs).

For *ALB_01* (bluntnose sixgill shark), modelled DO concentrations ranged from 167.1 - 251.6 µmol/L, whereas *in situ* Tag values spanned 80.1 - 229.8 µmol/L (Fig. 3a). The two datasets were highly correlated (Spearman's r = 0.98, $p < 0.001$, $R^2 = 0.93$); however, the model systematically had lower DO values, with a mean difference of –51.9 ± 16.1 µmol/L (mean RE = 21.3 %). The linear regression (Tag DO = 161.4 + 0.44 × Model DO) revealed a moderate slope, with the largest offset occurring between approximately 85 and 115 m depth (–34 to –37 µmol/L) (Table II).

For *BLU_01* (blue shark), modelled DO concentrations ranged between 186.4 and 255.3 µmol/L, whereas *in situ* Tag values extended from 268.2 to 396.7 µmol/L (Fig. 3b). Despite a strong correlation between datasets (Spearman's r = 0.93, $p < 0.001$, $R^2 = 0.61$), the model with lower DO, with a mean difference of –83.8 ± 27.3 µmol/L (mean RE = 27.4 %). The linear regression (Tag DO = 1.06 + 1.38 × Model DO) suggested an increased offset at higher oxygen concentration levels (Table II).

In *PIN_03* (whale shark), modelled DO concentrations ranged from 181.6 to 264.9 µmol/L, compared to 316.8 – 410.3 µmol/Lfrom Tag data (Fig. 3c). Although the correlation was strong (Spearman's r = 0.92, $p < 0.001$, $R^2 = 0.57$), the model again had lower DO values compared with the *in situ* values, with a mean difference of –122.8 ± 17.3 µmol/L (mean RE = 36.2 %). The regression (Tag DO = 195.4 + 0.67 × Model DO) indicated consistent lower DO values across depths (Table II).

In *JAM_01* (Chilean devil ray), modelled DO concentrations ranged from 160.9 to 258.1 µmol/L, while Tag observations varied between 221.4 to 271.9 µmol/L (Fig. 3d). The correlation was moderate (Spearman's r = 0.69, $p < 0.001$, $R^2 = 0.62$), with the model again with lower oxygen concentrations by –47.1 ± 16.7 µmol/L (mean RE = 20 %). The regression (Tag DO = 164.4 + 0.38 × Model DO) showed a shallow slope, suggesting weaker agreement across the concentration range (Table II).

Finally, *MAK_01* (shortfin mako shark), modelled DO concentrations ranged from 215.8 to 254.8 µmol/L, while Tag observations spanned a much wider range from 273.3 to 476.1 µmol/L (Fig. 3e). The correlation was weak (Spearman's r = 0.06, $p = 0.034$, $R^2 = 0.16$),

with the model substantially also with lower DO (–109.5 ± 69.5 µmol/L; mean RE = 29.2 %). The linear regression (Tag DO = –184.3 + 2.23 × Model DO) indicated poor agreement between datasets (Table II).

Table II. Summary of Spearman's correlation, coefficient of determination (R^2), and error metrics ((MAE- Mean Absolut Error, RMSE- Root Mean Squared Error) for comparisons between *in situ* (Tag) and modelled dissolved oxygen (DO) concentrations (µmol/L).

ID	*Spearman*	*R2*	*MAE*	*RMSE*
ALB_01	**0.96**	**0.93**	**51.88**	**54.25**
BLU_01	**0.93**	**0.61**	**83.83**	**88.00**
PIN_03	**0.92**	**0.57**	**122.78**	**123.94**
JAM_01	**0.69**	**0.62**	**47.09**	**49.94**
MAK_01	**0.06**	**0.16**	**109.52**	**128.26**

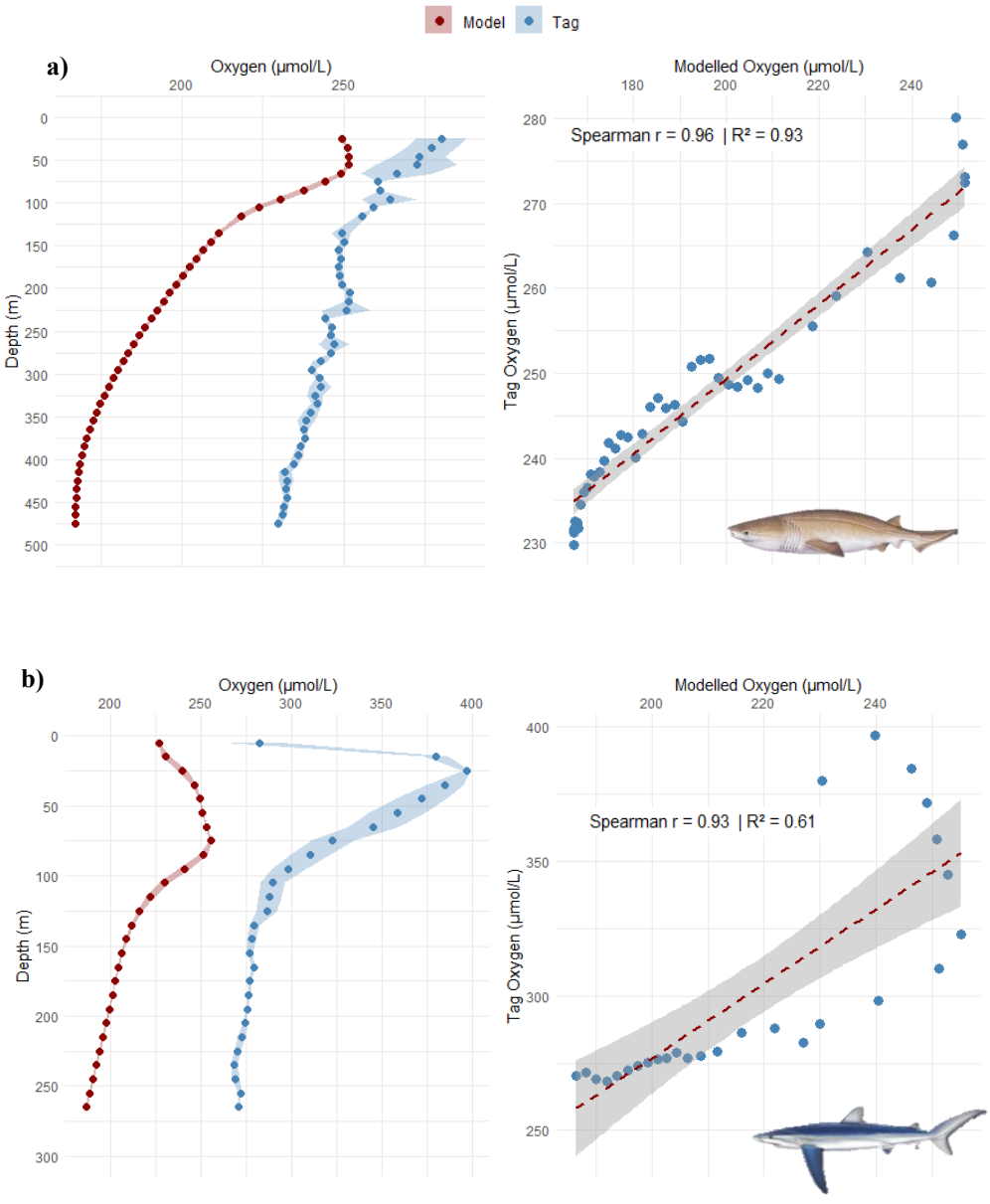

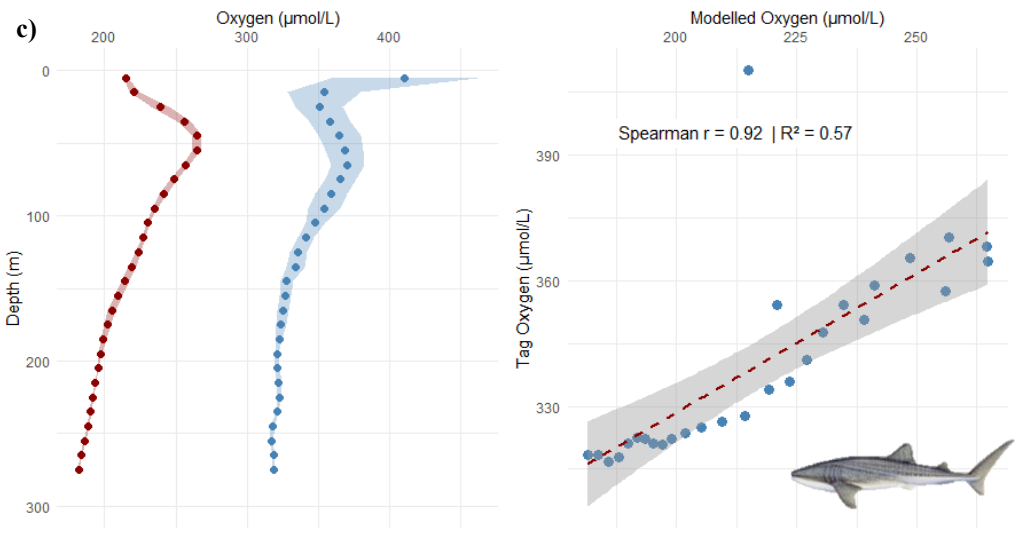
c)
Oxygen (µmol/L)
200
300
400
0
100
200
300
Depth (m)
Modelled Oxygen (µmol/L)
200
225
250
Spearman r = 0.92 | R² = 0.57
390
360
330
Tag Oxygen (µmol/L)

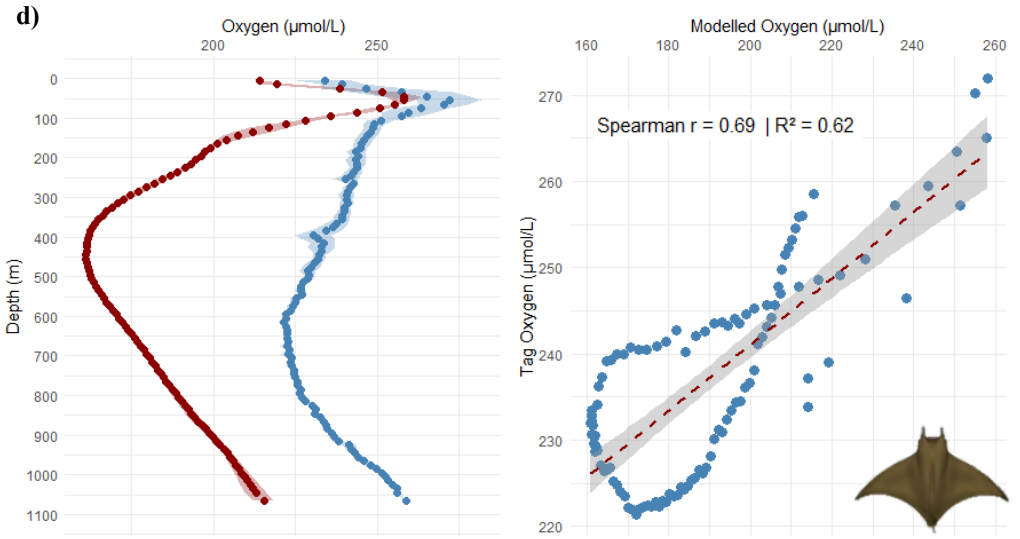
d)
Oxygen (µmol/L)
200
250
0
100
200
300
400
500
600
700
800
900
1000
1100
Depth (m)
Modelled Oxygen (µmol/L)
160
180
200
220
240
260
Spearman r = 0.69 | R² = 0.62
270
260
250
240
230
220
Tag Oxygen (µmol/L)

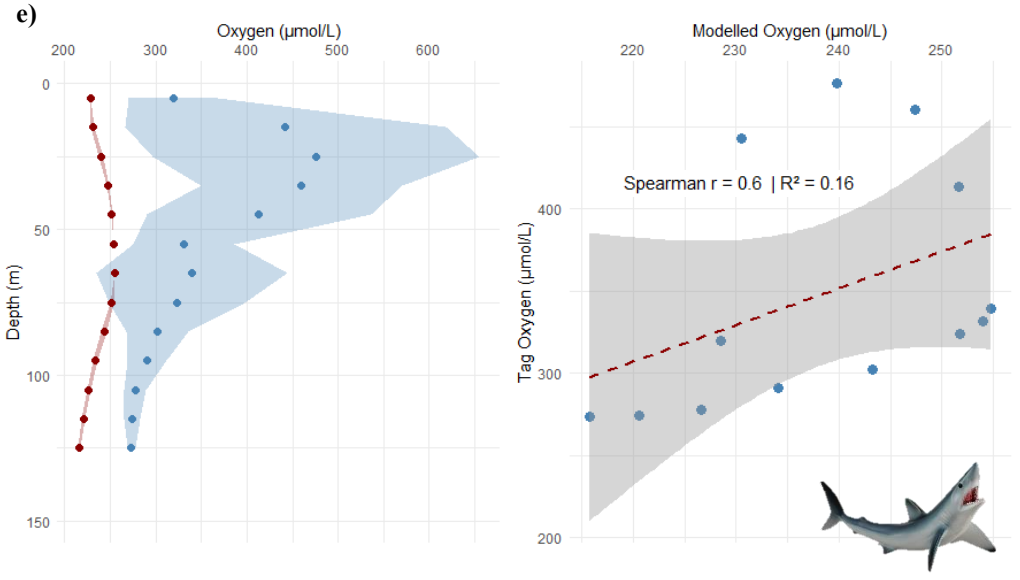
e)
Oxygen (µmol/L)
200
300
400
500
600
0
50
100
150
Depth (m)
Modelled Oxygen (µmol/L)
220
230
240
250
Spearman r = 0.6 | R² = 0.16
400
300
200
Tag Oxygen (µmol/L)

Figure 3. Dissolved oxygen (µmol/L) profiles from MAANTA tag measurements (blue, Tag) and CMEMS model outputs (red, Model), averaged in 10 m depth bins (±1 SD, left), and corresponding Spearman's rank correlations (right) for **(a)** bluntnose sixgill shark (ALB_01), **(b)** blue shark (BLU_01), **(c)** whale shark (PIN_03), **(d)** Chilean devil ray (JAM_01), and **(e)** shortfin mako shark (MAK_01).

For ALB_01, modelled temperatures ranged from 15.0 to 22.1 °C, while *in situ* Tag measurements varied between 12.6 and 21.1 °C (Fig. 4a). The datasets showed a very strong correlation (Spearman's r = 0.98, R^2 = 0.97, p < 0.001). However, the regression (Tag T = –5.24 + 1.18 × Model T) revealed a systematic positive offset, with the modelled temperatures consistently higher than Tag values. On average, modelled temperatures were higher than *in situ* temperatures by 1.4 ± 0.4 °C higher (MAE = 1.43, RMSE = 1.45; mean RE = 15.0 %) (Table III).

For BLU_01, modelled temperatures ranged from 15.0 to 22.1 °C, while Tag observations covered 12.6–21.1 °C (Fig. 4b). The datasets were almost perfectly aligned (Spearman's r = 1.0, R^2 = 1.0, p < 0.001). The fitted regression (Tag T= -1.45 + 1.00 × Model T) indicated a consistent positive offset, with modelled values exceeding Tag measurements by 2.2 ± 0.4 °C on average (MAE = 2.16, RMSE = 2.20; mean RE = 15.0 %) (Table III).

For JAM_01, modelled values spanned 11.7-25.4 °C, compared with 10.0–24.0 °C for the Tag data (Fig. 4c). The correlation was nearly perfect (Spearman's r = 1.0, R^2 = 1.0, p < 0.001). The regression (Tag T = -1.65 + 0.98 × Model T) suggested minimal systematic differences, although the modelled temperatures still slightly higher than *in situ* values, on average by 1.9 ± 0.2 °C (MAE = 1.89, RMSE = 1.90; mean RE = 14.6 %) (Table III).

For PIN_03, modelled profiles ranged from 14.1 to 25.9 °C, compared with 11.8–24.1 °C in the Tag data (Fig. 4d). The datasets were strongly correlated (Spearman's r = 1.0, R^2 = 0.99, p < 0.001). The regression (Tag T = –2.78 + 1.03 × Model T) indicated a consistent positive offset, with the model with higher temperatures Tag values by 2.3 ± 0.3 °C on average (MAE = 2.30, RMSE = 2.31; mean RE = 16.0 %) (Table III).

For MAK_01, modelled temperatures spanned 17.2–21.7 °C, whereas Tag measurements ranged from 14.5 to 20.1 °C (Fig. 4e). Correlation between datasets was strong (Spearman's r = 0.98, R^2 = 0.96, p < 0.001). The regression (Tag T = –4.24 + 1.08 × Model T) again highlighted a systematic positive offset, with modelled temperatures exceeding Tag values by 2.7 ± 0.4 °C on average (MAE = 2.68, RMSE = 2.71; mean RE = 16.7 %) (Table III).

Table III. Summary of Spearman's correlation, coefficient of determination (R^2), and error metrics (MAE- Mean Absolut Error, RMSE- Root Mean Squared Error) for comparisons between *in situ* (Tag) and modelled sea water temperature (TºC).

ID	*Spearman*	*R2*	*MAE(ºC)*	*RMSE(ºC)*
ALB_01	**0.98**	**0.97**	**1.43**	**1.45**
BLU_01	**1**	**1**	**2.16**	**2.2**
PIN_03	**1**	**0.99**	**2.3**	**2.31**
JAM_01	**1**	**1**	**1.89**	**1.90**
MAK_01	**0.98**	**0.96**	**2.68**	**2.71**

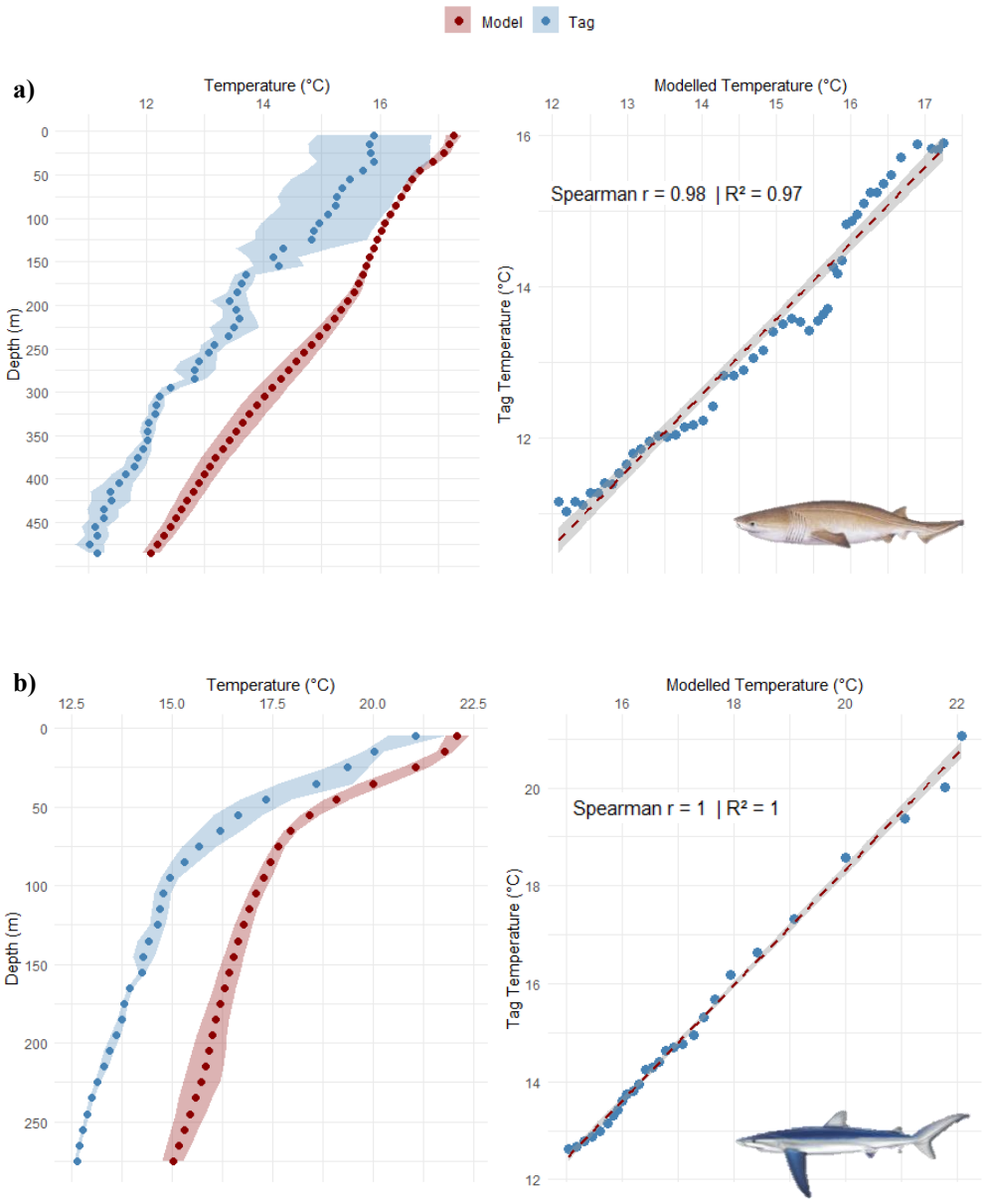

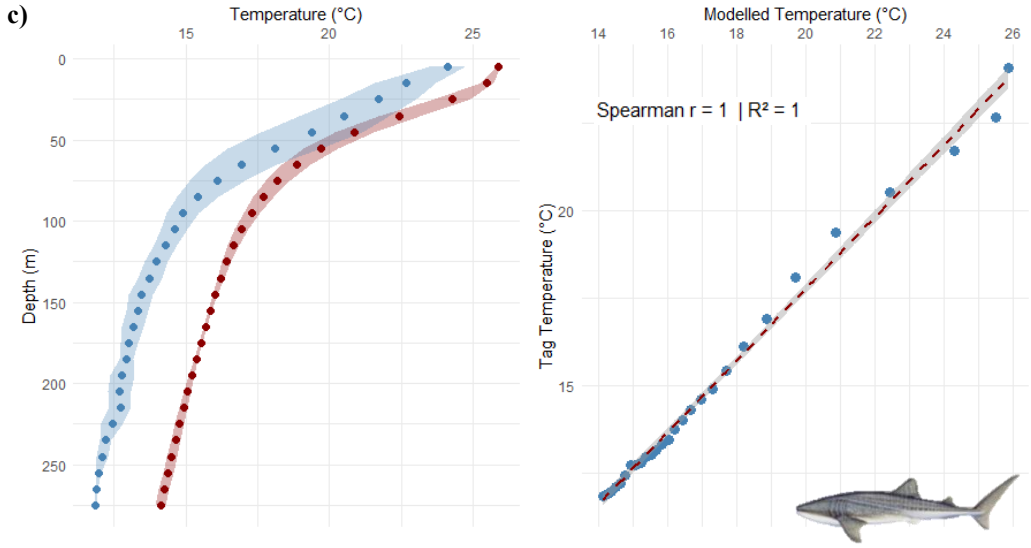
c)
Temperature (°C)
Depth (m)
Modelled Temperature (°C)
Tag Temperature (°C)
Spearman r = 1 | R² = 1

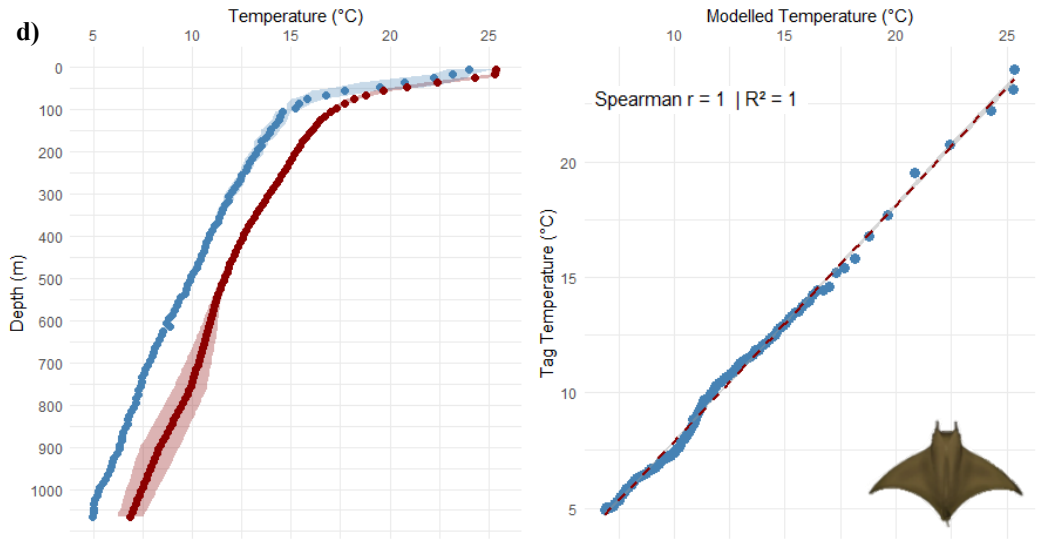
d)
Temperature (°C)
Depth (m)
Modelled Temperature (°C)
Tag Temperature (°C)
Spearman r = 1 | R² = 1

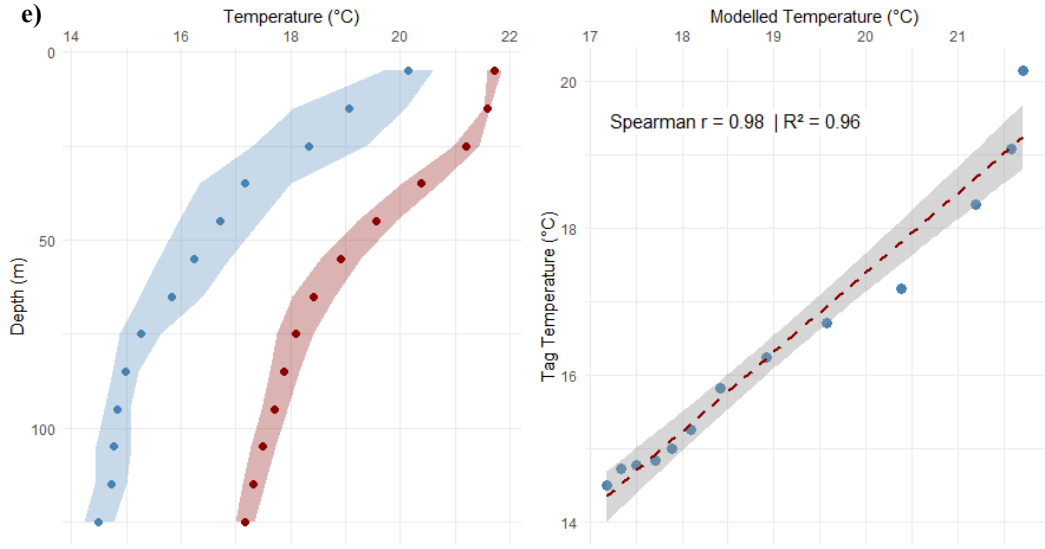
e)
Temperature (°C)
Depth (m)
Modelled Temperature (°C)
Tag Temperature (°C)
Spearman r = 0.98 | R² = 0.96

Figure 4. Temperature (ºC) profiles from MAANTA tag measurements (blue, Tag) and CMEMS model outputs (red, Model), averaged in 10 m depth bins (±1 SD, left), and corresponding Spearman's rank correlations (right) for **(a)** bluntnose sixgill shark (ALB_01), **(b)** blue shark (BLU_01), **(c)** whale shark (PIN_03), **(d)** Chilean devil ray (JAM_01), and **(e)** shortfin mako shark (MAK_01).

3.2 Multi-parameter sensor calibration comparison

Due to observed discrepancies between modelled and *in situ* measurements from the DO sensor, an extensive series of laboratory and field experiments using reference-calibrated instruments were conducted to improve data accuracy and reliability. Under controlled laboratory conditions, dissolved oxygen (DO) measurements from the LITE6142647b (LITEb) and LITE6143647e (LITEe) sensors were simultaneously compared with those from a PreSens® multi-parameter reference sensor, using a two-point (100–0%) oxygen saturation calibration over time.

In the 17th October laboratory experiment (Fig. 5a), the Kruskal–Wallis test revealed a statistically significant difference among all three sensors ($\chi^2 = 26.08$, df = 2, $p < 0.001$). Pairwise Wilcoxon rank-sum tests confirmed that all sensors differed significantly: LITEb vs LITEe ($p < 0.001$), LITEb vs PreSens ($p = 0.0073$), and LITEe vs PreSens ($p = 0.0080$). On average, LITEb measured 28.7 ± 29.1 µmol/L lower dissolved oxygen than the PreSens, while LITEe measured 6.3 ± 12.3 µmol/L higher. The difference between the two LITE units was 34.9 ± 24.7 µmol/L. Overall, LITEb consistently underestimated DO relative to both LITEe and the PreSens multi-parameter, a offset that became more pronounced at higher oxygen concentrations and diminished as DO levels decreases. Below 50 µmol/L, both LITE sensors tended to underestimate oxygen saturation compared with the PreSens multi-parameter system.

In the 6th December experiment, where deionized water was added to the oxygen sensors of both LITE units (Fig. 5b), the Kruskal–Wallis test again showed a significant difference among sensors ($\chi^2 = 70.32$, df = 2, $p < 0.001$). Pairwise Wilcoxon tests revealed that LITEb differed significantly from both LITEe ($p < 0.001$) and PreSens ($p < 0.001$), whereas LITEe and PreSens did not differ significantly ($p = 0.15$). Mean pairwise differences supported these results: LITEb measured 33.8 ± 23.3 µmol/L lower than PreSens, LITEe 4.9 ± 9.9 µmol/L lower, and the difference between the two LITE sensors was 29.0 ± 14.4 µmol/L. The overall magnitude of the differences was smaller compared to the 17th October experiment, indicating closer agreement between LITEe and PreSens. In general,

LITEe and the PreSens sensors recorded comparable oxygen concentrations, although LITEe tended to slightly underestimate values at higher oxygen levels and overestimate them at lower levels. In contrast, LITEb consistently underestimated oxygen concentration across the entire the trial.

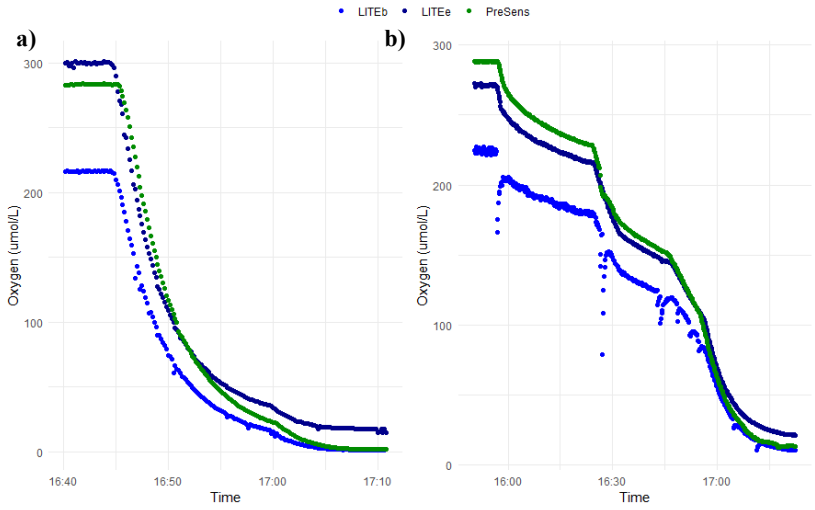

Figure 5. Dissolved oxygen concentration (O2 µmol/L) profiles comparing the PreSens® multi-parameter sensor with MAANTAb and MAANTAe **a)** 17th October 2024 **b)** 6th December 2024

Regarding temperature, in the 17th October 2024 experiment, both LITE sensors followed a similar trend to the PreSens® sensor, with minor deviations (Fig. 6a). The Kruskal–Wallis test indicated a significant difference between sensors ($\chi^2 = 482.98$, df = 2, $p < 0.001$). Pairwise Wilcoxon comparisons showed that all sensors differed significantly from one another (all adjusted $p < 0.001$). On average, LITEb measured 0.86 ± 0.04 °C lower and LITEe 0.17 ± 0.06 °C lower than PreSens, with a difference of 0.68 ± 0.04 °C between the two LITE sensors. Among the LITE units, LITEe aligned more closely with the PreSens multi-parameter measurements, while LITEb consistently underestimated temperature values, particularly at higher temperature levels.

In the 6th December 2024 experiment, after the addition of deionized water, both LITE sensors exhibited a progressive drift in temperature readings over time and a systematic underestimation compared with the PreSens sensor (Fig. 6b). The Kruskal–Wallis test confirmed a highly significant difference between sensors ($\chi^2 = 1443.7$, df = 2, $p < 0.001$), and pairwise Wilcoxon tests revealed significant differences between all pairs (all adjusted $p < 0.001$). LITEb and LITEe dissolved oxygen sensors respectively measured 2.07 ± 0.03 °C and 1.49 ± 0.02 °C lower than PreSens, with a 0.58 ± 0.04 °C difference between the two LITE sensors.

Overall, both LITE sensors accurately captured the general oxygen and temperature dynamics; however, LITEe produced results more consistent with the PreSens multi-parameter, whereas LITEb systematically underestimated both DO and temperature and exhibited greater thermal drift.

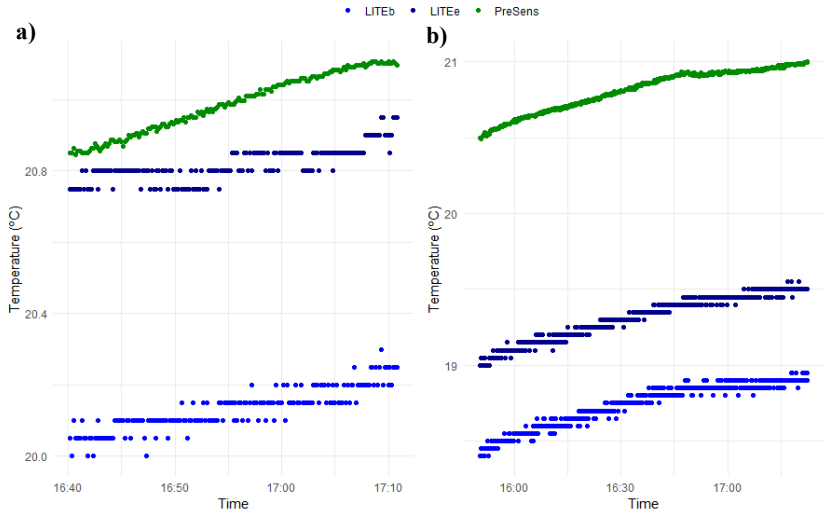

Figure 6. Temperature (ºC) profiles comparing the PreSens® multi-parameter sensor with MAANTAb and MAANTAe **a)** 17th October 2024 **b)** 6th December 2024.

3.3 CTD comparison tests

Following the summer of 2024 deployments, oxygen concentrations measured by the LITE sensors were compared *in situ* with a calibrated CTD sensor. Overall, oxygen concentrations differed significantly between the two sensors ($p= 2.43 \times 10^{-47}$), with a mean difference of 99.68 ± 12.41 µmol/L. Phase-specific analyses revealed a larger difference during the ascent (113 ± 10.9 µmol/L) compared to the descent (92.4 ± 5.18 µmol/L) though this difference was not statistically significant (p= 0.35) (Fig. 7a).

Following the removal of the LITE unit from the housing and addition of deionized water to the fiber-optic sensor, new CTD casts showed that the mean oxygen concentration difference decreased to 10.4 ± 3.5 µmol/L but remained statistically significant ($p=2.43 \times 10^{-47}$), with phase-specific differences still prominent for both ascent (13.4 ± 3.05 µmol/L) and descent (9.15 ± 2.82 µmol/L) (p= 0.009) (Fig. 7b).

The oxygen LITE sensors were then tested in two configurations: with a modified housing designed to enhance water flow (Full_LITE; see Annex II; Fig. 1b) and stand-alone without housing (Container_LITE). For the Container_LITE deployments, CTD measurements were 260 ± 17.0 µmol/L, while Container_LITEb and LITEe recorded

231 ± 19.1 µmol/L and 237 ± 16.0 µmol/L, respectively. Differences between the CTD and LITE sensors were significant ($p= 1.17 \times 10^{-28}$), as were differences between Container_LITEb and LITEe (p=0.02; Fig. 7c). For the fully assembled tags (Full_LITE), CTD oxygen concentrations were 260 ± 16.1 µmol/L, compared to 231 ± 16.6 µmol/L (Full_LITEb) and 239 ± 15.7 µmol/L (Full_LITEe), with post-hoc tests indicating significant differences between CTD and LITE sensors ($p=5.67\times 10^{-}30$) and between Full_LITEb and Full_LITEe (p=0.001; Fig. 7d). Comparisons between Full and Container LITE profiles showed no significant differences (Full = 235 ± 16.6 µmol/L; Container = 234 ± 17.8 µmol/L; p = 0.48).

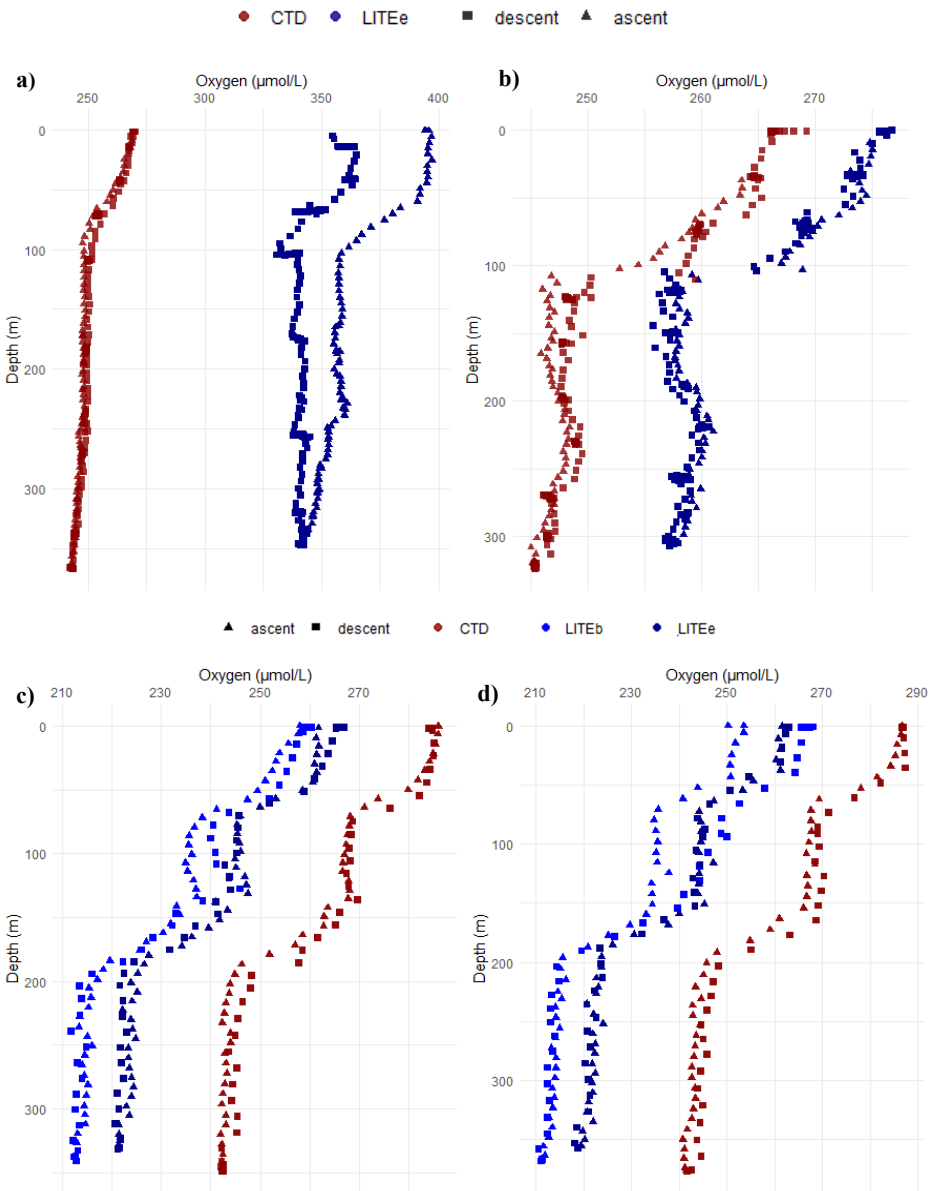

Figure 7. Cast of CTD along with the tags MAANTA6143647e and MAANTA6142647b showing the dissolved oxygen concentration (umol/L) over depth **a)** Before recalibrating **b)** Without housing and dionized water **c)** After recalibration and without housing (Full_LITE) **d)** After recalibration and with modified housing **(**Container_LITE).

Temperature measurements exhibited a similar trend to the oxygen results. In the first CTD cast, the temperature differences between the LITE sensors, when fully assembled, and the CTD were significant ($p=1.19 \times 10^{-48}$), with a mean difference of 1.33 ± 0.83 °C. Phase-specific analyses showed a larger difference during the ascent (2.21 ± 0.54 °C) than during the descent (0.83 ± 0.48 °C) (p= 0.65) (Fig. 8a). CTD cast was then repeated, after the MAANTA tag foam removal, i.e., using LITE container only and the addition of deionized water. The mean temperature difference was 1.60 ± 0.34 °C ($p= 1.19\times 10^{-48}$), with phase-specific differences of 1.31 ± 0.32 °C during ascent and 1.73 ± 0.26 °C during descent (p=0.97) (Fig. 8b).

For the Container_LITE sensors set-up, CTD temperatures registered 15.3 ± 1.30 °C, while Container_LITEb and Container_LITEe measured 13.1 ± 1.32 °C and 13.7 ± 1.34 °C, respectively. Differences between CTD and LITE sensors were significant ($p=1.17\times 10^{-28}$), as well as the difference between Container_LITEb and Container_LITEe (p=0.014; Fig. 10c). For the fully mounted tags, CTD temperature was 15.2 ± 1.25 °C, compared with 13.2 ± 1.28 °C (Full_LITEb) and 13.8 ± 1.30 °C (Full_LITEe), again showing significant differences between CTD and LITE sensors (p = 5.65 x 10 -30), as well as between Full_LITEb and Full_LITEe (p=0.007; Fig. 8d). Comparisons between Full and Container LITE profiles revealed no significant differences (p=0.41), with mean temperatures of 13.5 ± 1.25 °C for Full_LITE and 13.4 ± 1.36 °C for Container_LITE.

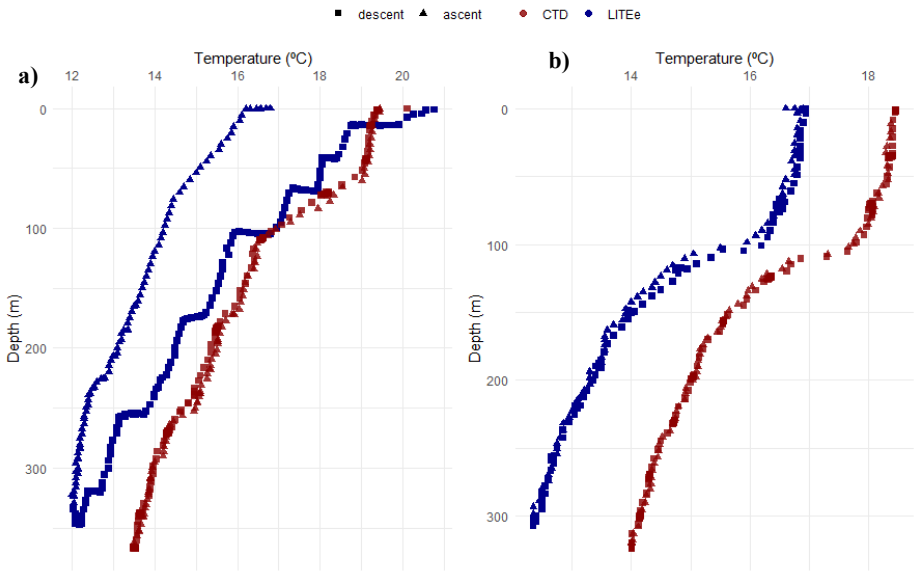

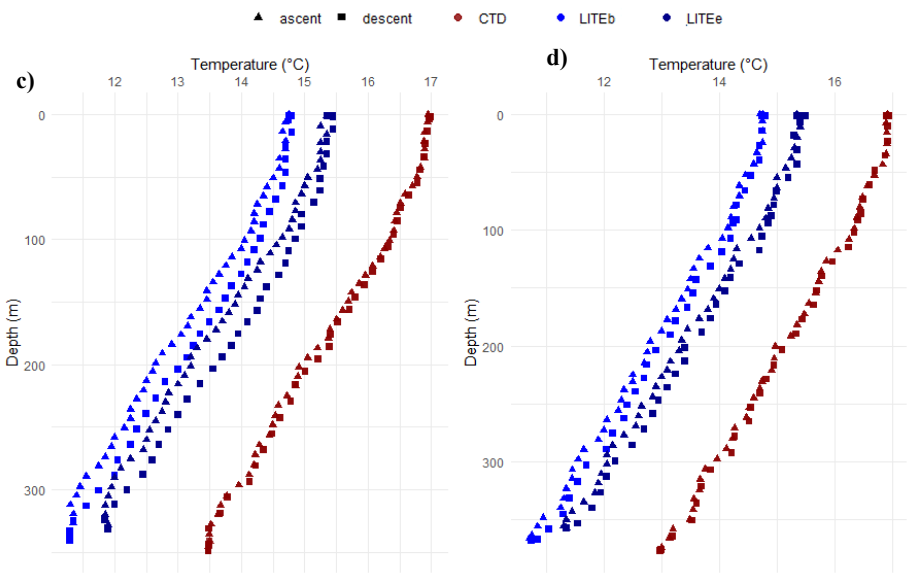

Figure 8. Cast of CTD along with the tags MAANTA6143647e and MAANTA6142647b showing the temperature (ºC) over depth **a**) Before recalibrating **b)** Without housing and dionized water **c)** After recalibration and without housing (Full_LITE) **d)** After recalibration and with modified housing (Container_LITE)

4. Discussion

4.1 Animal-borne oxygen sensing for dynamic ocean observation

Comparisons between *in situ* data from MAANTA tags and CMEMS model outputs revealed generally strong temperature agreement (r = 0.98–1.00) but more variable correlations for dissolved oxygen (r = 0.06–0.96). Across all deployments, CMEMS estimated lower DO concentrations (–47 to –123 µmol/L) and higher temperatures (+1.4 to +2.7 °C) than those recorded by the MAANTA tag.

Patterns varied among species and appeared closely linked to behaviour and physiology. The bluntnose sixgill shark (ALB_01) showed one of the strongest DO correlations (mean offset: –51.9 ± 16.1 µmol/L). This aligns with findings from early in situ oxygen tagging studies (Coffey & Holland, 2015), where slow-moving benthopelagic species yielded more stable measurements due to reduced flow-dependent sensor drift (Waller et al., 2024). In contrast, the shortfin mako shark (MAK_01) displayed the weakest correlation (mean offset: –109.5 ± 69.5 µmol/L), likely driven by its high-speed, oscillatory swimming, (Carey et al., 1981; Sepulveda et al., 2007; Waller et al., 2023) which can induce a sensor thermal lag response-time.

For the blue shark (BLU_01), CMEMS yield lower DO by –83.8 ± 27.3 µmol/L—greater than differences reported by Da Costa et al. (2024) 218–245 µmol/L, nevertheless, in a

different season. Similar temperature ranges (15–22 °C) were found in concurrent studies in the same region and season (Ciancia et al., 2016; Rovelli et al., 2022), suggesting that discrepancies likely reflect regional stratification and temporal averaging within CMEMS. The whale shark (PIN_03) also exhibited lower CMEMS-derived DO (–122.8 ± 17.3 µmol/L) and slightly higher temperature (+2.3 ± 0.3 °C) compared to in situ observations. Despite this, temperature (11.8–24.1 °C) it falls within known ecological tolerances already recorded (Graham et al., 2006; Fontes et al., 2023). DO ranged from 181–265 µmol/L; however, whale shark oxygen thresholds remain uncertain, with modelled data suggesting neonates may prefer waters below 170 µmol/L (Womersley et al., 2025). For the Chilean devil ray it represents the first in situ DO dataset, CMEMS yield lower DO (–47.1 ± 16.7 µmol/L) and yielded higher temperature (+1.9 ± 0.2 °C). This aligns with previous modelled estimates for *M. mobular* in moderately hypoxic waters (<220 µmol/L DO; Lezama-Ochoa et al., 2020) and within thermal ranges previously reported (Thorrold et al., 2014; Fontes et al., 2023).

Collectively, these findings demonstrate how animal-borne sensors provide valuable, high-resolution environmental data that complement modelled products. Differences between in situ and CMEMS datasets likely reflect a combination of species-specific behaviour (e.g., swimming speed, habitat use) and model or sensor limitations (e.g., spatial resolution, response time). Importantly, provides the first in situ oxygen measurements for mobulids and whale sharks, offering a foundation for refining oceanographic models through real-time biological sampling. Such “animal oceanographers” expand the reach of traditional monitoring systems and contribute to the democratization of ocean observation. Given this, all dataset are publicly available via ERDDAP (Environmental Research Division’s Data Access and Processing System): https://datanautilosh2020.eu/erddap/tabledap/animal_tag_ceiia_metadata.html.

4.2 MAANTA tag DO and temperature validation

Although the MAANTA tag’s sensors were initially assumed to be factory-calibrated, post-deployment analyses revealed that the PICO-O_2-SUB requires regular calibration to ensure accurate dissolved oxygen (DO) readings. Comparisons between tag data and modelled CMEMS products highlighted substantial discrepancies, prompting a detailed validation using calibrated CTDs and multiparameter reference sensors. These tests confirmed that sensors without calibration systematically underestimated DO, with mean

offsets near 100 µmol/L, but that accuracy markedly improved after applying deionized water on the optical surface of the DO sensor—reducing the bias to approximately 10 µmol/L. This straightforward procedure proved essential for restoring sensor sensitivity and stability. Nevertheless, small but systematic offsets among sensors are persistent, reinforcing the importance of post-deployment recalibration to correct for drift, as noted in previous studies (Körtzinger et al., 2005; Guinet et al., 2013; Coffey & Holland, 2015; Da Costa et al., 2024).

CTD comparisons showed that MAANTA temperature readings were consistently but slightly lower than reference measurements (typically 1–1.5 °C), well within the manufacturer's specified error range (±2 °C for the Keller 4LD sensor). The offset remained stable across tests, indicating that discrepancies were driven by sensor response time and thermal lag rather than housing interference. No significant differences were detected between the "Container-only" and "Full" configurations, confirming that the tag housing minimally affected water flow or sensor exposure. Minor variations between ascent and descent profiles were attributed to differing movement speeds during CTD–LITE casts—similar to the *in situ* patterns observed in fast-swimming species such as the mako shark, where rapid motion likely limits the sensor's response time.

Laboratory tests against a calibrated PreSens® multiparameter sensor confirmed that uncalibrated sensors underestimated DO and exhibited drift, especially at high oxygen concentrations. After conditioning with deionized water, LITEe achieved close agreement with the reference, while LITEb retained a small bias. Minor variability during low-oxygen phases was attributed to nitrogen bubbling over the optical surface. Temperature underestimations (0.8–2 °C) were consistent and likely due to response lag rather than systematic bias. The variability between otherwise identical sensors underscores the influence of sensor-specific drift, consistent with previous findings for optical oxygen sensors (Coffey & Holland, 2015; Da Costa et al., 2024). Unlike those studies, which evaluated drift over several days, our tests were conducted over a shorter interval (~1 h) using a comparable DO sensor model.

5. Conclusion

The MAANTA tag represents a significant advancement in biologging technology, being the first device to successfully record *in situ* dissolved oxygen (DO) data from free-swimming Chilean devil rays, whale and blue sharks. Validation through CTD

comparisons, laboratory calibrations, and sensor performance tests confirmed the tag's reliability in capturing fine-scale DO and water temperature profiles. Applying deionized water to the optical DO sensor prior to deployment markedly improved measurement accuracy and stability, while the foam housing modification had minimal effect on sensor performance. Temperature readings remained within the manufacturer's specified accuracy range (±2 °C), reinforcing confidence in the environmental data collected.

Performance differences among species were associated with behavioural and hydrodynamic factors, with greater variability observed in fast-swimming species such as the shortfin mako shark, where rapid movement likely affects sensor stabilization. These findings highlight the importance of species-specific deployment strategies and regular two-point calibration of the PICO-O_2-SUB sensor to minimize drift and maintain long-term accuracy. Future engineering improvements—particularly the integration of deeper-rated connectors (>1000 m)—will further enhance tag performance during deep-diving deployments. Overall, the MAANTA prototype demonstrates the feasibility of optical DO sensing in biologging and lays the groundwork for future studies linking oxygen variability with fine-scale behaviour in pelagic elasmobranchs.

6. References

Adams, K. R., Fetterplace, L. C., Davis, A. R., Taylor, M. D., & Knott, N. A. (2018). Sharks, rays and abortion: The prevalence of capture-induced parturition in elasmobranchs. Biological Conservation, 217, 11–27. https://doi.org/10.1016/j.biocon.2017.10.010

Afonso, P., Fontes, J., Giacomello, E., Magalhães, M. C., Martins, H. R., Morato, T., Neves, V., Prieto, R., Santos, R. S., Silva, M. A., & Vandeperre, F. (2020). The Azores: A mid-Atlantic hotspot for marine megafauna research and conservation. Frontiers in Marine Science, 6(January), 1-8. https://doi.org/10.3389/fmars.2019.00826

Arrowsmith, L. M., Sequeira, A. MM., Pattiaratchi, C. B., & Meekan, M. G. (2021). Water temperature is a key driver of horizontal and vertical movements of an ocean giant, the whale shark *Rhincodon typus*. *Marine Ecology Progress Series*, *679*, 101–114. https://doi.org/10.3354/meps13899

Aumont, O., Ethé, C., Tagliabue, A., Bopp, L., and Gehlen, M. (2015) PISCES-v2: an ocean biogeochemical model for carbon and ecosystem studies, Geosci. Model Dev., 8, 2465–2513, https://doi.org/10.5194/gmd-8-2465-2015.

Bailleul, F., Vacquie-Garcia, J., & Guinet, C. (2015). Dissolved oxygen sensor in animal-borne instruments: An innovation for monitoring the health of oceans and investigating the functioning of marine ecosystems. PLoS One, 10(7), e0132681. https://doi.org/10.1371/ journal.pone.0132681

Breitburg, D., Levin, L. A., Oschlies, A., Grégoire, M., Chavez, F. P., Conley, D. J., Garçon, V., Gilbert, D., Gutiérrez, D., Isensee, K., Jacinto, G. S., Limburg, K. E., Montes, I., Naqvi, S. W. A., Pitcher, G. C., Rabalais, N. N., Roman, M. R., Rose, K. A., Seibel, B. A., Telszewski, M., … Zhang, J. (2018). Declining oxygen in the global ocean and coastal waters. *Science (New York, N.Y.)*, *359*(6371), eaam7240. https://doi.org/10.1126/science.aam7240

Carey, F. G., Teal, J. M., & Kanwisher, J. W. (1981). The Visceral Temperatures of Mackerel Sharks (Lamnidae). *Physiological Zoology*, *54*(3), 334–344. http://www.jstor.org/stable/30159948

Carlson, J.K., Parsons, G.R. The Effects of Hypoxia on Three Sympatric Shark Species: Physiological and Behavioral Responses. *Environmental Biology of Fishes* **61**, 427–433 (2001). https://doi.org/10.1023/A:1011641302048

Casper, R.M. (2009). Guidelines for the instrumentation of wild birds and mammals. *Animal Behaviour, 78*, 1477-1483.

Ciancia, E., Loureiro, C. M., Mendonça, A., Coviello, I., Polito, C. D., Lacava, T., Pergola, N., Satriano, V., Tramutoli, V., & Martins, A. (2016). On the potential of an RST-based analysis of the MODIS- derived chl- a product over condor seamount and surrounding areas (Azores, NE Atlantic). Ocean Dynamics, 66(9), 1165–1180. https:// d o i . o r g / 1 0 . 1 0 0 7/ s 1 0 2 3 6- 0 1 6- 0 9 7 2- 9

Coffey, D. M., & Holland, K. N. (2015). First autonomous recording of in situ dissolved oxygen from free-ranging fish. Animal Biotelemetry, 3(1), 47. https://doi.org/10.1186/s40317-015-0088-x

Coffey, D. M., Royer, M. A., Meyer, C. G., & Holland, K. N. (2020). Diel patterns in swimming behavior of a vertically migrating deepwater shark, the bluntnose sixgill (Hexanchus griseus). *PloS one*, *15*(1), e0228253. https://doi.org/10.1371/journal.pone.0228253

Comfort, C.M., & Weng, K.C. (2015). Vertical habitat and behaviour of the bluntnose sixgill shark in Hawaii. *Deep-sea Research Part Ii-topical Studies in Oceanography, 115*, 116-126.

Compagno LJV (2001) Sharks of the world: an annotated and illustrated catalogue of shark species known to date, vol 2: Bullhead, mackerel and carpet sharks

(Heterodontiformes, Lamniformes and Orectolobiformes). FAO Species Catalogue for Fishery Purposes, no 1, vol 2, pp 269

Cortes, E., Arocha, F., Beerkircher, L., Carvalho, F., Domingo, A., Heupel, M., Holtzhausen, H., Santos, M. N., Ribera, M., & Simpfendorfer, C. (2010). Ecological risk assessment of pelagic sharks caught in Atlantic pelagic longline fisheries. Aquatic Living Resources, 23,25–34. https://doi.org/10.1051/alr/2009044

Crear, D. P., Latour, R. J., Friedrichs, M. A. M., St-Laurent, P., & Weng, K. C. (2020). Sensitivity of a shark nursery habitat to a changing climate. *Marine Ecology Progress Series, 652*, 123–136. https://doi.org/10.3354/meps13483

Da costa, I., Sims, D. W., Loureiro, B., et al. (2024). Measuring deoxygenation effects on marine predators: A new animal-attached archival tag recording in situ dissolved oxygen, temperature, fine-scale movements and behaviour. *Methods in Ecology and Evolution, 15*, 1360–1379. https://doi.org/10.1111/2041-210X.14360

Davila, X., Olsen, A., Lauvset, S. K., McDonagh, E. L., Brakstad, A., & Gebbie, G. (2023). On the origins of open ocean oxygen minimum zones. *Journal of Geophysical Research-Oceans*. **https://doi.org/10.1029/2023JC019677**

European Commission. (2015). *Copernicus: Europe's eyes on Earth*. Publications Office of the European Union. https://doi.org/10.2873/85954

Fontes, J., Castellano-González, G., Macena, B. C. L., & Afonso, P. (2023). Hitchhiking to the abyss. *Ecology and evolution*, *13*(5), e10126. https://doi.org/10.1002/ece3.10126

Fontes, J., Macena, B., Solleliet-Ferreira, S. Buyle, F., Magalhães, R., Bartolomeu, T., Liebsch, N., Meyer, C., Afonso, P. (2022). The advantages and challenges of non-invasive towed PILOT tags for free-ranging deep-diving megafauna. *Anim Biotelemetry* **10**, 39 (2022). https://doi.org/10.1186/s40317-022-00310-1

Graham, R. T., Roberts, C. M., & Smart, J. C. (2006). Diving behaviour of whale sharks in relation to a predictable food pulse. *Journal of the Royal Society, Interface*, *3*(6), 109–116. https://doi.org/10.1098/rsif.2005.0082

Grégoire, M. et al. (2021). A global ocean oxygen database and atlas for assessing and predicting deoxygenation and ocean health in the open and coastal ocean. 8https://doi.org/10.3389/fmars.2021.724913

Guinet, C., Xing, X., Walker, E., Monestiez, P., Marchand, S., Picard, B., *et al.* (2013). Calibration procedures and first dataset of Southern Ocean chlorophyll *a* profiles collected by elephant seals equipped with newly developed CTD-fluorescence tags. *Earth System Science Data, 5*(1), 15–29. https://doi.org/10.5194/essd-5-15-2013

Guinot, G., & Cavin, L. (2016). 'Fish' (Actinopterygii and Elasmobranchii) diversification patterns through deep time. Biological Reviews, 91(4), 950–981. https://doi.org/10.1111/brv.12203

Hammerschlag, N., Gallagher, A. J., & Lazarre, D. M. (2011). A review of shark satelMAANTA tagging studies. *Journal of Experimental Marine Biology and Ecology, 398*(1–2), 1–8. https://doi.org/10.1016/j.jembe.2010.12.012

Harcourt, R., Sequeira, A. M. M., Zhang, X., Roquet, F., Komatsu, K., Heupel, M., McMahon, C., Whoriskey, F., Meekan, M., Carroll, G., Brodie, S., Simpfendorfer, C., Hindell, M., Jonsen, I., Costa, D. P., Block, B., Muelbert, M., Woodward, B., Weise, M., ... Fedak, M. A. (2019). Animal-borne telemetry: An integral component of the ocean observing toolkit. *Frontiers in Marine Science*, *6*, Article 326. https://doi.org/10.3389/fmars.2019.00326

Hays, G. C., Ferreira, L. C., Sequeira, A. M. M., Meekan, M. G., Duarte, C. M., Bailey, H., Bailleul, F., Bowen, W. D., Caley, M. J., Costa, D. P., Eguíluz, V. M., Fossette, S., Friedlaender, A. S., Gales, N., Gleiss, A. C., Gunn, J., Harcourt, R., Hazen, E. L., Heithaus, M. R., Heupel, M., … Thums, M. (2016). Key Questions in Marine Megafauna Movement Ecology. *Trends in ecology & evolution*, *31*(6), 463–475. https://doi.org/10.1016/j.tree.2016.02.015

Hussey, N. E., Kessel, S. T., Aarestrup, K., Cooke, S. J., Cowley, P. D., Fisk, A. T., Harcourt, R. G., Holland, K. N., Iverson, S. J., & Kocik, J. F. (2015). Aquatic animal telemetry: A panoramic window into the underwater world. *Science, 348*, 1255642. https://doi.org/10.1126/science.1255642

Ito, T., Minobe, S., Long, M. C., Deutsch, C. (2017). Upper ocean O_2 trends: 1958–2015. *Geophysical Research Letters*. https://doi.org/10.1002/2017GL073613

Jensen, F. B., Nikinmaa, M., & Weber, R. E. (1993). Environmental perturbations of oxygen transport in teleost fishes: Causes, consequences, and compensations. In J. C. Rankin & F. B. Jensen (Eds.), *Fish ecophysiology* (pp. 161–179). Springer.

Körtzinger, A., Schimanski, J., & Send, U. (2005). High quality oxygen measurements from profiling floats: A promising new technique. *Journal of Atmospheric and Oceanic Technology, 22*(3), 302–308. https://doi.org/10.1175/JTECH1701.1

Lawson, C. L., Halsey, L. G., Hays, G. C., Dudgeon, C. L., Payne, N. L., Bennett, M. B., White, C. R., & Richardson, A. J. (2019). Powering Ocean Giants: The Energetics of Shark and Ray Megafauna. *Trends in ecology & evolution*, *34*(11), 1009–1021. https://doi.org/10.1016/j.tree.2019.07.001

Levin L. A. (2018). Manifestation, Drivers, and Emergence of Open Ocean Deoxygenation. *Annual review of marine science*, *10*, 229–260. https://doi.org/10.1146/annurev-marine-121916-063359

Lezama-Ochoa N, Lopez J, Hall M, Bach P, Abascal F, Murua H (2020) Spatio-temporal distribution of the spinetail devil ray Mobula mobular in the eastern tropical Atlantic Ocean. Endang Species Res 43:447-460 https://doi.org/10.3354/esr01082

Limburg, K. E., Breitburg, D., Swaney, D. P., Jacinto, G. (2020) Ocean deoxygenation: a primer. One Earth. https://doi.org/10.1016/j.oneear.2020.01.001

Maillard, T. C., Garzon, F., Hawkes, L. A., Tabor, G. R., & Witt, M. J. (2025). Refining Electronic Tagging of Marine Animals: Computational Fluid Dynamics and Pelagic Sharks. *Animals*, *15*(20), 2956. https://doi.org/10.3390/ani15202956

McKnight, J. C., Pass, C., Thompson, D., Balfour, S., Brasseur, S. M. J. M., Embling, C., Hastie, G., Milne, R., Kyte, A., Moss, S. E. W., Pemberton, R., & Russell, D. J. F. (2024). Quantifying and reducing the cost of tagging: combining computational fluid dynamics and diving experiments to reduce impact from animal-borne tags. *Proceedings. Biological sciences*, *291*(2034), 20241441. https://doi.org/10.1098/rspb.2024.1441

Musa, S. M., Ripley, D. M., Moritz, T., & Shiels, H. A. (2020). Ocean warming and hypoxia affect embryonic growth, fitness and survival of small-spotted catsharks, Scyliorhinus canicula. *Journal of fish biology*, *97*(1), 257–264. https://doi.org/10.1111/jfb.14370

Oschlies, A., Brandt, P., Stramma, L., & Schmidtko, S. (2018). Drivers and mechanisms of ocean deoxygenation. *Nature Geoscience*, 11, 467–473. https://doi.org/10.1038/s41561-018-0152-2

Payne, N. L., Meyer, C. G., Smith, J. A., Houghton, J. D. R., Barnett, A., Holmes, B. J., Nakamura, I., Papastamatiou, Y. P., Royer, M. A., Coffey, D. M., Anderson, J. M., Hutchinson, M. R., Sato, K., & Halsey, L. G. (2018). Combining abundance and performance data reveals how temperature regulates coastal occurrences and activity of a roaming apex predator. *Global change biology*, *24*(5), 1884–1893. https://doi.org/10.1111/gcb.14088

Petsch, S. T. (2003). The global oxygen cycle. Pp. 515 555 in Treatise on Geochemistry, H. D. Holland and K. K. Turekian, eds. Pergamon, Oxford. https://doi. org/10.1016/B0-08-043751-6/08159-7

Priede, I. G., Solbé, J. F. D. L. G., & Nott, J. E. (1988). An acoustic oxygen telemetry transmitter for the study of exposure of fish to variations in environmental dissolved oxygen. Journal of Experimental Biology, 140(1), 563–567. https://doi.org/10.1242/jeb.140.1.563

Prince, E. D., Luo, J., Goodyear, C. P., Hoolihan, J. P., Snodgrass, D., & Skomal, G. B. (2010). Ocean scale hypoxia-based habitat compression of Atlantic istiophorid billfishes. *Fisheries Oceanography, 19*(6), 448–462. https://doi.org/10.1111/j.1365-2419.2010.00556.x.

Queiroz, N., Humphries, N.E., Couto, A. *et al.* (2019) Global spatial risk assessment of sharks under the footprint of fisheries. *Nature* **572**, 461–466 (2019). https://doi.org/10.1038/s41586-019-1444-4

R Core Team (2024). *R: A Language and Environment for Statistical Computing*. R Foundation for Statistical Computing, Vienna, Austria.

Rohner, C. A., B. Norman, G. Araujo, J. Holmberg, & S. J. Pierce. (2021).“ Population Ecology of Whale Sharks.” In *Whale Sharks: Biology, Ecology, and Conservation*, 129–152. Florida, USA: CRC Press.

Roquet, F., Wunsch, C., Forget, G., Heimbach, P., Guinet, C., Reverdin, G., et al. (2013). Estimates of the Southern Ocean general circulation improved by animal-borne instruments [Dataset]. Geophysical Research Letters, 40(23), 6176–6180. https://doi.org/10.1002/2013gl058304

Rovelli, L., Carreiro- Silva, M., Attard, K., Rakka, M., Dominguez- Carrió, C., Bilan, M., Blackbird, S., Morato, T., Wolff, G., & Glud, R. (2022). Benthic O2 uptake by coral gardens at the condor seamount (Azores). Marine Ecology Progress Series, 688, 19–31. https://doi.org/10.3354/meps14021

Santos, R. S., Hawkins, S., Monteiro, L. R., Alves, M., and Isidro, E. J. (1995). Marine research, resources and conservation in the Azores. Aquat. Conserv. Mar. Freshw. Ecosyst. 5, 311–354. doi: 10.1002/aqc.3270050406

Schlaff, A.M., Heupel, M.R. & Simpfendorfer, C.A. (2014) Influence of environmental factors on shark and ray movement, behaviour and habitat use: a review. *Rev Fish Biol Fisheries* 24, 1089–1103. https://doi.org/10.1007/s11160-014-9364-8

Schmidtko, S., Stramma, L., & Visbeck, M. (2017). Decline in global oceanic oxygen content during the past five decades. *Nature*, *542*(7641), 335–339. https://doi.org/10.1038/nature21399

Semenza G. L. (2007). Oxygen-dependent regulation of mitochondrial respiration by hypoxia-inducible factor 1. *The Biochemical journal*, *405*(1), 1–9. https://doi.org/10.1042/BJ20070389

Sepulveda, C. A., J. B. Graham, & D. Bernal. (2007). “Aerobic Metabolic Rates of Swimming Juvenile Mako Sharks, Isurus oxyrinchus.” Marine Biology 152: 1087–1094.

Svendsen, J. C., Aarestrup, K., Steffensen, J. F., & Herskin, J. (2006). A novel acoustic dissolved oxygen transmitter for fish telemetry. Marine Technology Society Journal, 40(1), 103–108. https://doi.org/ 10.4031/002533206787353655

Thorrold, S. R., Afonso, P., Fontes, J., Braun, C. D., Santos, R. S., Skomal, G. B., & Berumen, M. L. (2014). Extreme diving behaviour in devil rays links surface waters and the deep ocean. Nature Communications, 5, 1–7. https://doi.org/10.1038/ncomms5274

Tokunaga, S., Chiang, W. C., Nakamura, I., Matsumoto, R., & Watanabe, Y. Y. (2025). Enhanced thermoregulation abilities of shortfin mako sharks as the key adaptive significance of regional endothermy in fishes. *The Journal of animal ecology*, 10.1111/1365-2656.70116. Advance online publication. https://doi.org/10.1111/1365-2656.70116

Vedor, M., Queiroz, N., Mucientes, G., Couto, A., Costa, I. D., Santos, A. D., Vandeperre, F., Fontes, J., Afonso, P., Rosa, R., Humphries, N. E., & Sims, D. W. (2021). Climate-driven deoxygenation elevates fishing vulnerability for the ocean's widest ranging shark. *eLife*, *10*, e62508. https://doi.org/10.7554/eLife.62508

Waller, M. J., Humphries, N. E., Womersley, F. C., Loveridge, A., Jeffries, A. L., Watanabe, Y., Payne, N., Semmens, J., Queiroz, N., Southall, E. J., & Sims, D. W. (2024). The vulnerability of sharks, skates, and rays to ocean deoxygenation: Physiological mechanisms, behavioral responses, and ecological impacts. Journal of Fish Biology, 105(2), 482–511. https://doi.org/10.1111/jfb.15830

Waller, M. J., Queiroz, N., Da costa, I., Cidade, T., Loureiro, B., Womersley, F. C., Fontes, J., Afonso, P., Macena, B. C. L., Loveridge, A., Humphries, N. E., Southall, E. J., & Sims, D. W. (2023). Direct measurement of cruising and burst swimming speeds of the shortfin mako shark (Isurus oxyrinchus) with estimates of field metabolic rate. *Journal of fish biology*, *103*(5), 864–883. https://doi.org/10.1111/jfb.15475

Watanabe, Y. Y., & Papastamatiou, Y. P. (2023). Biologging and Biotelemetry: Tools for Understanding the Lives and Environments of Marine Animals. Annual Review of Animal Biosciences, 11, 247–267. https://doi.org/10.1146/annurev-animal-050322-073657

Wearmouth, V. J., McHugh, M. J., Humphries, N. E., Naegelen, A., Ahmed, M. Z., Southall, E. J., Reynolds, A. M., & Sims, D. W. (2014). Scaling laws of ambush predator 'waiting' behaviour are tuned to a common ecology. *Proceedings. Biological sciences*, *281*(1782), 20132997. https://doi.org/10.1098/rspb.2013.2997

Williams, H. J., Taylor, L. A., Benhamou, S., Bijleveld, A. I., Clay, T. A., Grissac, S., Demšar, U., English, H. M., Franconi, N., Gómez- Laich, A., Griffiths, R. C., Kay, W. P., Morales, J. M., Potts, J. R., Rogerson, K. F., Rutz, C., Spelt, A., Trevail, A. M., Wilson, R. P., & Börger, L. (2020). Optimizing the use of biologgers for movement ecology

research. *Journal of Animal Ecology*, 89, 186– 206. https://doi. org/10.1111/1365-2656.13094

Womersley, F. C., Waller, M. J., & Sims, D. W. (2025). Do Whale Sharks Select for Specific Environments to Give Birth?. *Ecology and evolution*, *15*(2), e70930. https://doi.org/10.1002/ece3.70930

Chapter II: Practical case study – The dive behaviour of *Mobula tarapacana* in relation to dissolved oxygen

1. Introduction

Following the 2024 field deployments and calibration of the multisensory MAANTA oxygen-measuring tag, the 2025 deployment season enabled the collection of additional *in situ* data for sensor validation and a preliminary investigation of the diving behaviour of the Chilean devil ray (*Mobula tarapacana*) in relation to dissolved oxygen (DO) and temperature.

The Chilean devil ray (*M. tarapacana* Philippi, 1892) belongs to the Mobula genus that has 9 extant species (Notarbartolo-di-Sciara et al. 2019; Hosegood et al., 2020) with a 10th recently proposed (Bucair et al., 2025). It is distinguished from other mobulids by the olive-green to brown dorsal coloration and a distinctive white ventral region (Mendonça et al., 2020; White et al., 2018). This large pelagic species can reach a maximum disc width (DW) of up to 3.7 m (Lezama-Ochoa et al., 2019; Rambahiniarison et al., 2018; White et al., 2018). The Chilean devil ray has a cosmopolitan distribution across tropical, subtropical, and temperate waters of the Atlantic, Pacific, and Indian Oceans (Couturier et al., 2012; Pate et al., 2023).

Like other mobulids, Chilean devil rays display slow growth and late sexual maturity, with age-at-pregnancy estimates ranging from 5 to 12 years (Couturier et al., 2012; Croll et al., 2012; Rambahiniarison et al., 2018). Such life-history traits make the species particularly vulnerable to anthropogenic pressures, including targeted fishing and bycatch. The international demand for gill plates used in traditional Asian medicine (White et al., 2006; Pate et al., 2023), along with incidental capture in gillnets, purse seines, and longlines, contributes to high mortality rates (Guirhem et al., 2021; Lezama-Ochoa et al., 2019; Palacios et al., 2023; Putra et al., 2020). As a result, the most recent IUCN Red List assessment listed *M. tarapacana* as *Critically Endangered (CR)* (Jabado et al., 2025). Major gaps persist in understanding its movement ecology, reproduction,

age and growth, and population trends (Laglbauer et al., 2025; Lezama-Ochoa et al., 2019; Pate et al., 2023; Stewart et al., 2018).

This elusive and understudied species is typically observed in aggregations linked to feeding, cleaning, social, and reproductive behaviours, particularly around seamounts such as Princess Alice and Ambrósio in the Azores, as well as off the coast of Brazil (Mendonça et al., 2018, 2020; Morato et al., 2010; Palacios et al., 2023). These seamounts act as biological hotspots, supporting high biodiversity and attracting a variety of pelagic megafauna (Morato et al., 2010). In the Azores, three species of mobula—*M. tarapacana, M. mobular, and M. birostris (Fontes pers. obs.)* — have been observed with seasonal aggregations on shallow seamounts and island shores.

Once thought to be primarily surface-dwelling filter feeders, *M. tarapacana* can undertake long-distance migrations of up to 3,800 km across oligotrophic tropical and subtropical waters and to perform deep dives exceeding 1,800 m into waters colder than 4°C (Thorrold et al., 2014). These deep dives often reach the deep scattering layer (DSL), a zone rich in mesopelagic fish and squid (Irigoien et al., 2014) and frequented by deep-diving predators (Braun et al., 2023). Diving into the bathypelagic zone is limited by physiological and energetic constraints associated with low temperatures, high pressure, and reduced oxygen availability, all of which can significantly affect animal fitness (Braun et al., 2022; Sutton et al., 2008).

This deep diving behaviour requires thermoregulatory adaptations that allow heat generation and retention in critical tissues (Thorrold et al.,2014). In lamnid sharks and scombroid fishes, the convergent evolution of cranial endothermy has been linked to the maintenance of brain function and visual acuity during foraging in deep, cold waters (Block & Finnerty, 1994). *M. tarapacana* similarly possesses specialized *retia mirabilia* surrounding the cranial cavity, supporting cranial endothermy (Schwitzer & Notarbartolo-di-Sciara, 1986). Earlier studies (Alexander, 1995; 1996) suggested that the *retia* warms the brain, though the counter-current system and its functional advantage remained unclear in mobula species not typically exposed to cold waters. Recent findings, however, propose that cranial endothermy in mobulids evolved through temperature-driven selection for enhanced thermogenic capacity, enabling stable brain temperatures and improved neural performance in low temperature environments (Arostegui et al., 2024).

How mobulid rays respond to low dissolved oxygen remains unknown. In elasmobranchs, hypoxia tolerance varies widely: highly mobile species typically avoid low-oxygen zones (Waller et al., 2024), while slower benthic species may rely on compensatory mechanisms such as increased ventilation, bradycardia (Butler & Metcalfe, 1988), or elevated haematocrit to maintain aerobic metabolism (Waller et al., 2024). Some deep-diving sharks, such as the bigeye thresher (*Alopias superciliosus*), even possess enlarged gill surface areas to enhance oxygen uptake (Wootton et al., 2015). Given their repeated exposure to low-oxygen depths, mobulas may exhibit similar adaptations, but these physiological mechanisms remain unstudied.

In this study, we provide the first insights into the relationship between dissolved oxygen concentration and the diving behaviour of the endangered Chilean devil ray using the MAANTA NAUTILOS biologging tag. Specifically, we aim to assess how dissolved oxygen and temperature influence the vertical distribution and dive behaviour of the Chilean devil ray.

2. Materials and methods

2.1 Animal ethical approval

Provided in Part I, Section 2.5 (Animal ethical approval).

2.2 Field deployment

The deployment procedures for the MAANTA tag on the mobulid are described in Part I, Section 2.3 (Field Deployment) (Fig. 1). Detailed specifications of the MAANTA tag, including its integrated dissolved oxygen, temperature, and fine-scale movement sensors, are provided in Part I, Section 2.1 (Tag Specifications).

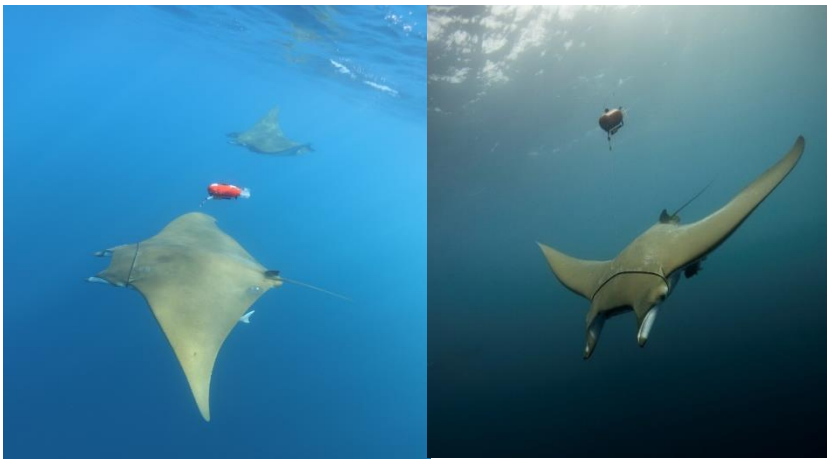

Figure 1. MAANTA tag deployment on a sickefin devil ray (*Mobula tarapacana*) (Source: J. Fontes Okeanos- ImagDOP©

2.3 Study area

Deployments were carried out between August and September 2025 at the Ambrósio seamount, located approximately 3 miles off Santa Maria Island in the eastern group of the Azores Archipelago, Portugal. Recovery sites included Mar de Prata and Maria Celeste seamounts, and nearshore areas of Santa Maria. In total, three Chilean devil rays were successfully tagged (Fig. 2).

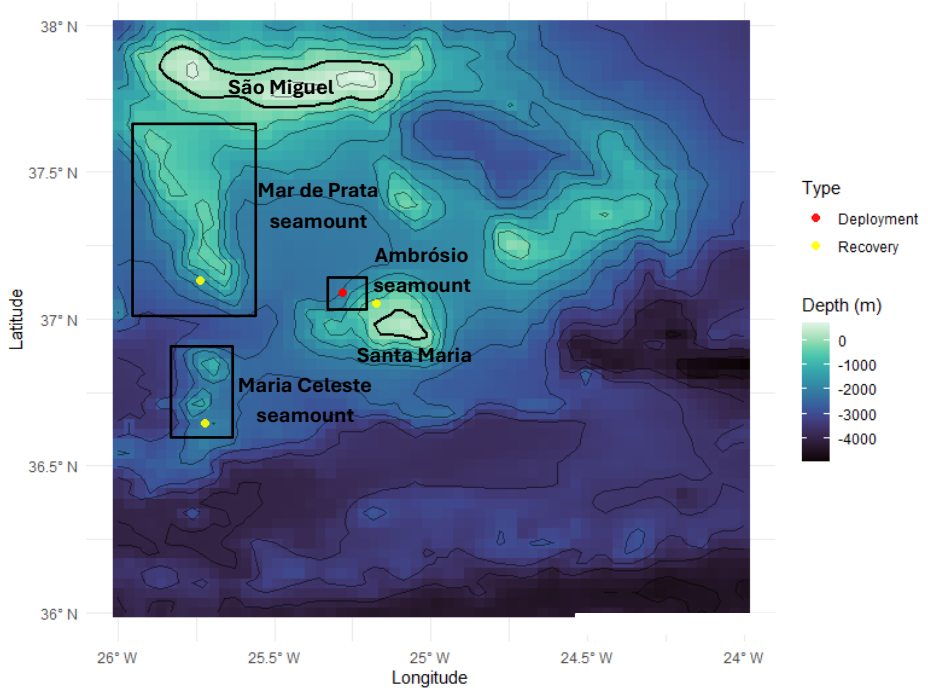

Figure 2. Map of the eastern group of the Azores archipelago and adjacent seamounts showing tag deployment sites (red circles) and recovery locations (yellow circles).

2.4 Data analysis

2.4.1 Oxygen and Temperature gradients

To visualize vertical environmental structure, dive profiles were colour-coded according to concurrent temperature and dissolved oxygen measurements recorded every 10 seconds. These data were used to illustrate thermal and oxygen gradients along the dive trajectories. Mean values (± SD) of temperature and dissolved oxygen were calculated for each individual across the full depth range.

2.4.2 Environmental variables profiles

Time-at-depth (TAD), time-at-oxygen (TAO), and time-at-temperature (TAT) profiles were calculated to describe *M. tarapacana* habitat use across diel cycles. Depth, oxygen, and temperature data were grouped into bins: oxygen concentrations in 20 µmol/L

intervals, temperature in 2°C intervals, and depth at 0, 2, 5, 10, 20, 50, 100, 200, 300, 400, 600, and 2000 m. Based on the time resolution of each deployment, the proportion of time spent within each bin was calculated as a percentage of the total deployment duration. Day and night periods were defined as 20:00–07:00 to allow comparisons of vertical and environmental occupancy between diel phases.

All *M. tarapacana* individuals were included (n = 3), and data were restricted to the period between deployment and tag pop-off, ensuring only biologically relevant records were analyzed. Oxygen concentration, temperature, and time were standardized as percentages relative to the total recording duration to enable comparisons among individuals. Extreme outliers were identified and removed using the 95th percentile threshold prior to analysis.

2.4.3 Vertical velocity dive profiles

Vertical velocity (VV) (m/s) was estimated to assess the fine-scale diving behaviour of mobulids. Depth data were first smoothed using a 10-point simple moving average (SMA) window, applied with a centered alignment to reduce short-term fluctuations and sensor noise while preserving the main dive profile. Given the 20 Hz sampling rate, this smoothing corresponds to approximately 10 seconds of data. Vertical velocity was then calculated as the rate of change in smoothed depth over time—i.e., the difference between consecutive depth values divided by the elapsed time between measurements:

$$VV = \frac{\Delta \text{Depth}}{\Delta \text{Time}}$$

This produced a measure of instantaneous vertical speed (m/s), from which the absolute vertical velocity (|VV|) was also derived to quantify movement intensity regardless of direction. Dives were further segmented into descent and ascent phases, with VV summarized for each phase to obtain mean (± SD) and maximum velocities. Differences in vertical velocity between ascent and descent phases were tested using the Wilcoxon rank-sum test on individual mean velocities.

To account for diel patterns in vertical behaviour, dives were classified as either daytime or nighttime (night: 20h00–07h00). Finally, VV was correlated (Spearman's rank) with concurrent oxygen and temperature data to assess whether environmental conditions influenced the energetic costs of vertical movement.

3. Results

Three Chilean devil rays (IDs: JAM_08, JAM_09, and JAM_10) were tagged with the LITE multisensor device LITE6142647b (LITEb) and LITE6143647e (LITEe) in August and September of 2025 (Table IV). Tag deployment durations ranged from 17 to 26 hours. Sex was determined through direct visual observation during tagging, based on the presence of claspers in males and their absence in females. The minimum linear distance, i.e., the straight-line distance travelled between the tagging and pop-up locations, ranged from 10 to 63 km.

Table IV. Summary metadata of the tagged *M.tarapacana*

*Distance travelled refers to the straight-line distance from tagging to pop-up location.

Shark ID	Tag ID	Species	Sex	Tagging date	Pop-up date	Deployment duration (h)	*Distance travelled (Km)
JAM_08	LITE6142647b	*M. tarapacana*	-	29-08-2025	30-08-2025	25.15	~10.4
JAM_09	LITE6143647e	*M. tarapacana*	M	30-08-2025	31-08-2025	26.57	~40.9
JAM_10	LITE6142647b	*M. tarapacana*	F	31-08-2025	01-09-2025	17.08	~62.8

3.1 Oxygen and Temperature gradients

Oxygen concentrations exhibited similar ranges across all individuals (Fig. 3). For JAM_08, values ranged from 204 to 263 ± 10 µmol/L (Fig. 3 Ia); for JAM_09 (Fig. 3. IIa), from 183 to 253 ± 13 µmol/L; and for JAM_10, from 200 to 269 ± 11 µmol/L (Fig.3 IIIa). The highest oxygen concentrations consistently occurred within the oxycline, at depths of approximately 40–50 m, while the lowest values were recorded in the deepest layers (500–600 m).

Temperature profiles showed a comparable vertical pattern among individuals. For JAM_08, temperatures ranged from 9 to 23 ± 3 °C (Fig. 3Ib); for JAM_09, from 9 to 24 ± 4 °C (Fig. 3 IIb); and for JAM_10, from 9 to 23 ± 3 °C (Fig.3. IIIb). The warmest temperatures were observed in surface waters (0–2 m), decreasing sharply through the thermocline at 40–50 m depth, with the lowest temperatures in the deepest layers (500–600 m).

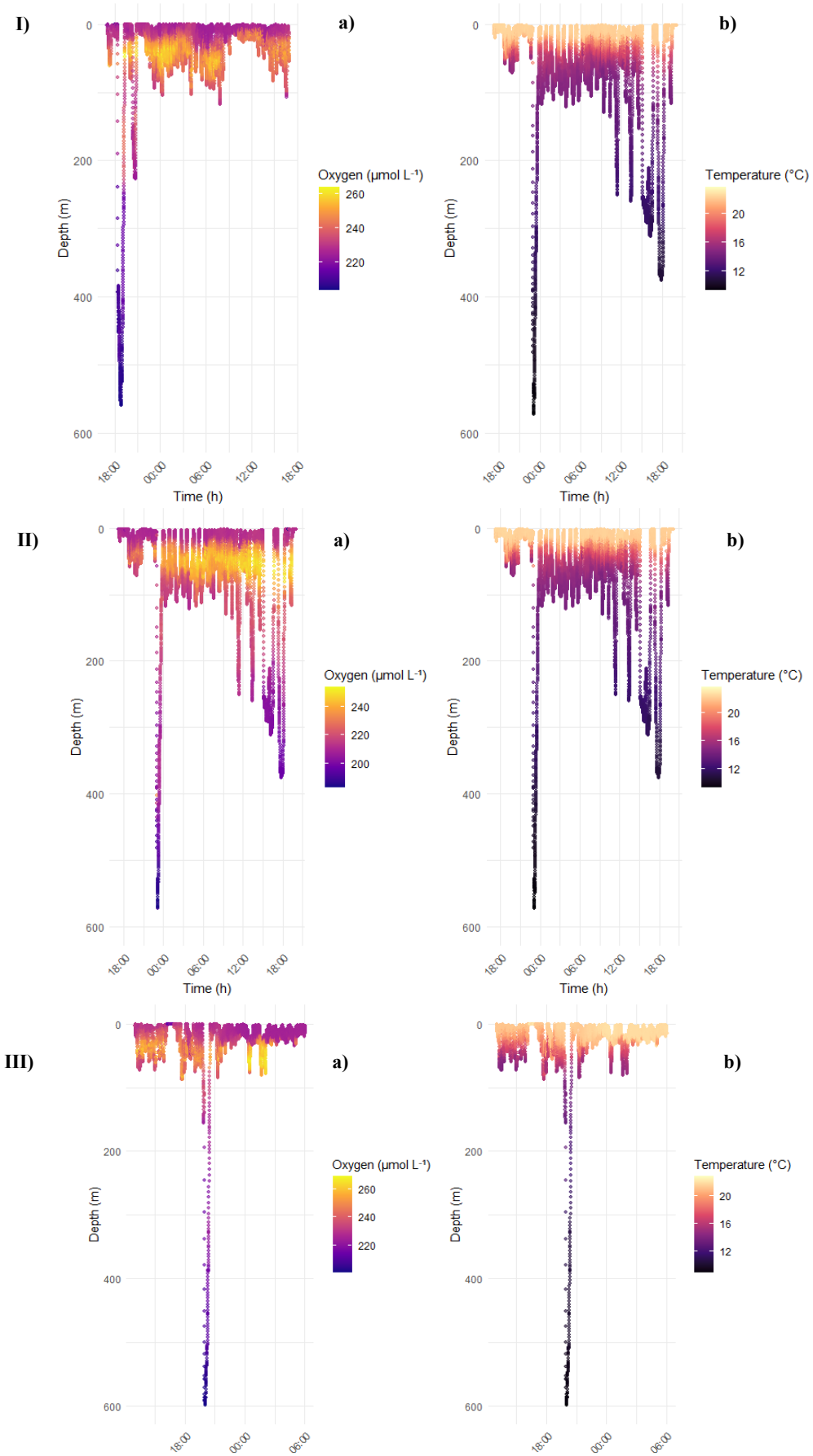

Figure 3. Dive profiles of *Mobula tarapacana* over time I)- JAM_08 II)- JAM_09 II)- JAM_10, color-coded by **(a)** dissolved oxygen concentration (µmol/L) and **(b)** temperature (°C).

3.2 TAD (time at depth) /TAO (time at oxygen) and TAT (time at temperature)

The Chilean devil rays displayed a predominant use of the epipelagic zone and multiple incursions to the mesopelagic zone, spending the majority of their time in the upper water column, with individuals occupying the top 100 m for an average of 91 ± 11% (JAM_08) (Fig. 4 Ia), 82 ± 8% (JAM_09) (Fig. 4 IIa), and 97 ± 4% (JAM_10) (Fig. 4 IIIa) of the tracking period. The optimal temperature range where devil rays spent the majority of time was (21-23ºC) and the lower temperatures experienced were (7-11ºC).

Day–night comparisons revealed distinct vertical habitat preferences among individuals. JAM_08 spent more time near the surface during the day (28 ± 13% at 10–20 m) but also exhibited deep daytime dives (36% at 400–600 m). JAM_09 showed a more balanced vertical distribution, spending 33 ± 19% of daytime at 20–50 m and 35 ± 34% of nighttime at 50–100 m. JAM_10 primarily occupied shallow waters both during the day (46% at 20–50 m) and at night (44 ± 10% at 10–20 m). Overall, nighttime behaviour was characterized by increased use of deeper layers, with dives extending to depths of up to 600 m (Fig. 4a).

TAO profiles indicated that JAM_08 and JAM_10 spent more than 50% of their time in waters with high DO concentrations, between 220–230 µmol/L, whereas JAM_09 occupied slightly lower DO concentrations (210–220 µmol/L). Despite inter-individual variability, DO values remained within a narrow range. TAT profiles showed that all individuals spent most of the time in waters between 21 and 23 °C, suggesting thermal preferences (Fig. 4b, c).

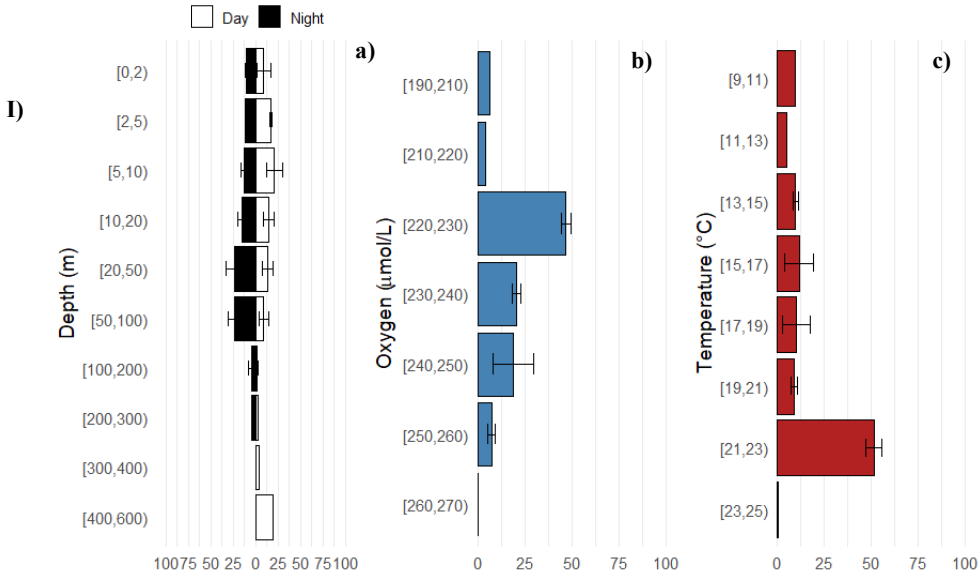

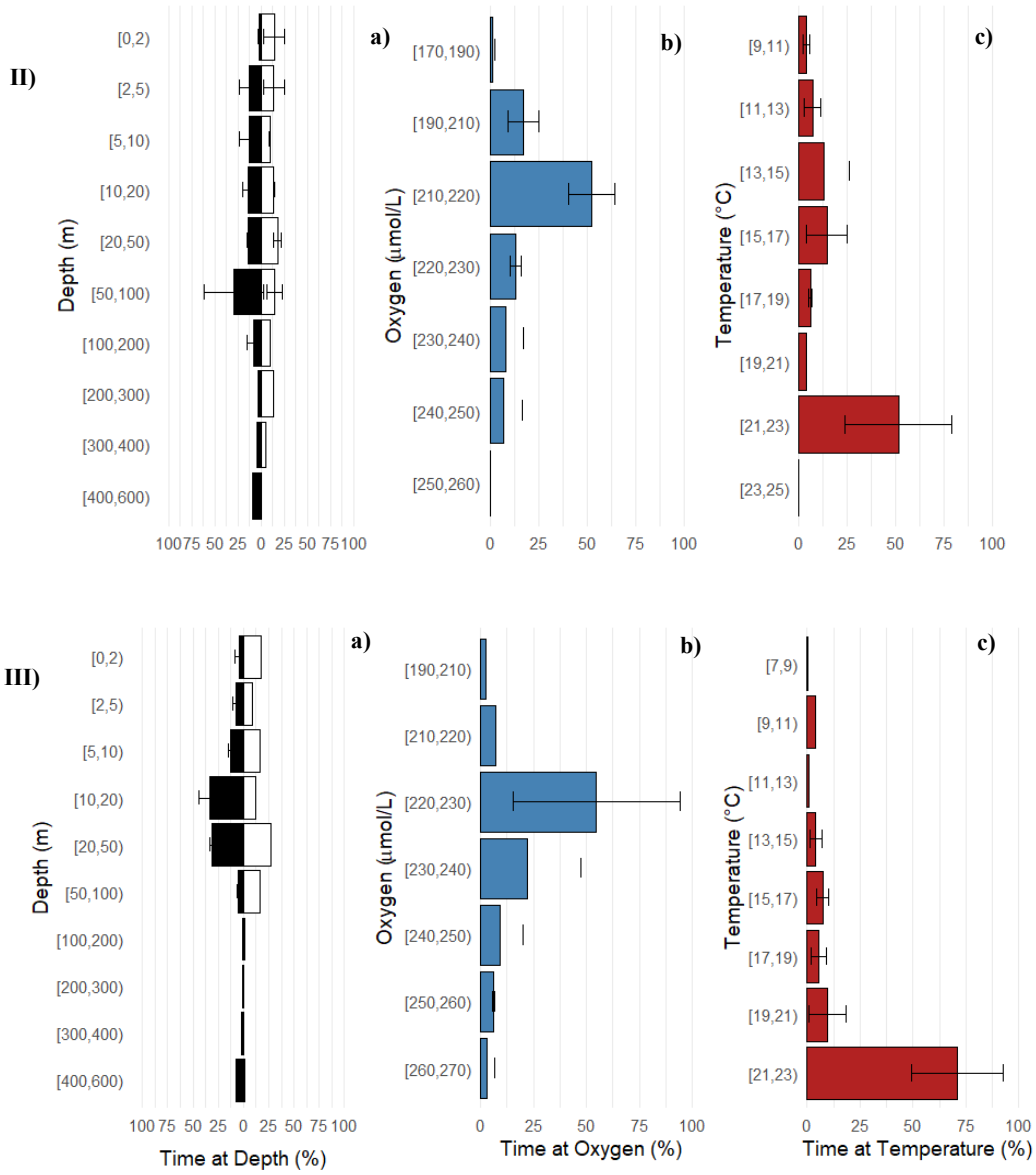

Figure 4. (**a**) Time at depth (TAD) (**b**) Time at temperature (TAT) (**c**) Time at oxygen (TAO) profiles of I)- JAM_08 II)- JAM_09 III)- JAM_10.

3.3 Diving behaviour and vertical movement patterns

Across the ~24-hour deployments, all individuals displayed a consistent diel pattern, characterized by frequent shallow dives during the day and a single deep dive occurring predominantly at night—except for JAM_08, which dove deepest at dusk. During daylight hours, JAM_08 and JAM_10 remained mostly within the upper 150 m, with JAM_08 performing three dives below 100 m, while JAM_10 did not exceed this depth. In contrast, JAM_09 exhibited a different profile, performing four dives that extended beyond 250 m. Overall, the individuals spent most of their time within the upper 100 m of the water column, where temperature and oxygen levels were highest. (Fig. 5a, b).

The deepest dives recorded reached 600 m (JAM_10), with a rapid descent followed by a slower, stepwise ascent to the surface. Each deep-dive cycle lasted approximately 60 minutes, typically followed by 10–40 minutes near the surface (0–2 m) before descending again to ~100 m (Fig. 5b). Time to reach maximum depth varied notably among individuals: JAM_08 performed a steep descent to 450 m, briefly ascended by ~50 m, then continued downward to 560 m, taking 28.1 minutes to descend and 25.1 minutes to ascend. In contrast, JAM_09 reached 584 m in just 8.1 minutes, ascending in 50.0 minutes, while JAM_10 descended to 600 m in 15.1 minutes and ascended in 34.1 minutes.

Maximum vertical velocity occurred during descents (JAM_08: 5.14 m/s; JAM_09: 4.59 m/s; JAM_10: 5.41 m/s), emphasizing the steep and rapid nature of downward movements occurred in deep dives. For JAM_08, mean descent velocities were significantly higher than ascent velocities (0.114 ± 0.121 m/s vs. 0.082 ± 0.159 m/s; $p < 0.001$), and a similar pattern was observed for JAM_10 (0.131 ± 0.132 m/s vs. 0.118 ± 0.238 m/s; $p < 0.001$). In contrast, JAM_09 showed no significant difference between both phases ($p = 0.87$), with comparable mean speeds in both ascent (0.115 ± 0.167 m/s) and descent (0.106 ± 0.105 m/s).

Overall, VV tended to be greater during descents, although this trend was not consistent across all individuals. When averaged across the entire time series, descents were slightly slower overall (JAM_08: ascent = 0.18 ± 0.15 m/s, descent = 0.10 ± 0.18 m/s; JAM_09: ascent = 0.15 ± 0.13 m/s, descent = 0.14 ± 0.20 m/s; JAM_10: ascent = 0.18 ± 0.16 m/s, descent = 0.14 ± 0.24 m/s), reflecting individual variability in diving behaviour (Fig. 5a).

The correlation between the VV and environmental gradients across all individuals, showed a weak to moderate positive correlation with DO, indicating that individuals tended to dive faster in more oxygenated waters (JAM_08: $\rho = +0.423$, $p < 0.001$; JAM_09: $\rho = +0.380$, $p < 0.001$; JAM_10: $\rho = +0.225$, $p < 0.001$). In contrast, temperature exhibited a moderate negative correlation with the VV, suggesting reduced vertical movement in warmer layers and increased in cooler waters (JAM_08: $\rho = –0.521$, $p < 0.001$; JAM_09: $\rho = –0.353$, $p < 0.001$; JAM_10: $\rho = –0.348$, $p < 0.001$).

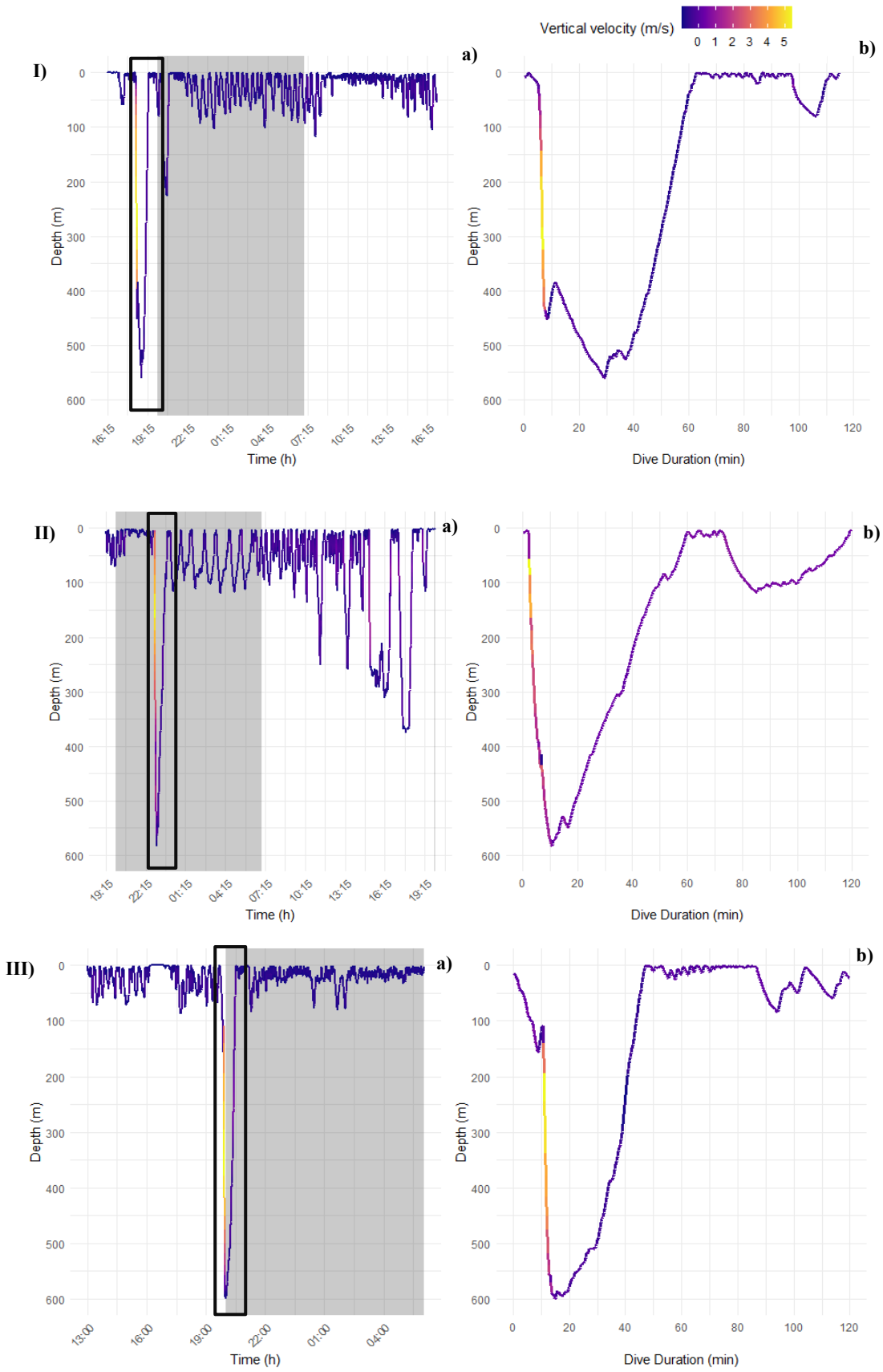

Figure 5. (**a**) Dive profiles of *Mobula tarapacana* I)- JAM_08 II)- JAM_09 III)- JAM_10, with depth trajectories color-coded by vertical velocity (m/s). Shaded gray areas indicate nighttime (20h00 – 7h00). Square highlights the identified deep-dive event. (**b**) Detailed profiles of the highlighted deep dives, showing depth against dive duration (min).

4. Discussion

4.1 Vertical distribution, horizontal movement and environmental context

Chilean devil rays in this study travelled between a minimum of 10 to 63 km over 17–25 hours, consistent with previous estimates of 24–44 km per day (Thorrold et al., 2014), indicating similar horizontal mobility across regions. Dissolved oxygen (DO) ranged from 183 to 269 µmol/L, comparable to earlier observations in the Azores (217–253 µmol/L; Da Costa et al., 2014), though those observations were made at shallower depths and during a different season. Despite the generally oligotrophic nature of the Azores (Amorim et al., 2017), its seamounts function as localized productivity hotspots ("oceanic seamount ecosystem areas"; Da Silva & Pinho, 2007), where hydrodynamic upwelling enhances zooplankton concentrations and attracts large pelagic fauna, including *M. tarapacana* (Gargan et al., 2017; Solleliet-Ferreira et al., 2020). These well-oxygenated, productive conditions likely promote both surface residency and deep-diving behaviour, possibly linked to foraging activity (Braun et al., 2022), underscoring the ecological significance of seamounts for *M. tarapacana*.

Although the physiological effects of low oxygen have not been directly studied in mobulids, their presence in OMZs—such as Cape Verde (Stramma et al., 2008; Thorrold et al., 2014) and the Costa Rica Dome (Lezama-Ochoa et al., 2019; Karstensen et al., 2008)—suggests a broad tolerance to hypoxia. Their deep-diving behaviour and repeated exposure to cold, oxygen-poor waters further imply the existence of yet-undocumented physiological adaptations. Comparable challenges in other elasmobranchs are met through strategies such as the "breath-holding" thermoregulation observed in scalloped hammerhead sharks (Sphyrna lewini), which temporarily reduce gill ventilation during deep dives to conserve heat and oxygen, though at the cost of anaerobic by-product accumulation (Royer et al., 2023). Elasmobranchs' high glycogen reserves and well-developed white muscle support anaerobic metabolism (Bernal et al., 2001; Nilsson & Östlund-Nilsson, 2008), and ram-ventilating species may increase post-dive swimming speeds to enhance oxygen uptake (Wegner et al., 2010). In contrast, the Azores region——is relatively well oxygenated, with average saturation around 94% above 550 m (Palma et al., 2012) suggesting that the DO range used by the Chilean devil ray likely reflects the stable, well-oxygenated conditions of the local environment rather than physiological limitations.

Water temperatures ranged from 9°C at depth to 24°C near the surface, aligning with previous findings for *M. tarapacana* in the Azores (7.2–23.9°C; Fontes et al., 2023). Individuals showed a preference for 21–23°C, similar to optimal ranges reported for other mobulids (20–30°C; Canese et al., 2011; Croll et al., 2012; Couturier et al., 2012) although they tolerated much colder waters. This broad thermal tolerance—from 4.2°C (Thorrold et al., 2014) to 24°C— is possible due to physiological adaptations such as cranial endothermy via retia mirabilia in the pectoral fins and brain (Alexander et al., 1995, 1996; Schweitzer & Notarbartolo-di-Sciara, 1986), enabling sensory and neural efficiency during deep, cold-water forays (Thorrold et al., 2014; Bernal et al., 2012). Such adaptations likely evolved under temperature-driven selection to enhance neural efficiency in cooler environments (Arostegui, 2024).

4.2 Deep diving behaviour and diel patterns

Mobulas were once considered surface-dwelling species, and in this study spent over 80% of their time within the upper 100 m, consistent with patterns observed in other mobulid species (Canese et al., 2011; Croll et al., 2012b) Nevertheless, this assumption is now recognized as inaccurate, as biologging studies revealed their deep dive behaviour (Thorrold et al.,2014). Deep dives exceeding 1,800 m have been reported for Chilean devil rays (Thorrold et al., 2014), highlighting their remarkable physiological adaptations. In the present study, the deepest dive reached 600 m (JAM_10), comparable to maximum depths reported for other mobulids, including *M. mobular* (Canese et al., 2011) and *M. alfredi* (Lassauce et al., 2020), both reaching up to ~700 m. Collectively, these findings confirm that mobulids routinely exploit mesopelagic to bathypelagic zones, with *M. tarapacana* representing the deepest-diving member of the genus.

Although overall depth use did not differ significantly between day and night, detailed dive profiles revealed consistent diel patterns. Individuals typically performed a single deep dive at night (except JAM_08, which dived at dusk), lasting ~60 minutes, followed by 10–40 minutes at the surface (0–2 m). Two main diving strategies were observed: (1) a steep, rapid descent followed by an oscillatory ascent (JAM_08), resembling whale shark foraging behaviour (Brunnschweiler et al., 2009); and (2) a fast descent (8–15 min) followed by a prolonged, stepwise ascent (34–50 min; JAM_09/10), consistent with dive profiles in *M. alfredi* and several shark species exhibiting prey-searching behaviour (Lassauce et al., 2020; Carey et al., 1990).

The stepwise ascent patterns observed in JAM_09 and JAM_10 suggest active foraging within the deep scattering layer (DSL). Although mobulids are primarily filter feeders, their diets include euphausiids, copepods, small fish, and squid (Rohner et al., 2017; Stewart et al., 2017), prey commonly associated with the DSL. Comparable nocturnal deep-diving and daytime basking patterns have been observed in *M. alfredi* (Lassauce et al., 2020), other mobulids (Couturier et al., 2013; Stewart et al., 2016) and whale sharks (Gleiss et al., 2013), supporting the hypothesis of nocturnal foraging on vertically migrating prey.

Regarding the diel behaviour, the pattern of daytime surface residency, likely acts as a thermoregulation mechanism, allowing individuals to increase body temperature (Canese et al., 2011; Thorrold et al., 2014; Stewart et al., 2016; Lassauce et al., 2022), which could indicate enhanced metabolic efficiency before descending into colder, deeper waters at night (Palacios et al., 2023). The daytime surface residency as also been observed in Chilean devil rays (Solleliet-Ferreira et al., 2020; Thorrold et al., 2014) and other mobulids (Canese et al., 2011; Stewart et al., 2016b). Fonseca-Ponce et al., 2022 even suggested that this behaviour in *M. birostris*, could act as a thermal refugia after deep foraging dives.

Some studies, however, have reported deeper daytime dives in *M. tarapacana* during their oceanic migrations (Thorrold et al., 2014). These differences likely reflect regional prey distribution patterns, as generally vertically migrating organisms typically remain at depth during the day and ascend at night (Kaartvedt et al., 2009). The contrasting diel patterns may also be driven by habitat differences: while Thorrold et al., 2014 tracked individuals along open-ocean migratory routes, the present study focused on seamount-associated habitats. This contrast highlights *M. tarapacana*'s behavioural plasticity, with shallower dives reflecting local prey dynamics or social behaviour aggregations rather than physiological limitations.

4.3 Dive behaviour classification and possible influences

Dive-type classification provides additional insight into the functional significance of the observed patterns (Queiroz et al., 2017). Typically, "V-shaped" dives—characterized by rapid descents and ascents with minimal bottom time—are associated with travelling or prey-searching, whereas "U-shaped" dives—with extended bottom phases—indicate active foraging (Queiroz et al., 2017; Schreer et al., 1996; Wilson et al., 2009). For

mobulids, Braun et al. (2014) described asymmetrical V-shaped dives, where brief descents and rapid ascents likely reflect efficient, gliding-based movement.

In this study, dive profiles ranged from short, shallow dives to prolonged, deep descents, possibly reflecting both behavioural types. The long, deep U-shaped dives observed in JAM_08 likely represent foraging events targeting prey aggregations at depth, while the shorter, V-shaped dives of JAM_09 and JAM_10 are more consistent with exploratory or prey-searching behaviour.

Lunar illumination may also influence diving depth and prey distribution. Andrzejaczek et al. (2024) reported that many pelagic species dive deeper during periods of higher moonlight, likely following prey that shift to greater depths during the full moon. Similarly, Barr and Abelson (2019) found that increased moonlight enhances plankton and mobulid aggregations, improving foraging opportunities. During this study, the moon phase was waxing crescent, reaching the first quarter during JAM_10's deployment (https://tabuademares.com/calendario-lunar). This intermediate illumination may have concentrated prey at moderate rather than extreme depths, potentially explaining the absence of very deep nocturnal dives. However, given the limited sample size and short deployment period, these patterns should be interpreted cautiously.

4.4 Vertical velocity

Vertical velocity data confirmed that *Mobula tarapacana* is among the fastest-swimming marine animals. During the deepest recorded dive, individual JAM_10 reached a maximum descent rate of 5.41 m/s, closely matching the ~6 m/s reported by Thorrold et al. (2014). For comparison deep diving organisms such as the Cuvier's and sperm whales typically descend at 1–2 m/s (Robinson et al., 2012; Watwood et al., 2006), while Atlantic and yellowfin tunas reach 4–5 m/s (Dagorn et al., 2006; Lawson et al., 2010). These values reaffirm that *M. tarapacana* exhibits some of the highest vertical swimming speeds recorded among both fish and marine mammals.

Vertical velocity increased in cooler, well-oxygenated waters, suggesting a behavioural strategy in which individuals descend into deeper, cooler layers during dives and reduce movement in warmer, shallower waters consistent with diel vertical migration. Variability

in correlation strength among individuals likely reflects differences in diving strategy as the tagged mobulas probably remained within the thermal and DO optimal limits.

Comparisons between ascent and descent rates showed that vertical velocity was generally higher during descents, though not consistently across individuals. On average, descents were slightly slower overall, likely reflecting passive gliding to conserve energy during shallow dives In contrast, that may require yet-unidentified oxygen regulation strategies, such as reduced gill ventilation (Royer et al., 2023) or elevated blood haematocrit levels (Waller et al., 2024). Furthermore, the retia mirabilia within the brain and pectoral fins likely facilitate rapid descents by transferring heat generated during swimming to the brain, supporting cranial endothermy and maintaining sensory performance in colder, deeper waters (Bernal et al., 2012).

4.5 DO sensor tool validation

To verify the performance of the MAANTA tag in the 2025 deployments, raw dissolved oxygen (DO) data were recalculated using the manufacturer's correction tool (PyroScience,; see Annex V). This allowed comparison between *in situ* measurements and the sensor's internal DO calculations. The recalculated values showed strong correlations within *in situ* readings (Spearman's $\rho \geq 0.996$), although small but significant differences were detected ($p < 0.05$). Overall, the PYRO recalculations closely followed the temporal patterns of the MAANTA tag data but tended to slightly overestimate DO concentrations, likely due to minor variations in the correction algorithm or discrepancies in input environmental parameters.

5. Conclusion

This study provides the first high-resolution, *in situ* characterization of the vertical distribution, with concurrent dissolved oxygen (DO) measurements, and diving behaviour of the critically endangered Chilean devil ray (*Mobula tarapacana*). The MAANTA biologging tag, showed that individuals primarily occupied waters with DO concentrations of 210–230 µmol/L and temperatures between 9–24 °C, demonstrating broad thermal and oxygen tolerance within the well-oxygenated seamount environment of the Azores. Two main dive types—U-shaped and V-shaped—were identified, possibly, corresponding to active foraging and exploratory or gliding behaviour, reflecting the species' behavioural plasticity.

Vertical velocity analyses revealed *M. tarapacana* to be among the fastest vertically moving marine species (up to 5.41 m/s). Shallower and slower dives may indicate gliding behaviour, whereas higher vertical velocities observed in deeper dives could be related to a thermal and oxygen regulation strategy. Despite the limited sample size, the MAANTA tag performed strongly in capturing fine-scale DO and temperature data following the 2024 calibration improvements.

Overall, this state-of-the-art case study validates the MAANTA tag as a reliable, non-invasive tool for integrated behavioural and environmental monitoring. Offering novel insights into the oxygen ecology, thermoregulation, and diving physiology of the Chilean devil ray, establishing them as biological sentinels for monitoring deoxygenation in a changing ocean.

6. References

Alexander, R. L. (1995). Evidence of a counter-current heat exchanger in the ray, Mobula tarapacana (Chondrichthyes: Elasmobranchii: Batoidea: Myliobatiformes). J. Zool. Lond. 237, 377–384. 9. https://doi.org/10.1111/j.1096-3642.1996.tb00224.x

Alexander, R. L. (1996). Evidence of brain-warming in the mobulid rays, Mobula tarapacana and Manta birostris (Chondrichthyes: Elasmobranchii: Batoidea: Myliobatiformes). Zool. J. Linnean Soc. 118, 151–164. **https://doi.org/10.1111/j.1096-3642.1996.tb00224.x**

Amorim, P., Perán, A. D., Pham, C., Kim, J. M., Cardigos, F., Tempera, F., Morato, T. (2017): Ocean climatology in the Azores region (North Atlantic) and seabed characteristics, links to GIS layers in ArcGIS format [dataset]. PANGAEA, https://doi.org/10.1594/PANGAEA.872601,

Andrzejaczek, S., DiGiacomo, A. E., Mikles, C. S., Pagniello, C. M. L. S., Reimer, T. E. J., & Block, B. A. (2024). Lunar cycle effects on pelagic predators and fisheries: Insights into tuna, billfish, sharks, and rays. Reviews in Fish 94. https://doi.org/10.1007/s11160-024-09914-7 Biology and Fisheries, 35(1), 7

Arostegui M. C. (2025). Cranial endothermy in mobulid rays: Evolutionary and ecological implications of a thermogenic brain. *The Journal of animal ecology*, *94*(1), 11–19. https://doi.org/10.1111/1365-2656.14200

Barr, Y., & Abelson, A. (2019). Feeding - cleaning trade-off: Manta ray "Decision-Making" as a conservation tool. Frontiers in https://doi.org/10.3389/fmars.2019.00088

Bernal, D., Carlson, J. K., Goldman, J. & Lowe, C. G. Energetics, Metabolism, and Endothermy in Sharks and Rays in Biology of Sharks and Their Relatives 2nd edn (eds Carrier, J. C., Musick, J. A. & Heithaus, M. R.) (CRC Press, 2012). https://doi.org/10.1201/b11867-10

Block, B. A. & Finnerty, J. R. (1994) Endothermy in fishes: a phylogenetic analysis of constraints, predispositions, and selection pressures. Environ. Biol. Fish 40, 283–302. https://doi.org/10.1007/BF00002518

Braun, C,., Skomal, G., Thorrold, S., Berumen, M., "DivingBehaviorof theReef MantaRayLinksCoralReefs with Adjacent Deep Pelagic Habitats". (2014) PLoS ONE.2014; 9(2):e88170. https://doi.org/10.1371/journal. pone.0088170 PMID:24516605

Braun, C. D., Arostegui, M. C., Thorrold, S. R., Papastamatiou, Y. P., Gaube, P., Fontes, J., Afonso, P. (2022). The Functional and Ecological Significance of Deep Diving by Large Marine Predators. Annual Review of Marine Science. 2022 Jan;14:129-159. DOI: 10.1146/annurev-marine-032521-103517. PMID: 34416123.

Braun, C. D., Della Penna, A., Arostegui, M. C., Afonso, P., Berumen, M. L., Block, B. A., Brown, C. A., Fontes, J., Furtado, M., Gallagher, A. J., Gaube, P., Golet W. J., Kneebone, J., Macena, B. C. L., Mucientes, G., Orbesen, E. S., Queiroz, N., Shea, B. D. Schratwieser, J. Sims, D. W., Skomal, G. B., Snodgrass, D., Thorrold, S. R. (2023) Linking vertical movements of large pelagic predators with distribution patterns of biomass in the open ocean, Proc. Natl. Acad. Sci. U.S.A. 120 (47) e2306357120, https://doi.org/10.1073/pnas.2306357120.

Brunnschweiler, J. M., Baensch, H., Pierce, S. J., & Sims, D. W. (2009). Deep-diving behaviour of a whale shark Rhincodon typus during long-distance movement in the western Indian Ocean. *Journal of fish biology*, *74*(3), 706–714. https://doi.org/10.1111/j.1095-8649.2008.02155.x

Bucair, N., Hinojosa-Alvarez, S., Marshall, A.D. *et al.* (2025). An integrative taxonomy investigation unravels a cryptic species of *Mobula* Rafinesque, 1810 (Mobulidae, Myliobatiformes), from the Atlantic Ocean. *Environ Biol Fish* (2025). https://doi.org/10.1007/s10641-025-01727-2

Butler, P. J., & Metcalfe, J. D. (1988). Cardiovascular and respiratory systems. In T. J. Shuttleworth (Ed.), *Physiology of elasmobranch fishes* (pp. 1–47). Springer.

Caldeira, R. M. A., & Reis, J. C. (2017). The Azores confluence zone. Frontiers in Marine Science, 4(FEB), 1–14. https://doi.org/10.3389/fmars.2017.00037

Caldeira, R. M. A., & Reis, J. C. (2017). The Azores confluence zone. Frontiers in Marine Science, 4(FEB), 1–14. https://doi.org/10.3389/fmars.2017.00037

Carey, F.G., Scharold, J.V., Kalmijn, A.J.Movements of blue sharks (*Prionace glauca*) in depth and course. *Mar. Biol.* **106**, 329–342 (1990). https://doi.org/10.1007/BF01344309

Clark, T. (2010) Abundance, homerange and movement patterns of manta rays (Maanta alfredi, M. birostris) in Hawaií. Doctoral dissertation, The University of Hawaii http://hdl.handle.net/10125/101865

Couturier, L. I. E., Marshall, A. D., Jaine, F. R. A., Kashiwagi, T., Pierce, S. J., Townsend, K. A., Weeks, S. J., Bennett, M. B., & Richardson, A. J. (2012). Biology, ecology and conservation of the Mobulidae. Journal of Fish Biology, 80(5), 1075–1119. https://doi.org/10.1111/j.1095 8649.2012.03264.x

Couturier, L. I., Rohner, C. A., Richardson, A. J., Marshall, A. D., Jaine, F. R., Bennett, M. B., Townsend, K. A., Weeks, S. J., & Nichols, P. D. (2013). Stable isotope and signature fatty acid analyses suggest reef manta rays feed on demersal zooplankton. *PloS one*, *8*(10), e77152. https://doi.org/10.1371/journal.pone.0077152

Croll, D. A., Newton, K. M., Weng, K., Galván-Magaña, F., O'Sullivan, J., & Dewar, H. (2012). Movement and habitat use by the spine-tail devil ray in the Eastern Pacific Ocean. Marine Ecology Progress Series, 465, 193–200. https://doi.org/10.3354/meps09900

Da Costa, I., Sims, D. W., Loureiro, B., et al. (2024). Measuring deoxygenation effects on marine predators: A new animal-attached archival tag recording in situ dissolved oxygen, temperature, fine-scale movements and behaviour. *Methods in Ecology and Evolution, 15*, 1360–1379. https://doi.org/10.1111/2041-210X.14360

Da Silva, P. M., & Pinho, M. R. (2007). "Small-size-scale fishing on seamounts," in *Seamounts: Ecology Fisheries and Conservation*, eds T. J. Pitcher, T. Morato, P. J. B. Hart, M. R. Clark, N. Haggan, and R. S. Santos (Oxford: Fisheries and Aquatic Resource Series; Blackwell Scientific), 335–360.

Dagorn, L., Holland, K. N., Hallier, J.-P., Taquet, M., Moreno, G., Sancho, G., … Fonteneau, A. (2006). Deep diving behavior observed in yellowfin tuna(Thunnus albacares). *Aquatic Living Resources*, *19*(1), 85–88. doi:10.1051/alr:2006008

Fonseca-Ponce, I. A., Zavala-Jiménez, A. A., Aburto-Oropeza, O., Maldonado Gasca, A., Galván-Magaña, F., González-Armas, R., et al. (2022). Physical and environmental drivers of oceanic manta ray mobula birostris sightings at an aggregation site in bahía de banderas, Mexico. Mar. Ecol. Prog. Series. 694, 133–148. doi: 10.3354/meps14106

Fontes, J., Castellano-González, G., Macena, B. C. L., & Afonso, P. (2023). Hitchhiking to the abyss. *Ecology and evolution*, *13*(5), e10126. https://doi.org/10.1002/ece3.10126

Fontes, J., Castellano-González, G., Macena, B. C. L., Afonso, P. (2023) Hitchhiking to the abyss. Ecol Evol 13: e10126. https://doi.org/10.1002/ece3.10126

Gargan, L. M., Morato, T., Pham, C. K., Finarelli, J. A., Carlsson, J. E. L., & Carlsson, J. (2017). Development of a sensitive detection method to survey pelagic biodiversity using eDNA and quantitative PCR: a case study of devil ray at seamounts. Marine Biology, 164(5), 1–9. https://doi.org/10.1007/s00227-017-3141-x

Gleiss, A., Wright, S., Liebsch, N., Wilson, R., Norman, B., (2013) Contrasting diel patterns in vertical movement and locomotor activity of whale sharks at Ningaloo Reef. Marine Biology. 2013; 160(11):2981–2992. https://doi.org/10.1007/s00227-013-2288-3

Guirhem, G., Arrizabalaga, H., Lopetegui, L., Murua, H., Ochoa, N. L., Griffiths, S., Gondra, J. R., Sabarros, P. S., Carlos Baez, J., & Juan-Jordá, M. J. (2021). A Preliminary Habitat Suitability Model for Devil Rays in the Western Indian Ocean. 17.

Hight, B. V., and Lowe, C. G. (2007). Elevated body temperatures of adult female leopard sharks, Triakis semifasciata, while aggregating in shallow nearshore embayments: evidence for behavioral thermoregulation? J. Exp. Mar. Bio.l Ecol. 3521, 114–128. doi: 10.1016/j.jembe.2007.07.021

Hosegood J, Humble E, Ogden R et al (2020) Phylogenomics and species delimitation for effective conservation of manta and devil rays. Mol Ecol 29:4783–4796. https:// doi. org/ 10. 1111/ mec. 15683

Hueter, R. E., Tyminski, J. P., & de la Parra, R. (2013). Horizontal movements, migration patterns, and population structure of whale sharks in the Gulf of Mexico and northwestern Caribbeansea. *PloSone*, *8*(8),e71883.https://doi.org/10.1371/journal.pone.0071883Schmidtko, S., Stramma, L., & Visbeck, M. (2017). Decline in global oceanic oxygen content during the past five decades. *Nature*, *542*(7641), 335–339. https://doi.org/10.1038/nature21399

Irigoien, X., Klevjer, T. A., Røstad, A., Martinez, U., Boyra, G., Acuña, J. L., Bode, A., Echevarria, F., Gonzalez-Gordillo, J. I., Hernandez-Leon, S., Agusti, S., Aksnes, D. L., Duarte, C. M., & Kaartvedt, S. (2014). Large mesopelagic fishes biomass and trophic efficiency in the open ocean. *Nature communications*, *5*, 3271. https://doi.org/10.1038/ncomms4271

Jabado, R.W., Marshall, A., Stevens, G., Laglbauer, B., Barros, N., D'Costa, N., Carter, R., De Bruyne, G., Doherty, P., Fernando, D., Metcalfe, K., Mvomo Minko, Y. & Rohner, C.A. (2025). *Mobula tarapacana*. *The IUCN Red List of Threatened Species* 2025: e.T60199A279077133.

Jaine, F. R. A., Rohner, C. A., Weeks, S. J., Couturier, L. I. E., Bennett, M. B., Townsend, K. A., & Richardson, A. J. (2014). Movements and habitat use of reef manta rays off eastern Australia: offshore excursions, deep diving and eddy affinity revealed by satellite telemetry. *Marine Ecology Progress Series*, *510*, 73-86. https://doi.org/10.3354/meps10910

Kaartvedt, S., Røstad, A., Klevjer, T. A., & Staby, A. (2009). Use of bottom-mounted echo sounders in exploring behavior of mesopelagic fishes. *MARINE ECOLOGY PROGRESS SERIES*, *395*, 109-118. https://doi.org/10.3354/meps08174

Karstensen, J., Stramma, L., & Visbeck, M. (2008). Oxygen minimum zones in the eastern tropical Atlantic and Pacific oceans. *Progress in Oceanography*, *77*(4), 331-350.

Laglbauer, B.J.L., Salim, M.G., Fahmi, Oktaviyani, S., Gozali, I. C., Tawang, F., Rizal, H. S., Rosady, V. P., Rudianto, D., Ender, I., Fontes, J. M. R., Afonso, P., Bennett, M. B., Stevens, G. M. W. (2025) High take of mobulid rays in East Java, Indonesia: landing trends and socio-economic context. *Environ Biol Fish* **108**, 1925–1949 (2025). https://doi.org/10.1007/s10641-025-01749-w

Lassauce, H., Chateau, O., Erdmann, M. V., & Wantiez, L. (2020). Diving behavior of the reef manta ray (Mobula alfredi) in New Caledonia: More frequent and deeper night-time diving to 672 meters. *PloS one*, *15*(3), e0228815. https://doi.org/10.1371/journal.pone.0228815

Lawson, G. L., Castleton, M. R. & Block, B. A. (2010) Movements and diving behavior of Atlantic bluefin tuna Thunnus thynnus in relation to water column structure in the northwestern Atlantic. Mar. Ecol. Prog. Ser. 400, 245–265. https://doi.org/10.3354/meps08394

Lezama-Ochoa, N., Hall, M. A., Pennino, M. G., Stewart, J. D., López, J., & Murua, H. (2019). Environmental characteristics associated with the presence of the spinetail devil ray (Mobula mobular) in the eastern tropical 24. https://doi.org/10.1371/journal.pone.0220854

Mendonça, S. A., Macena, B. C. L., Afonso, A. S., & Hazin, F. H. V. (2018). Seasonal aggregation and diel activity by the Chilean devil ray Mobula tarapacana off a small, equatorial outcrop of 74 the Mid-Atlantic Ridge. Journal of Fish Biology, 93(6), 1121 1129. https://doi.org/10.1111/jfb.13829

Mendonça, S. A., Macena, B. C. L., de Araújo, C. B. B., Bezerra, N. P. A., & Hazin, F. H. V. (2020). Dancing with the devil: Courtship behaviour, mating evidences and population structure of Mobula tarapacana (Myliobatiformes: Mobulidae) in a remote archipelago in the equatorial mid-Atlantic ocean. Neotropical Ichthyology, 18(3), 1-14. https://doi.org/10.1590/1982-0224 2020-0008

Morato, T., Hoyle, S. D., Allain, V., & Nicol, S. J. (2010). Seamounts are hotspots of pelagic biodiversity in the open ocean. Proceedings of the National Academy of Sciences of the United States of America, 107(21), 9707–9711. https://doi.org/10.1073/pnas.0910290107

Nilsson, G. E., & Ostlund-Nilsson, S. (2008). Does size matter for hypoxia tolerance in fish?. *Biological reviews of the Cambridge Philosophical Society*, *83*(2), 173–189. https://doi.org/10.1111/j.1469-185X.2008.00038.x

Notarbartolo-di-Sciara G, Adnet S, Bennett M et al (1849) (2019) Taxonomic status, biological notes, and conser vation of the longhorned pygmy devil ray Mobula ere goodoo (Cantor. Aquat Conserv Mar Freshw Ecosyst 30(1):104–122. https:// doi. org/ 10. 1002/ aqc. 3230

Palacios, M. D., Stewart, J. D., Croll, D. A., Cronin, M. R., Trejo-Ramírez, A., Stevens, G. M. W., Lezama-Ochoa, N., Zilliacus, K. M., González−Armas, R., Notarbartolo di Sciara, G., & Galván−Magaña, F. (2023). Manta and devil ray aggregations: conservation challenges and developments in the field. Frontiers

Palma, C., Lillebø, A. I., Borges, C., Souto, M., Pereira, E., Duarte, A. C., & de Abreu, M. P. (2012). Water column characterisation on the Azores platform and at the sea mounts south of the archipelago. *Marine pollution bulletin*, *64*(9), 1884–1894. https://doi.org/10.1016/j.marpolbul.2012.06.015

Pate, J. H., Wilmott, J. R., Jones, C., Horn, C., & Farmer, N. A. (2023). Multiple datasets confirm range extension of the Chilean devil ray Mobula tarapacana in the western North Atlantic Ocean off the eastern USA. Journal of the Marine Biological Association of the United Kingdom, 103(1), 1–8. https://doi.org/10.1017/S002531542300022X

Putra, M. I. H., Setyawan, E., Laglbauer, B. J. L., Lewis, S., Dharmadi, D., Sianipar, A., & Ender, I. (2020). Predicting mobulid ray distribution in coastal areas of Lesser Sunda Seascape: Implication for spatial and fisheries management. Ocean and Coastal Management, 198(May 2019), 105328. https://doi.org/10.1016/j.ocecoaman.2020.105328

Queiroz, N., Vila-Pouca, C., Couto, A., Southall, E., Mucientes, G., Humphries, N., Sims, D. (2017) Convergent Foraging Tactics of Marine Predators with Different Feeding Strategies across Heterogeneous Ocean Environ ments. Frontiers in Marine Science. 2017; 4. https://doi.org/10.3389/fmars.2017.00239

Rambahiniarison, J. M., Lamoste, M. J., Rohner, C. A., Murray, R., Snow, S., Labaja, J., Araujo, G., & Ponzo, A. (2018). Life history, growth, and reproductive biology of four mobulid species in the bohol sea, Philippines. Frontiers in Marine Science, 5(AUG), 1–16. https://doi.org/10.3389/fmars.2018.00269

Robinson, P. W., Costa, D. P., Crocker, D. E., Gallo-Reynoso, J. P., Champagne, C. D., Fowler, M. A., Goetsch, C., Goetz, K. T., Hassrick, J. L., Hückstädt, L. A., Kuhn, C. E., Maresh, J. L., Maxwell, S. M., McDonald, B. I., Peterson, S. H., Simmons, S. E., Teutschel, N. M., Villegas-Amtmann, S., & Yoda, K. (2012). Foraging behavior and success of a mesopelagic predator in the northeast Pacific Ocean: insights from a data-rich species, the northern elephant seal. *PloS one*, *7*(5), e36728. https://doi.org/10.1371/journal.pone.0036728

Rohner, C. A., Burgess, K. B., Rambahiniarison, J. M., Stewart, J. D., Ponzo, A., & Richardson, A. J. (2017). Mobulid rays feed on euphausiids in the Bohol Sea. Royal Society Open Science, 4(5), 161060. https://doi.org/10.1098/rsos.161060

Royer, M., Meyer, C., Royer, J., Maloney, K., Cardona, E., Blandino, C., Fernandes da Silva, G., Whittingham, K., & Holland, K. N. (2023). "Breath holding" as a thermoregulation strategy in the deep-diving scalloped hammerhead shark. *Science (New York, N.Y.)*, *380*(6645), 651–655. https://doi.org/10.1126/science.add4445

Santos, M., Moita, M. T., Bashmachnikov, I., Menezes, G. M., Carmo, V., Loureiro, C. M., Mendonça, A., Silva, A. F., & Martins, A. (2013). Phytoplankton variability and oceanographic conditions at condor seamount, Azores (NE Atlantic). Deep Sea Research Part II: Topical Studies in Oceanography, 98, 52–62. https://doi.org/10.1016/j.dsr2.2013.05.037

Schlaff, A. M., Heupel, M. R., and Simpfendorfer, C. A. (2014). Influence of environmental factors on shark and ray movement, behaviour and habitat use: a review. Rev. Fish Biol. Fish. 24, 1089–1103. doi: 10.1007/s11160-014-9364-8

Schreer, J. F. & Testa, J. W. Classification of Weddell seal diving behavior. *Mar. Mamm. Sci.* 12, 227–250 (1996). https://doi.org/10.1111/j.1748-7692.1996.tb00573.x

Schweitzer, J., & Notarbartolo-Di-Sciara, G. (1986). The rete mirabile cranica in the genus Mobula: A comparative study. *Journal of morphology*, *188*(2), 167–178. https://doi.org/10.1002/jmor.1051880204

Solleliet-Ferreira, S., Macena, B. C. L., Laglbauer, B. J. L., Sobral, A. F., Afonso, P., & Fontes, J. (2020). Chilean devilray and common remora prey jointly on baitfish.

Environmental Biology of Fishes, 103(8), 993–1000. https://doi.org/10.1007/s10641-020-00990-9

Stewart, J. D., Hoyos-Padilla, E. M., Kumli, K. R., & Rubin, R. D. (2016). Deep-water feeding and behavioral plasticity in Manta birostris revealed by archival tags and submersible observations. *Zoology (Jena, Germany)*, *119*(5), 406–413. https://doi.org/10.1016/j.zool.2016.05.010

Stewart, J. D., Jaine, F. R. A., Armstrong, A. J., Armstrong, A. O., Bennett, M. B., Burgess, K. B., Couturier, L. I. E., Croll, D. A., Cronin, M. R., Deakos, M. H., Dudgeon, C. L., Fernando, D., Froman, N., Germanov, E. S., Hall, M. A., Hinojosa-Alvarez, S., Hosegood, J. E., Kashiwagi, T., Laglbauer, B. J. L., … Stevens, G. M. W. (2018). Research priorities to support effective Manta and Devil Ray conservation. Frontiers in Marine Science, 5(SEP), 1–27. https://doi.org/10.3389/fmars.2018.00314

Stewart, J. D., Rohner, C. A., Araujo, G., Avila, J., Fernando, D., Forsberg, K., Ponzo, A., Rambahiniarison, J. M., Kurle, C. M., & Semmens, B. X. (2017). Trophic overlap in mobulid rays: Insights from stable isotope analysis. Marine Ecology Progress Series, 580, 131 151. https://doi.org/10.3354/meps12304

Stramma, L., Brandt, P., Schafstall, J., Schoot, F., Fischer, J., Körtzinger, A. (2008) Oxygen minimum zone in the North Atlantic south and east of the Cape Verde Islands Journal of Geophysical Research: Oceans, 113 . C04014. DOI 10.1029/2007JC004369.

Sutton, T. T., Porteiro, F. M., Heino, M., Byrkjedal, I., Langhelle, G., Anderson, C. I. H., Horne, J., Søiland, H., Falkenhaug, T., Godø, O. R., Bergstad, O. A. (2008) Vertical structure, biomass and topographic association of deep-pelagic fishes in relation to a mid-ocean ridge system. Deep Sea Res. II 55, 161–184. https://doi.org/10.1016/j.dsr2.2007.09.013

Tenzing, P. (2014). The eco-physiology of two species of tropical stingrays in an era of climate change (Townsville, AUS: James Cook University).

Thorrold, S. R., Afonso, P., Fontes, J., Braun, C. D., Santos, R. S., Skomal, G. B., & Berumen, M. L. (2014). Extreme diving behaviour in devil rays links surface waters and the deep ocean. Nature Communications, 5, 1–7. https://doi.org/10.1038/ncomms5274

Waller, M. J., Humphries, N. E., Womersley, F. C., Loveridge, A., Jeffries, A. L., Watanabe, Y., Payne, N., Semmens, J., Queiroz, N., Southall, E. J., & Sims, D. W. (2024). The vulnerability of sharks, skates, and rays to ocean deoxygenation: Physiological mechanisms, behavioral responses, and ecological impacts. Journal of Fish Biology, 105(2), 482–511. https://doi.org/10.1111/jfb.15830

Watwood, S. L., Miller, P. J., Johnson, M., Madsen, P. T., & Tyack, P. L. (2006). Deep-diving foraging behaviour of sperm whales (Physeter macrocephalus). *The Journal of animal ecology*, *75*(3), 814–825. https://doi.org/10.1111/j.1365-2656.2006.01101.x

White, W. T., Corrigan, S., Yang, L., Henderson, A. C., Bazinet, A. L., Swofford, D. L., & Naylor, G. J. P. (2018). Phylogeny of the manta and devilrays (Chondrichthyes: Mobulidae), with an updated taxonomic arrangement for the family. Zoological Journal of the Linnean Society, 182(1), 50–75. https://doi.org/10.1093/zoolinnean/zlx018

White, W. T., Giles J, Potter IC (2006). Data on the bycatch fishery and reproductive biology of mobulid rays (Myliobatiformes) in Indonesia. Fish. Res. 82: 65–73 https://doi.org/10.1016/j.fishres.2006.08.008

Wilson, S., Block, B., (2009) "Habitat use in Atlantic bluefin tuna Thunnus thynnus inferred from diving behavior". Endangered SpeciesResearch.2009; 10:355–367 doi: 10.3354/esr00240

Wootton, T. P., Sepulveda, C. A., & Wegner, N. C. (2015). Gill morphometrics of the thresher sharks (Genus Alopias): Correlation of gill dimensions with aerobic demand and environmental oxygen. *Journal of morphology*, *276*(5), 589–600. https://doi.org/10.1002/jmor.20369

Annexes

Annex I: State of the art

1.1 Ocean deoxygenation

Oxygen is vital for the survival and fitness of aerobic organisms, playing a critical role from the molecular level to the ecosystem scale and biogeochemical cycles (Breitburg et al. 2018; Petsch, 2003; Schlaff et al. 2014). O_2 serves as a primary electron acceptor in cellular respiration, enabling energy production through the electron transport chain (Semenza 2007). Additionally has a main role in modulating metabolic pathways and cellular activities (Nelson, 2016).

The levels of dissolved oxygen (DO) in both open ocean and coastal water are decreasing, a phenomenon known as ocean deoxygenation. Since 1960, global ocean levels have decreased an estimated 2% (Oschlies et al., 2018; Schmidtko et al., 2017) and projections indicate that can further suffer a decrease of 1%-7% by 2100 (Breitburg et al., 2018; Schmidtko et al., 2017). Historical and paleontological records indicate that previous mass extinctions were influenced by widespread deoxygenation, revealing its potential to drive large-scale biodiversity loss (Penn et al., 2018)

The ongoing deoxygenation is closely linked to global warming, driven by increased greenhouse gas emissions, affecting a range of physiological and biological processes (Boop et al 2013). The human-induced temperature increase generates an excess heat, that is taken up by the ocean, reducing oxygen solubility in the water column (Ito et al 2017). This warming creates more stable surface layers, intensifying thermo-haline stratification, as warmer, less dense water remains at the surface, limiting mixing with colder and denser layers bellow (Venegas et al., 2023). Consequently, there is a reduction in the vertical mixing, limiting the transport of oxygen-rich surface layers to deep oxygen-depleted layers (Breitburg et al. 2018). In addition, the slowing down of the ocean´s circulation system leads to a restricted nutrient exchange with deeper layers, diminishing primary productivity and increased microbial respiration, further reducing dissolved oxygen (Lozier et al., 2017; Breitburg et al., 2018; Levin, 2018). The warmer and deoxygenated environment accelerates the metabolic rate increasing oxygen consumption, hence, accelerating oxygen depletion (Breitburg et al., 2018; Gilly et al., 2013).

In coastal and estuarine ecosystems oxygen deficiency is intensified by the anthropogenic nutrients input, particularly from agricultural runoff. This influx of nutrients promotes eutrophication leading to decreased oxygen concentrations and the emergence of hypoxic zones (Fennel and Testa, 2019; Kessouri et al., 2021). In shallow shelf regions (<50m), seasonal temperature increases combined with coastal upwelling can further intensify oxygen depletion, leading to hypoxic conditions (Chan et al., 2008; Grantham et al., 2004).

The reduction of DO has cascading effects across biological scales. At the microbial level, it alters microbial activity impacting nutrient cycling (Levin & Le Bris, 2015). On an individual scale the reduction of the suitable oxygen threshold can affect the behaviour and physiology, affecting the individual fitness (Waller et al., 2024). At the population level it can lead to periodic distribution shifts influencing local abundance and recruitment (Gilly et al., 2013). These alterations interfere with trophic dynamics compromising nutrient cycling and gene flow, threatening the resilience of entire ecosystems (Gilly et al., 2013). When it comes to ecosystem services, the displacement of species distributions and abundance increases exposure to fishing pressure (Deutsch et al., 2015; Prince & Goodyear, 2006).

Particularly severe deoxygenation occurs near the eastern boundary upwelling areas, where oxygen is depleted through the respiration and decomposition of organic matter exported from highly productive waters. The processes give rise to persistent low-oxygen areas know as oxygen minimum zones (OMZ) (Davila et al., 2023; Levin, 2018; Schmidtko et al., 2017; Sonnerup et al.,2019). The persistent hypoxic water form in the depth range of 200-800 meters (Gilly et al., 2013) representing 5% of the ocean´s volume (Zhou et al., 2022). The oxygen levels in hypoxic conditions can reach < 20 μmol kg^{-1} (Levin, 2018) while in normoxic conditions is equivalent to 200–320 μmol kg^{-1} depending on temperature and salinity (Schmidtko et al., 2017). As ocean warming intensifies, OMZs are expected to expand, further amplifying the effects of deoxygenation (Gilly et al., 2013).

1.2 Elasmobranchs

Elasmobranchs are a subclass of cartilaginous fish that includes sharks, skates and rays, comprising over 1000 extant species (Guinot & Cavin, 2016). Most species occur in the marine realm but distribute from estuarine, coastal and shelf ecosystems to open ocean. Many elasmobranchs are highly migratory, capable of undertaking extensive migrations between coastal and oceanic waters (Ferretti et al., 2010).

Elasmobranchs are broadly known for their key ecological role as apex and meso-predators. They exert significant influence on marine food webs by regulating trophic dynamics, facilitating nutrient cycling and playing a crucial role in maintaining ecosystems balance (Hammerschlag et al., 2011). The removal of these top-predator can trigger mesopredator release compromising ecosystem structure and resilience and a breakdown of trophic cascades and predator-prey relationships (Ferretti et al., 2010; Nowicki et al., 2021; Spiers et al., 2016). Such disruption may result in the decline of prey populations or even species replacement (Frid et al., 2008).

Overexploitation, both from targeted fisheries and bycatch is driving significant declines in elasmobranch population. An estimated 80 million sharks are harvested annually for the meat and fin trade (Worm et al., 2024), contributing to the fisheries industry valued over $1 billion (Dent & Clarke, 2015). Since 1970 is estimated that shark and ray populations have decreased by 71% (Pacoureau et al., 2021) and 32% are classified in risk of extinction (Dulvy et al., 2021). Despite the scale of exploitation in elasmobranchs, remains weakly regulated and poorly managed (Das & Afonso, 2017). This contributes

to the underestimation of total weight of harvest due to unrecorded catches, discards at sea and misidentification (Ferreti et al., 2010).

Their biological traits of slow growth and maturation rates in combination with low fecundity further enhances elasmobranchs vulnerability to overexploitation limiting population resilience and stock recovery (Adams et al., 2018; Cortes et al., 2010).

1.3 Elasmobranchs oxygen requirements

Understanding the oxygen requirements of elasmobranchs and how these vary across species and physiological traits is essential for assessing their vulnerability to deoxygenation and its impacts on individual fitness. The oxygen demand required for the aerobic metabolism varies within elasmobranchs species due to their high variability of biological and physiological adaptations (Watanabe & Payne, 2023).

One of the key factors influencing oxygen requirements is the species´ ventilation strategies (Lawson et al., 2019). Obligate ram-ventilating species, such as the blue shark (Prionace glauca, Linnaeus, 1758) and the shortfin mako shark (Isurus oxyrinchus Rafinesque, 1810) rely on a constant flow across the gills. The shortfin mako, a regionally endothermic species, exhibits higher oxygen and metabolic demands when compared to ectothermic species like the blue shark, in order to sustain bot physical activity and thermoregulation (Bernal et al., 2012; Carlson et al., 2004; Lawson et al., 2019).

In contrast, buccal-ventilating ectotherms, such as the nurse shark (*Ginglymostoma cirratum*, Bonnaterre, 1788), can actively pump water over their gills while stationary, allowing them to tolerate lower oxygen levels and exhibit lower metabolic and oxygen demands (Bernal et al., 2012; Graham et al., 1990; Sepulveda et al., 2007; Whitney et al., 2016).

1.3.1 How oxygen requirements are measured?

Traditionally oxygen requirements have been measured through laboratory experiments using respirometry and continuous-swim tunnel systems, accessing aerobic performance under controlled conditions (Lawson et al., 2019; Carlson & Parsons, 2001). However, these methods are often offseted towards smaller captive species of elasmobranchs. Advances in biologging now allow to estimate oxygen demands in free-swimming elasmobranchs by measuring physiological parameters such as heart rate, swimming speed and acceleration which are use to build bioenergetic models serving as proxies to

metabolic demands (Lawson et al., 2019; Waller et al., 2023; Watanabe et al., 2019). Hypoxic thresholds can also be inferred by comparing the vertical and horizontal movements with modelled DO concentrations, revealing the hypoxia threshold and species-specific tolerance levels (Abascal et al., 2011; Coffey et al., 2015; Da costa et al., 2024; Vedor et al., 2021)

1.3.2 Physiological responses to hypoxia

Elasmobranch responses to hypoxia vary by species, mobility and physiology. While highly mobile pelagic sharks may avoid low-oxygen zones (Waller et al., 2024), slower-moving benthic skates may rely on compensatory mechanisms (Wearmouth et al., 2014; Jensen et al., 1993). Regarding the ventilatory mechanisms, some species are oxyregulators, increasing oxygen uptake under hypoxia, while others are oxyconformers, reducing uptake as oxygen declines (Fritsche & Nilsson, 1993).

Physiological responses include increased ventilation and bradycardia, as seen in small-spotted catshark (*Scyliorhinus canicular*, Linnaeus 1758), enhancing cardiac efficiency during hypoxia (Butler & Metcalfe, 1988). Haematocrit levels as also been linked to maintaining aerobic metabolism under hypoxia (Waller et al., 2024), with endothermic species like the mako shark exhibiting higher values when compared to ectotherms species (Emery, 1986).

To optimise oxygen uptake, elasmobranchs have evolved a variety of gill architecture morphologies (Waller et al., 2024). Highly active species that frequent hypoxic zones such as the bigeye thresher shark (*Alopias superciliosus*, Lowe, 1841) present the largest gill surface among elasmobranchs (Wootton et al., 2015). The shortfin mako shark, another active species, exhibit thickened gill lamellae enhancing diagonal blood flow (Wegner et al., 2010).

When oxygen availability becomes critically low, some elasmobranchs rely on anaerobic metabolism as an alternative energy pathway (Richards, 2009). Large-bodied elasmobranchs like the shortfin mako shark, possess greater glycogen reserves and white muscle, highlighting a higher capacity for anaerobic energy production, (Bernal et al., 2001; Coffey et al., 2020; Nilsson & Östlund-Nilsson, 2008). In order to oxidize the anaerobic by-product, it has been suggested that ram-ventilating species may also increase swimming speed (Wegner et al., 2010).

1.3.3 Behavioural responses to hypoxia

Elasmobranchs are known to be highly migratory so it is expected that they would avoid areas where oxygen concentration is below the optimal threshold (Parsons & Hoffmayer, 2005). The blue shark, a cosmopolitan ocean distributed species is known to reduce dive depth in response to shoaling hypoxic layers in OMZs (Vedor et al., 2021).

Species with higher metabolic oxygen demands, such as regionally endothermic lamnids are particularly sensitive to low oxygen environments due to elevated energetic needs and specialised physiology (e.g. large gill surface, large heart mass and higher myoglobin concentration) (Bernal et al., 2010). Whereas, smaller, less active species often display oxyconforming responses (Musa et al., 2020). Behavioural strategies under hypoxia may also include increased mouth gape to enhance oxygen uptake (Carlson & Parsons, 2001).

1.3.4 Ecological impacts of deoxygenation on elasmobranchs

Elasmobranchs exhibit both physiological and behavioural strategies to tackle low oxygen conditions, either by avoid or tolerate them (Waller et al., 2024). Nevertheless, deoxygenation can still lead to significant ecological consequences. One of the most prominent effects is habitat compression, within expanding OMZs, forcing species into oxygen-rich surface layers. This not only reduces foraging space but also increases interspecific competition, and increased exposure to fisheries (Prince et al., 2010; Vedor et al., 2021).

Prolonged hypoxic conditions also elevate mortality risk, especially in benthic species with low mobility, which are less prone to escape deteriorating environments (Wrarmouth et al., 2014). Moreover, trophic dynamics are affected as prey species redistribute along oxygen gradients. While prey aggregate in surface waters, may temporarily enhance foraging opportunities for predators, leading to imbalanced predator-prey interactions (Gilly et al., 2013).

Inter and intraspecific interactions may shift, favouring more hypoxia-tolerant species, providing a competitive advantage, reducing predation risk and reshaping community structure (Crear et al., 2020). As deoxygenation intensifies such ecological shifts have long-term consequences in the ecosystems balance and trophic dynamics (Waller et al., 2024).

1.4 Modelled and *in situ* DO data

Electronic tags have become more sophisticated enhancing the knowledge gap of species ecology, behaviour, and, increasingly, their interaction with dynamic environmental variables such as dissolved oxygen (DO) (Coffey et al., 2020; Hussey et al., 2015). Prior, most studies on the effects of deoxygenation relied in DO modelled concentration instead of *in situ* measurements (e.g. Copernicus Marine Environment Monitoring Service, CMEMS; World Ocean Atlas, WOA) (Coffey et al., 2020; Prince et al., 2010; Prince & Goodyear, 2006; Vedor et al., 2021). These models are based on prediction of DO concentration within a grid cell across defined spatial and temporal scales (Waller et al., 2024), often using satelMAANTA- derived data as input (European Commission, 2015). However, the coarse resolution of these models can limit the ability to detect fine-scale behavioural responses, particularly in mobile marine species (Hussey et al., 2015).

Modelled DO at greater depths may diverge significantly from the actual concentration experienced by the animal, leading to potentially offseted interpretations of the behavioural impacts of deoxygenation in elasmobranchs (Coffey & Holland, 2015; Da costa et al., 2024). In contrast, *in situ* DO measurements provide more accurate concentrations, allowing for real-time assessment of the environmental conditions encountered by free-ranging elasmobranchs (Coffey & Holland, 2015; Coffey et al., 2020; Da costa et al., 2024).

The development of biologging devices equipped with dissolved oxygen sensors has enabled elasmobranchs to serve as "animal oceanographers", enabling them to collect high-resolution environmental data that can refine existing models and improve overall understanding of ocean variables (Harcourt et al., 2019). These biologging platforms offer valuable opportunities to enhance data coverage in undersampled regions, such as the Southern Ocean, where sampling is constrained by sea ice coverage (Roquet et al., 2013), thereby improving regional oceanographic models (Hussey et al., 2015). Additionally, the integration of triaxial accelerometers with these tags provides critical insights into how elasmobranchs respond behaviourally to deoxygenation (Vedor et al., 2021; Waller et al., 2023). To further support the collection of essential ocean variables (EOVs), the Animal-Borne Ocean Sensors (AniBOS) network has been established as a standardized framework for leveraging biologging data in ocean observation (McMahon et al., 2021).

1.5 Biotelemetry and biologging

Studying elusive and worldwide distributed marine animals can be a challenge. Nonetheless the advancements of modern technology have allowed the development of animal-borne electronic devices to collect behavioural, biological, physiological, and environmental data (Watanabe et al., 2023).

The study of movement patterns and distribution of aquatic animals began with mark-recapture methods, which offered a limited resolution, revealing only the tagging and recapture locations (Cren, 1965). With the advent of the technology era this approach evolved to telemetry (Siber, 2001). A breakthrough that led to the development of electronic devices known as “transmitters” or “tags” on free-ranging animals that autonomously transmitted data to datalogging or relay receiving stations (Hussey et al., 2015).

Biotelemetry was developed to enable *in situ* remote tracking through the creation of animal-attached transmitters. Initially, systems relied on radio signals, detected through signal triangulation from multiple receivers (Thums et al.,2018). However, since radio waves do not propagate through saltwater, biotelemetry evolved into two primary methods: acoustic (Donaldson et al., 2014) and satelMAANTA telemetry (Hazen et al., 2012). Acoustic telemetry involves receivers placed either at fixed locations or attached to mobile platforms (Grothues, 2009) which are retrieved periodically. SatelMAANTA telemetry, on the other hand, transmits data from tagged animals to land based receivers via orbiting satelMAANTAs (Hussey et al. 2015).

The advent of biologging, revolutionized the study of behaviour, movement and ecology of marine organisms with the use of animal borne tags (Hussey et al. 2015; Hays et al. 2016; Rutz & Hays, 2009). The major difference between biotelemetry and biologging lies in the data collection method. In biotelemetry information is transmitted from the tag (transmitter) to a receiver, while in biologging the information recorded is stored in an animal-borne device and downloaded when the device is retrieved (Cooke, 2008; Watanabe & Papastamatiou, 2023). Nevertheless, both concepts overlap as modern technologies are capable of simultaneously track animal movements and record environmental, movement and behavioural data (Watanabe & Papastamatiou, 2023).

Initially, biologging required the physical recapture of the animal to retrieve the data. However, recovery methods have since evolved with the development of mechanical releasing devices, such as galvanic time release (GTR) systems, which enable dataloggers

to detach automatically (Watanabe et al., 2004). Once released, the devices can be recovered using satelMAANTA or radio telemetry, significantly reducing the need for animal recapture and increasing data recovery rates (Watanabe et al., 2004).

The major stepping stone of the biologging data transmission and storage came with the launch of the ARGOS satelMAANTA (Advanced Research and Global observation satelMAANTA) in the late 1970s, enabling the first animal tracking via satelMAANTA transmitters in polar bears and basking sharks (Schweinburg & Lee, 1982; Priede, 1984). Since then, advancements in technology have led to miniaturization of the tags and the expansion of the range of species and life stages that can be monitored (Hussey et al. 2015). Improvements in battery life and the integration of Global Positioning System (GPS) has enabled longer and more accurate deployments, while software developments allow for finer-scale movement data (Dujon et al., 2014).

Biologging has enabled the study of animal movements in three dimensions (Hussey et al. 2015). Tracking horizontal movements is essential for defining habitat use, species distribution and population dynamics (Cheke & Tratalos, 2007, Dean et al., 2014). Vertical movement is key to understand diving behaviour and, when combined with essential ocean variables (EOVs)- such as temperature, pressure, salinity, and oxygen (Miloslavich et al., 2018; Muller-Karger et al., 2018), provides a comprehensive third dimension to understanding an organism's depth-specific behaviours and environmental interactions (e.g., Elliot et al., 2022). Sensors integrated into the transmitters collect this data, offering a detailed vertical profile of both the animal’s movements and the surrounding ocean conditions (Williams et al., 2020).

Despite these advances, a significant portion of the collected data remains inaccessible, highlighting the need for a standardized framework to facilitate data sharing and streamline data flow among stakeholders (Sequeira et al., 2021).

1.6 Animal-borne sensors

Animal-borne sensors, also known as bio-loggers started in the 1960s with time-depth recording dataloggers in Weddell seals (Kooyman, 1965) and later Adélie penguins in 1990 (Naito et al., 1990). By the 1990s with technology advancements the analog dataloggers were replaced by digital ones, enabling both the miniaturization and expanding the range of the parameters recorded (Watanabe & Papastamatiou, 2023). Not only recorded animal movements but also measured additional data such as body

acceleration (Yoda et al., 1999), video images (Davis et al., 1999) and echolocation (Nowacek et al., 1998), offering valuable insights regarding their physiology and behaviour.

A major breakthrough came with the development of the pop-up satelMAANTA archival tags in the late 1990s. These tags were capable of recording depth, temperature and light levels for geolocation. Pre-programmed to detach after a set period and float to the surface further transmitting summarized data via the ARGOS satelMAANTA (Block et al., 1998). This innovation made it possible to track pelagic fishes, previously limited to air-breathing marine species (Block et al., 1998; Watanabe & Papastamatiou, 2023).

Attachment methods of the tags vary, ranging from intramuscular anchors to drilling through the dorsal fins to secure the tag (Ferreira et al., 2018). The invasive techniques require capturing and restraining the animal, which can interfere with the animal´s fitness both during and after the deployment (Hammerschlag et al., 2011; Kohler & Turner 2001). Post-release stress may also alter the natural behaviour, requiring a recovery period. This is particularly significant in short-term behavioural studies, compromising the accuracy of the collected data (Whitney et al., 2016).

To mitigate these impacts, non-invasive tags have been developed. The first non-invasive towed tag in whale sharks (Rhincodon typus) represented a significant step forward (Gleiss et al., 2009). Subsequent innovations include clamping attachment methods (Fontes et al., 2018) and harness systems (Fontes et al., 2022), both of which show minimal behavioural impact. These approaches enable high-resolution monitoring of fine-scale behaviour and swimming performance in free ranging animals with minimal disturbance (Fontes et al., 2022).

1. References

Adams, K. R., Fetterplace, L. C., Davis, A. R., Taylor, M. D., & Knott, N. A. (2018). Sharks, rays and abortion: The prevalence of capture-induced parturition in elasmobranchs. Biological Conservation, 217, 11–27. https://doi.org/10.1016/j.biocon.2017.10.010

Bernal, D., Dickson, K. A., Shadwick, R. E., & Graham, J. B. (2001). Review: Analysis of the evolutionary convergence for high performance swimming in lamnid sharks and tunas. *Comparative biochemistry and physiology. Part A, Molecular & integrative physiology*, *129*(2-3), 695–726. https://doi.org/10.1016/s1095-6433(01)00333-6.

Block, B. A., Dewar, H., Farwell, C., & Prince, E. D. (1998). A new satelMAANTA technology for tracking the movements of Atlantic bluefin tuna. *Proceedings of the National Academy of Sciences of the United States of America*, *95*(16), 9384–9389. https://doi.org/10.1073/pnas.95.16.9384

Bopp, L., Resplandy, L., Orr, J. C., Doney, S. C., Dunne, J. P., Gehlen, M., Halloran, P., Heinze, C., Ilyina, T., Séférian, R., Tjiputra, J., & Vichi, M. (2013). Multiple stressors of ocean ecosystems in the 21st century: Projections with CMIP5 models. *Biogeosciences, 10*(12), 6225–6245. https://doi.org/10.5194/bg-10-6225-2013.

Breitburg, D., Levin, L. A., Oschlies, A., Grégoire, M., Chavez, F. P., Conley, D. J., Garçon, V., Gilbert, D., Gutiérrez, D., Isensee, K., Jacinto, G. S., Limburg, K. E., Montes, I., Naqvi, S. W. A., Pitcher, G. C., Rabalais, N. N., Roman, M. R., Rose, K. A., Seibel, B. A., Telszewski, M., … Zhang, J. (2018). Declining oxygen in the global ocean and coastal waters. *Science (New York, N.Y.)*, *359*(6371), eaam7240. https://doi.org/10.1126/science.aam7240

Butler, P. J., & Metcalfe, J. D. (1988). Cardiovascular and respiratory systems. In T. J. Shuttleworth (Ed.), *Physiology of elasmobranch fishes* (pp. 1–47). Springer.

Carlson, J.K., Parsons, G.R. The Effects of Hypoxia on Three Sympatric Shark Species: Physiological and Behavioral Responses. *Environmental Biology of Fishes* **61**, 427–433 (2001). https://doi.org/10.1023/A:1011641302048

Chan, F., Barth, J. A., Lubchenco, J., Kirincich, A., Weeks, H., Peterson, W. T., & Menge, B. A. (2008). Emergence of anoxia in the California current large marine ecosystem. *Science (New York, N.Y.)*, *319*(5865), 920. https://doi.org/10.1126/science.1149016

Cheke, R. A., Tratalos J. A. (2007) Migration, patchiness, and population processes illustrated by two migrant pests. *Bioscience* 57, 145–154. doi: 10.1641/B570209

Coffey, D. M., Royer, M. A., Meyer, C. G., & Holland, K. N. (2020). Diel patterns in swimming behavior of a vertically migrating deepwater shark, the bluntnose sixgill (Hexanchus griseus). *PloS one*, *15*(1), e0228253. https://doi.org/10.1371/journal.pone.0228253

Coffey, D.M., Holland, K.N. First autonomous recording of in situ dissolved oxygen from free-ranging fish. *Anim Biotelemetry* **3**, 47 (2015). https://doi.org/10.1186/s40317-015-0088-x

Cooke, S. J. (2008). Biotelemetry and biologging in endangered species research and animal conservation: Relevance to regional, national, and IUCN Red List threat

assessments. Endangered Species Research, 4(1–2), 165–185. https://doi.org/10.3354/esr00063

Cortes, E., Arocha, F., Beerkircher, L., Carvalho, F., Domingo, A., Heupel, M., Holtzhausen, H., Santos, M. N., Ribera, M., & Simpfendorfer, C. (2010). Ecological risk assessment of pelagic sharks caught in Atlantic pelagic longline fisheries. Aquatic Living Resources, 23,25–34. https://doi.org/10.1051/alr/2009044

Crear, D. P., Latour, R. J., Friedrichs, M. A. M., St-Laurent, P., & Weng, K. C. (2020). Sensitivity of a shark nursery habitat to a changing climate. *Marine Ecology Progress Series, 652*, 123–136. https://doi.org/10.3354/meps13483

Da costa, I., Sims, D. W., Loureiro, B., et al. (2024). Measuring deoxygenation effects on marine predators: A new animal-attached archival tag recording in situ dissolved oxygen, temperature, fine-scale movements and behaviour. *Methods in Ecology and Evolution, 15*, 1360–1379. https://doi.org/10.1111/2041-210X.14360

Das, D., & Afonso, P. (2017). Review of the diversity, ecology, and conservation of elasmobranchs in the Azores Mid-North Atlantic. https://doi.org/10.3389/fmars.2017.00354

Davila, X., Olsen, A., Lauvset, S. K., McDonagh, E. L., Brakstad, A., & Gebbie, G. (2023). On the origins of open ocean oxygen minimum zones. *Journal of Geophysical Research-Oceans*. **https://doi.org/10.1029/2023JC019677**

Davis, R. W., Fuiman, L. A., Williams, T. M., Collier, S. O., Hagey, W. P., Kanatous, S. B., Kohin, S., & Horning, M. (1999). Hunting behavior of a marine mammal beneath the antarctic fast Ice. *Science (New York, N.Y.)*, *283*(5404), 993–996. https://doi.org/10.1126/science.283.5404.993

Dean, M. J., Hoffman, W. S., Zemeckis, D. R., Armstrong M. P. (2014) Fine-scale diel and gender-based patterns in behaviour of Atlantic cod (*Gadus morhua*) on a spawning ground in the Western Gulf of Maine. ICES J. Mar. Sci. 71, 1474–1489. doi: 10.1093/icesjms/fsu040

Dent, F., & Clarke, S. (2015). *State of the global market for shark products*. FAO Fisheries and Aquaculture Technical Paper No. 590. Food and Agriculture Organization of the United Nations

Deutsch, C., Ferrel, A., Seibel, B., Pörtner, H. O., & Huey, R. B. (2015). Ecophysiology. Climate change tightens a metabolic constraint on marine habitats. *Science (New York, N.Y.)*, *348*(6239), 1132–1135. https://doi.org/10.1126/science.aaa1605

Donaldson, M. R., Hinch, S. G., Suski, C. D., Fisk, A. T., Heupel, M. R., & Cooke, S. J. (2014). Making connections in aquatic ecosystems with acoustic telemetry monitoring. *Frontiers in Ecology and the Environment, 12*(10), 565–573. https://doi.org/10.1890/130283

Dujon, A. M., Lindstrom, R. T., & Hays, G. C. (2014). The accuracy of Fastloc GPS locations and implications for animal tracking. *Methods in Ecology and Evolution, 5*(11), 1162–1169. https://doi.org/10.1111/2041-210X.12286

Dulvy, N. K., Pacoureau, N., Rigby, C. L., Pollom, R. A., Jabado, R. W., Ebert, D. A., Finucci, B., Pollock, C. M., Cheok, J., Derrick, D. H., Herman, K. B., Sherman, C. S., VanderWright, W. J., Lawson, J. M., Walls, R. H. L., Carlson, J. K., Charvet, P., Bineesh, K. K., Fernando, D., Ralph, G. M., … Simpfendorfer, C. A. (2021). Overfishing drives over one-third of all sharks and rays toward a global extinction crisis. *Current biology : CB*, *31*(21), 4773–4787.e8. https://doi.org/10.1016/j.cub.2021.08.062

Elliott, R. G., Montgomery, J. C., Della Penna, A., Radford, C. A. (2022) SatelMAANTA tags describe movement and diving behaviour of blue sharks *Prionace glauca* in the southwest Pacific. Mar Ecol Prog Ser 689:77-94. https://doi.org/10.3354/meps14037

Emery, S. H. (1986). Hematological comparisons of endothermic vs. ectothermic elasmobranch fishes. *Copeia, 1986*(3), 700–705.

European Commission. (2015). *Copernicus: Europe's eyes on Earth*. Publications Office of the European Union. https://doi.org/10.2873/85954

Fennel, K., & Testa, J. M. (2019). Biogeochemical Controls on Coastal Hypoxia. *Annual review of marine science*, *11*, 105–130. https://doi.org/10.1146/annurev-marine-010318-095138

Ferreira, L. C., Mansfield, K. L., Thums, M., & Meekan, M. G. (2018). SatelMAANTA tracking technologies and their application to shark movement ecology. In *Shark research: Emerging technologies and applications for the field and laboratory* (pp. 357–377)

Ferretti, F., Worm, B., Britten, G. L., Heithaus, M. R., & Lotze, H. K. (2010). Patterns and ecosystem consequences of shark declines in the ocean. Ecology Letters, 13(8), 1055–1071. https://doi.org/10.1111/j.1461-0248.2010.01489.x

Fontes, J., Baeyaert, J., Prieto, R., Graça, G., Buyle, F., Afonso, P. (2018). New non-invasive methods for short-term electronic tagging of pelagic sharks and rays. *Mar Biol* **165**, 34 (2018). https://doi.org/10.1007/s00227-018-3289-z

Fontes, J., Macena, B., Solleliet-Ferreira, S. Buyle, F., Magalhães, R., Bartolomeu, T., Liebsch, N., Meyer, C., Afonso, P. (2022). The advantages and challenges of non-invasive

towed PILOT tags for free-ranging deep-diving megafauna. *Anim Biotelemetry* **10**, 39 (2022). https://doi.org/10.1186/s40317-022-00310-1

Frid, A., Baker, G. G., & Dill, L. M. (2008). Do shark declines create fear-released systems? Oikos, 117(2), 191–201. https://doi.org/10.1111/j.2007.0030-1299.16134.x

Fritsche, R., & Nilsson, S. (1993). Cardiovascular and ventilatory control during hypoxia. In J. C. Rankin & F. B. Jensen (Eds.), *Fish ecophysiology* (pp. 180–206). Springer.

Gilly, W. F., Beman, J. M., Litvin, S. Y., & Robison, B. H. (2013). Oceanographic and biological effects of shoaling of the oxygen minimum zone. *Annual review of marine science*, *5*, 393–420. https://doi.org/10.1146/annurev-marine-120710-100849

Gleiss, A. C., Norman, B., Liebsch, N., Francis, C., & Wilson, R. P. (2009). A new prospect for tagging large free-swimming sharks with motion-sensitive data-loggers. *Fisheries Research, 97*(1–2), 11–16. https://doi.org/10.1016/j.fishres.2008.12.012

Grantham, B. A., Chan, F., Nielsen, K. J., Fox, D. S., Barth, J. A., Huyer, A., Lubchenco, J., & Menge, B. A. (2004). Upwelling-driven nearshore hypoxia signals ecosystem and oceanographic changes in the northeast Pacific. *Nature*, *429*(6993), 749–754. https://doi.org/10.1038/nature02605

Grothues, T.M. (2009). A Review of Acoustic Telemetry Technology and a Perspective on its Diversification Relative to Coastal Tracking Arrays. In: Nielsen, J.L., Arrizabalaga, H., Fragoso, N., Hobday, A., Lutcavage, M., Sibert, J. (eds) Tagging and Tracking of Marine Animals with Electronic Devices. Reviews: Methods and Technologies in Fish Biology and Fisheries, vol 9. Springer, Dordrecht. https://doi.org/10.1007/978-1-4020-9640-2_5

Guinot, G., & Cavin, L. (2016). 'Fish' (Actinopterygii and Elasmobranchii) diversification patterns through deep time. Biological Reviews, 91(4), 950–981. https://doi.org/10.1111/brv.12203

Hammerschlag, N., Gallagher, A. J., & Lazarre, D. M. (2011). A review of shark satelMAANTA tagging studies. *Journal of Experimental Marine Biology and Ecology, 398*(1–2), 1–8. https://doi.org/10.1016/j.jembe.2010.12.012
Harcourt, R., Sequeira, A. M. M., Zhang, X., Roquet, F., Komatsu, K., Heupel, M., McMahon, C., Whoriskey, F., Meekan, M., Carroll, G., Brodie, S., Simpfendorfer, C., Hindell, M., Jonsen, I., Costa, D. P., Block, B., Muelbert, M., Woodward, B., Weise, M., ... Fedak, M. A. (2019). Animal-borne telemetry: An integral component of the ocean observing toolkit. *Frontiers in Marine Science*, *6*, Article 326. https://doi.org/10.3389/fmars.2019.00326

Hays, G. C., Ferreira, L. C., Sequeira, A. M. M., Meekan, M. G., Duarte, C. M., Bailey, H., Bailleul, F., Bowen, W. D., Caley, M. J., Costa, D. P., Eguíluz, V. M., Fossette, S., Friedlaender, A. S., Gales, N., Gleiss, A. C., Gunn, J., Harcourt, R., Hazen, E. L.,

Heithaus, M. R., Heupel, M., … Thums, M. (2016). Key Questions in Marine Megafauna Movement Ecology. *Trends in ecology & evolution*, *31*(6), 463–475. https://doi.org/10.1016/j.tree.2016.02.015

Hazen, E. L., Maxwell, S. M., Bailey, H., Bograd, S. J., Hamann, M., Gaspar, P., Godley, B. J., Shillinger, G. L. (2012) Ontogeny in marine tagging and tracking science: technologies and data gaps. Mar Ecol Prog Ser 457:221-240 https://doi.org/10.3354/meps09857

Hussey, N. E., Kessel, S. T., Aarestrup, K., Cooke, S. J., Cowley, P. D., Fisk, A. T., Harcourt, R. G., Holland, K. N., Iverson, S. J., & Kocik, J. F. (2015). Aquatic animal telemetry: A panoramic window into the underwater world. *Science, 348*, 1255642. https://doi.org/10.1126/science.1255642

Ito, T., Minobe, S., Long, M. C., Deutsch, C. (2017). Upper ocean O_2 trends: 1958–2015. *Geophysical Research Letters*. https://doi.org/10.1002/2017GL073613

Jensen, F. B., Nikinmaa, M., & Weber, R. E. (1993). Environmental perturbations of oxygen transport in teleost fishes: Causes, consequences, and compensations. In J. C. Rankin & F. B. Jensen (Eds.), *Fish ecophysiology* (pp. 161–179). Springer.

Kessouri, F., McWilliams, J. C., Bianchi, D., Sutula, M., Renault, L., Deutsch, C., Feely, R. A., McLaughlin, K., Ho, M., Howard, E. M., Bednaršek, N., Damien, P., Molemaker, J., & Weisberg, S. B. (2021). Coastal eutrophication drives acidification, oxygen loss, and ecosystem change in a major oceanic upwelling system. *Proceedings of the National Academy of Sciences of the United States of America*, *118*(21), e2018856118. https://doi.org/10.1073/pnas.2018856118

Kohler, N. E., & Turner, P. A. (2001). Shark tagging: A review of conventional methods and studies. In *The behavior and sensory biology of elasmobranch fishes: An anthology in memory of Donald Richard Nelson* (pp. 191–224). https://doi.org/10.1023/A:1007679303082

Kooyman, G. L. (1965). Techniques used in measuring diving capacities of Weddell seals.*Polar Record, 12*(79), 391–394. https://doi.org/10.1017/S003224740005484X

Le Cren, E. D. (1965). A note on the history of mark-recapture population estimates. *Journal of Animal Ecology, 34*(3), 453–454. https://doi.org/10.2307/2661

Levin L. A. (2018). Manifestation, Drivers, and Emergence of Open Ocean Deoxygenation. *Annual review of marine science*, *10*, 229–260. https://doi.org/10.1146/annurev-marine-121916-063359

Levin, L. A., & Le Bris, N. (2015). The deep ocean under climate change. *Science (New York, N.Y.)*, *350*(6262), 766–768. https://doi.org/10.1126/science.aad0126

Lozier, M. S., Bacon, S., Bower, A. S., Cunningham, S. A., de Jong,M. F., de Steur, L., et al. (2017). Overturning in the subpolar northatlantic program a new international ocean observing system. Bull. Am.Meteorol. Soc. 98, 737–52 *(PDF) AMOC Recent and Future Trends: A Crucial Role for Oceanic Resolution and Greenland Melting?*. DOI: 10.1175/BAM

McMahon, C. R., Roquet, F., Baudel, S., Belbeoch, M., Bestley, S., Blight, C., Boehme, L., Carse, F., Costa, D. P., Fedak, M. A., Guinet, C., Harcourt, R., Heslop, E., Hindell, M. A., Hoenner, X., Holland, K., Holland, M., Jaine, F. R. A., Jeanniard du Dot, T., Jonsen, I., Keates, T. R., Kovacs, K. M., Labrousse, S., Lovell, P., Lydersen, C., March, D., Mazloff, M., McKinzie, M. K., Muelbert, M. M. C., O'Brien, K., Phillips, L., Portela, E., Pye, J., Rintoul, S., Sato, K., Sequeira, A. M. M., Simmons, S. E., Tsontos, V. M., Turpin, V., van Wijk, E., Vo, D., Wege, M., Whoriskey, F. G., Wilson, K., & Woodward, B. (2021). Animal Borne Ocean Sensors (AniBOS) – An essential component of the Global Ocean Observing System. *Frontiers in Marine Science, 8*, 751840. https://doi.org/10.3389/fmars.2021.751840

Miloslavich, P., Bax, N. J., Simmons, S. E., Klein, E., Appeltans, W., Aburto-Oropeza, O., Andersen Garcia, M., Batten, S. D., Benedetti-Cecchi, L., Checkley, D. M., Jr, Chiba, S., Duffy, J. E., Dunn, D. C., Fischer, A., Gunn, J., Kudela, R., Marsac, F., Muller-Karger, F. E., Obura, D., & Shin, Y. J. (2018). Essential ocean variables for global sustained observations of biodiversity and ecosystem changes. *Global change biology*, *24*(6), 2416–2433. https://doi.org/10.1111/gcb.14108

Muller- Karger, F. E., Miloslavich, P., Bax, N. J., Simmons, S., Costello, M. J., Pinto, I. S., Canonico, G., Turner, W., Gill, M., Montes, E., Best, B. D., Pearlman, J., Halpin, P., Dunn, D., Benson, A., Martin, C. S., Weatherdon L. V., Appeltans, W., Provoost, P., … Geller, G. (2018). Advancing marine biological observations and data requirements of the complementary essential ocean variables (EOVs) and essential biodiversity variables (EBVs) frameworks. *Frontiers in Marine Science*, 5, 211. https://doi.org/10.3389/fmars.2018.00211

Musa, S. M., Ripley, D. M., Moritz, T., & Shiels, H. A. (2020). Ocean warming and hypoxia affect embryonic growth, fitness and survival of small-spotted catsharks, Scyliorhinus canicula. *Journal of fish biology*, *97*(1), 257–264. https://doi.org/10.1111/jfb.14370

Naito, Y., Asaga, T., & Ohyama, Y. (1990). Diving behavior of Adélie penguins determined by time-depth recorders. *Condor, 92*(3), 582–586. https://doi.org/10.2307/1368676

Nelson J. A. (2016). Oxygen consumption rate v. rate of energy utilization of fishes: a comparison and brief history of the two measurements. *Journal of fish biology*, *88*(1), 10–25. https://doi.org/10.1111/jfb.12824

Nilsson, G. E., & Ostlund-Nilsson, S. (2008). Does size matter for hypoxia tolerance in fish?. *Biological reviews of the Cambridge Philosophical Society*, *83*(2), 173–189. https://doi.org/10.1111/j.1469-185X.2008.00038.x

Nowacek, D. P., Tyack, P. L., Wells, R. S., & Johnson, M. P. (1998). An onboard acoustic data logger to record biosonar of free-ranging bottlenose dolphins. *The Journal of the Acoustical Society of America, 103*(5), 2908. https://doi.org/10.1121/1.421851

Nowicki, R. J., Thomson, J. A., Fourqurean, J. W., Wirsing, A. J., & Heithaus, M. R. (2021). Loss of predation risk from apex predators can exacerbate marine tropicalization caused by extreme climatic events. Journal of Animal Ecology, 90(9), 2041–2052. https://doi.org/10.1111/1365-2656.13424

Oschlies, A., Brandt, P., Stramma, L., & Schmidtko, S. (2018). Drivers and mechanisms of ocean deoxygenation. *Nature Geoscience*, 11, 467–473. https://doi.org/10.1038/s41561-018-0152-2

Pacoureau, N., Rigby, C. L., Kyne, P. M., Sherley, R. B., Winker, H., Carlson, J. K., Fordham, S. V., Barreto, R., Fernando, D., Francis, M. P., Jabado, R. W., Herman, K. B., Liu, K. M., Marshall, A. D., Pollom, R. A., Romanov, E. V., Simpfendorfer, C. A., Yin, J. S., Kindsvater, H. K., & Dulvy, N. K. (2021). Half a century of global decline in oceanic sharks and rays. *Nature*, *589*(7843), 567–571. https://doi.org/10.1038/s41586-020-03173-9

Parsons, G. R., & Hoffmayer, E. R. (2005). Seasonal changes in the distribution and relative abundance of the Atlantic sharpnose shark *Rhizoprionodon terraenovae* in the north central Gulf of Mexico. *Copeia, 2005*(4), 914–920.

Payne, N. L., Meyer, C. G., Smith, J. A., Houghton, J. D. R., Barnett, A., Holmes, B. J., Nakamura, I., Papastamatiou, Y. P., Royer, M. A., Coffey, D. M., Anderson, J. M., Hutchinson, M. R., Sato, K., & Halsey, L. G. (2018). Combining abundance and performance data reveals how temperature regulates coastal occurrences and activity of a roaming apex predator. *Global change biology*, *24*(5), 1884–1893. https://doi.org/10.1111/gcb.14088

Penn, J. L., Deutsch, C., Payne, J. L., & Sperling, E. A. (2018). Temperature-dependent hypoxia explains biogeography and severity of end-Permian marine mass extinction. *Science (New York, N.Y.)*, *362*(6419), eaat1327. https://doi.org/10.1126/science.aat1327

Petsch, S. T. (2003). The global oxygen cycle. Pp. 515 555 in Treatise on Geochemistry, H. D. Holland and K. K. Turekian, eds. Pergamon, Oxford. https://doi. org/10.1016/B0-08-043751-6/08159-7

Priede, I. (1984) A basking shark (*Cetorhinus maximus*) tracked by satelMAANTA together with simultaneous remote sensing. Fish. Res. 2,201–216. doi: 10.1016/0165-7836(84)90003-1

Prince, E. D., & Goodyear, C. P. (2006). Hypoxia-based habitat compression of tropical pelagic fishes. *Fisheries Oceanography, 15*(6), 451–464. https://doi.org/10.1111/j.1365-2419.2005.00393.x

Prince, E. D., Luo, J., Goodyear, C. P., Hoolihan, J. P., Snodgrass, D., & Skomal, G. B. (2010). Ocean scale hypoxia-based habitat compression of Atlantic istiophorid billfishes. *Fisheries Oceanography, 19*(6), 448–462. https://doi.org/10.1111/j.1365-2419.2010.00556.x.

Richards, J. G. (2009). Metabolic and molecular responses of fish to hypoxia. In J. G. Richards, A. P. Farrell, & C. J. Brauner (Eds.), *Fish physiology* (Vol. 27, pp. 443–485). Academic Press.

Roquet, F., Wunsch, C., Forget, G., Heimbach, P., Guinet, C., Reverdin, G., et al. (2013). Estimates of the Southern Ocean general circulation improved by animal-borne instruments [Dataset]. Geophysical Research Letters, 40(23), 6176–6180. https://doi.org/10.1002/2013gl058304

Rutz, C., & Hays, G. C. (2009). New frontiers in biologging science. *Biology Letters, 5*(3), 289–292. https://doi.org/10.1098/rsbl.2009.0089

Schlaff, A.M., Heupel, M.R. & Simpfendorfer, C.A. Influence of environmental factors on shark and ray movement, behaviour and habitat use: a review. *Rev Fish Biol Fisheries* **24**, 1089–1103 (2014). https://doi.org/10.1007/s11160-014-9364-8

Schmidtko, S., Stramma, L., & Visbeck, M. (2017). Decline in global oceanic oxygen content during the past five decades. *Nature*, *542*(7641), 335–339. https://doi.org/10.1038/nature21399

Schweinsburg, R. E., & Lee, L. J. (1982). Movement of four satelMAANTA-monitored polar bears in Lancaster Sound, Northwest Territories. *Arctic, 35*(3), 504–511. https://doi.org/10.14430/arctic2357

Semenza G. L. (2007). Oxygen-dependent regulation of mitochondrial respiration by hypoxia-inducible factor 1. *The Biochemical journal*, *405*(1), 1–9. https://doi.org/10.1042/BJ20070389

Sequeira, A. M. M., O'Toole, M., Keates, T. R., McDonnell, L. H., Braun, C. D., Hoenner, X., Jaine, F. R. A., Jonsen, I. D., Newman, P., Pye, J., Bograd, S. J., Hays, G. C., Hazen, E. L., Holland, M., Tsontos, V. M., Blight, C., Cagnacci, F., Davidson, S. C., Dettki, H., … Weise, M. (2021). A standardisation framework for bio-logging data to advance ecological research and conservation. *Methods in Ecology and Evolution, 12*(6), 996–1007. https://doi.org/10.1111/2041-210X.13593

Sibert, J. R. (2001). Electronic tagging and tracking in marine fisheries. In J. R. Sibert & J. L. Nielsen (Eds.), *Electronic tagging and tracking in marine fisheries* (pp. 3–17). Springer. https://doi.org/10.1007/978-94-017-1402-0_1

Sonnerup, R. E., Chang, B. X., Warner, M. J., & Mordy, C. W. (2019). Time scales of ventilation and consumption of oxygen and fixed nitrogen in the eastern tropical South Pacific oxygen deficient zone from transient tracers. Deep Sea Research Part I: Oceanographic Research Papers. https://doi.org/10.1016/j.dsr.2019.103080

Spiers, E. K. A., Stafford, R., Ramirez, M., Vera Izurieta, D. F., Cornejo, M., & Chavarria, J. (2016). Potential role of predators on carbon dynamics of marine ecosystems as assessed by a Bayesian belief network. Ecological Informatics, 36, 77–83. https://doi.org/10.1016/j.ecoinf.2016.10.003

Thums, M., Fernandez-Gracia, J., Sequeira, A. M. M., Eguiluz, V. M., Duarte, C. M., & Meekan, M. G. (2018). How big data fast tracked human mobility research and the lessons for animal movement ecology. *Frontiers in Marine Science, 5*, 21. https://doi.org/10.3389/fmars.2018.00021

Vedor, M., Queiroz, N., Mucientes, G., Couto, A., Costa, I. D., Santos, A. D., Vandeperre, F., Fontes, J., Afonso, P., Rosa, R., Humphries, N. E., & Sims, D. W. (2021). Climate-driven deoxygenation elevates fishing vulnerability for the ocean's widest ranging shark. *eLife*, *10*, e62508. https://doi.org/10.7554/eLife.62508

Venegas, R., Acevedo, J., & Treml, E. (2023). Three decades of ocean warming impacts on marine ecosystems: A review and perspective (Version 1). Deakin University. https://hdl.handle.net/10779/DRO/DU:25720035.v1

Waller, M. J., Humphries, N. E., Womersley, F. C., Loveridge, A., Jeffries, A. L., Watanabe, Y., Payne, N., Semmens, J., Queiroz, N., Southall, E. J., & Sims, D. W. (2024). The vulnerability of sharks, skates, and rays to ocean deoxygenation: Physiological mechanisms, behavioral responses, and ecological impacts. Journal of Fish Biology, 105(2), 482–511. https://doi.org/10.1111/jfb.15830

Waller, M. J., Queiroz, N., Da costa, I., Cidade, T., Loureiro, B., Womersley, F. C., Fontes, J., Afonso, P., Macena, B. C. L., Loveridge, A., Humphries, N. E., Southall, E. J., & Sims, D. W. (2023). Direct measurement of cruising and burst swimming speeds of the shortfin

mako shark (Isurus oxyrinchus) with estimates of field metabolic rate. *Journal of fish biology*, *103*(5), 864–883. https://doi.org/10.1111/jfb.15475

Watanabe, Y. Y., & Papastamatiou, Y. P. (2023). Biologging and Biotelemetry: Tools for Understanding the Lives and Environments of Marine Animals. Annual Review of Animal Biosciences, 11, 247–267. https://doi.org/10.1146/annurev-animal-050322-073657

Watanabe, Y., Baranov, E. A., & Sato, K. (2004). Foraging tactics of Baikal seals differ between day and night. *Marine Ecology Progress Series, 279*, 283–289. https://doi.org/10.3354/meps279283

Wearmouth, V. J., McHugh, M. J., Humphries, N. E., Naegelen, A., Ahmed, M. Z., Southall, E. J., Reynolds, A. M., & Sims, D. W. (2014). Scaling laws of ambush predator 'waiting' behaviour are tuned to a common ecology. *Proceedings. Biological sciences*, *281*(1782), 20132997. https://doi.org/10.1098/rspb.2013.2997

Wegner, N. C., Sepulveda, C. A., Olson, K. R., Hyndman, K. A., & Graham, J. B. (2010). Functional morphology of the gills of the shortfin mako, Isurus oxyrinchus, a lamnid shark. *Journal of morphology*, *271*(8), 937–948. https://doi.org/10.1002/jmor.10845

Whitney, N. M., White, C. F., Gleiss, A. C., Schwieterman, G. D., Anderson, P., Hueter, R. E., & Skomal, G. B. (2016). A novel method for determining post-release mortality, behavior, and recovery period using acceleration data loggers. *Fisheries Research, 183*, 210–221. https://doi.org/10.1016/j.fishres.2016.06.003

Williams, H. J., Taylor, L. A., Benhamou, S., Bijleveld, A. I., Clay, T. A., Grissac, S., Demšar, U., English, H. M., Franconi, N., Gómez- Laich, A., Griffiths, R. C., Kay, W. P., Morales, J. M., Potts, J. R., Rogerson, K. F., Rutz, C., Spelt, A., Trevail, A. M., Wilson, R. P., & Börger, L. (2020). Optimizing the use of biologgers for movement ecol ogy research. *Journal of Animal Ecology*, 89, 186– 206. https://doi. org/10.1111/1365-2656.13094

Wootton, T. P., Sepulveda, C. A., & Wegner, N. C. (2015). Gill morphometrics of the thresher sharks (Genus Alopias): Correlation of gill dimensions with aerobic demand and environmental oxygen. *Journal of morphology*, *276*(5), 589–600. https://doi.org/10.1002/jmor.20369

Worm, B., Orofino, S., Burns, E. S., D'Costa, N. G., Manir Feitosa, L., Palomares, M. L. D., Schiller, L., & Bradley, D. (2024). Global shark fishing mortality still rising despite widespread regulatory change. *Science (New York, N.Y.)*, *383*(6679), 225–230. https://doi.org/10.1126/science.adf8984

Yoda, K., Sato, K., Niizuma, Y., Kurita, M., Bost, C., Le Maho, Y., & Naito, Y. (1999). Precise monitoring of porpoising behaviour of Adélie penguins determined using acceleration data loggers. *The Journal of experimental biology*, *202*(Pt 22), 3121–3126. https://doi.org/10.1242/jeb.202.22.3121

Zhou, Y. T., Gong, H. J., & Zhou, F. (2022). Responses of horizontally expanding oceanic oxygen minimum zones to climate change based on observations. Geophysical Research Letters, 49, e2022GL097724. https://doi.org/10.1029/2022GL097724

Annex II: MAANTA tag design

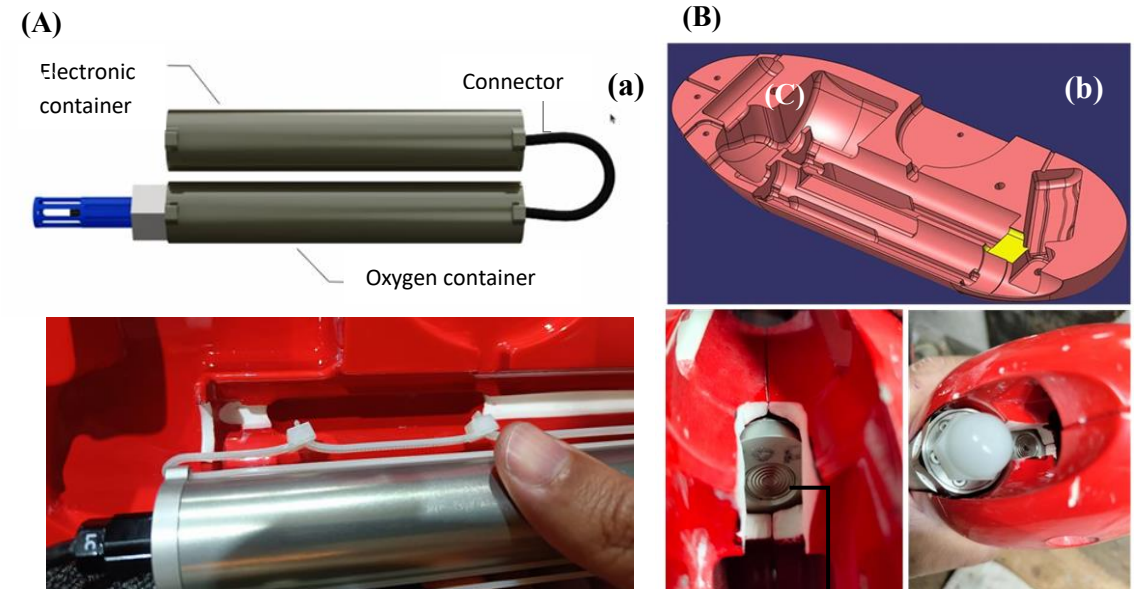

Figure 1. (a) New conector and Zip tie addition with housing modification **(b)** Modified housing container to improve water flow to pressure sensor.

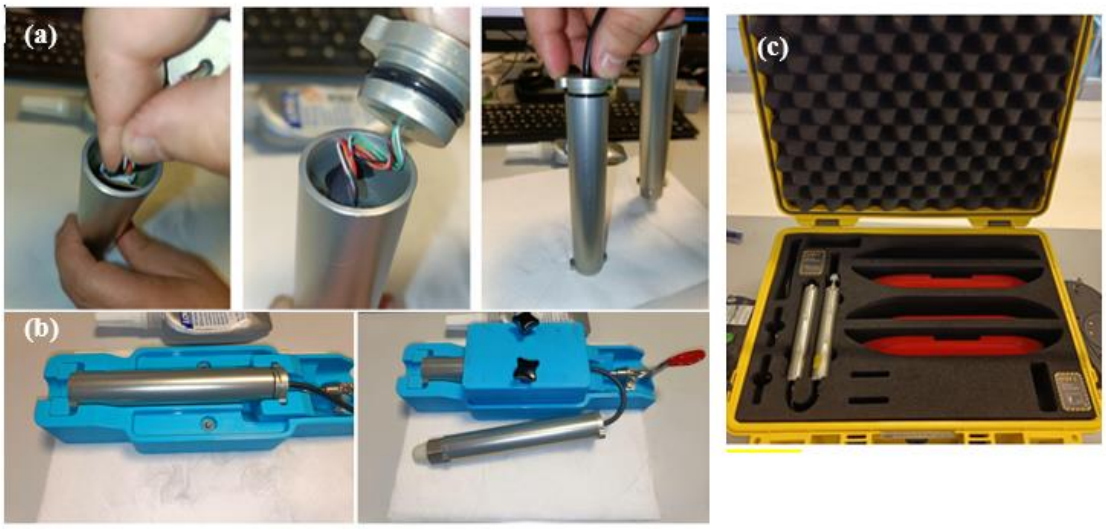

Figure 2. (a) Cable insertion into the electronic housing, **(b)** auxiliary tool used for sealing the housing, and **(c)** protective transport case for the MAANTA tag.

Annex III: Experiments set up

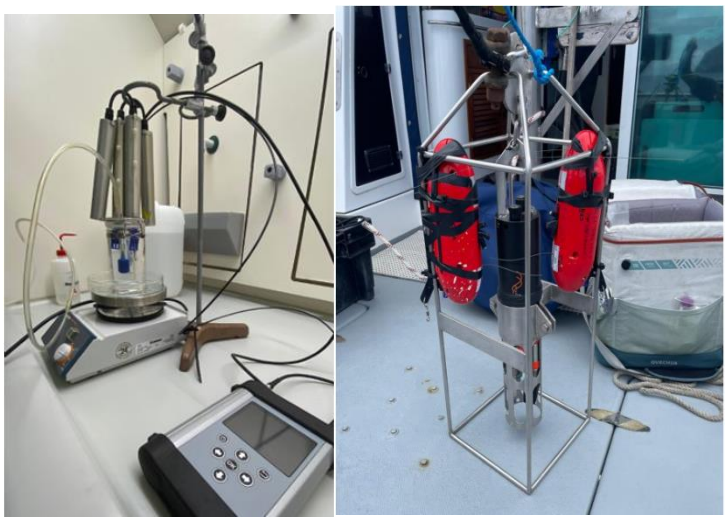

Figure 1. **(a)** Laboratory set-up for the comparison of units LITEe and LITEb with PreSens® multi-parameter. **(b)** CTD set-up with fully assembled LITEe and LITEb

Annex IV: Comparison between CMEMS and tag

Table I. Summary of Spearman's correlation, coefficient of determination (R^2), and error metrics ((MAE- Mean Absolut Error, RMSE- Root Mean Squared Error) for comparisons between *in situ* (Tag) and modelled dissolved oxygen (DO) concentrations

ID	*Spearman*	*R2*	*MAE(ºC)*	*RMSE(ºC)*
BLU_05	**-**	**-**	**-**	**-**
BLU_06	**0.54**	**0.59**	**644.86**	**645.23**
BLU_07	**0.49**	**0.57**	**239.70**	**240.28**
PIN_02	**0.87**	**0.74**	**196.14**	**196.52**
JAM_02	**0.41**	**0.03**	**183.38**	**187.36**
JAM_03	**0.62**	**0.58**	**140.01**	**141.18**
JAM_04	**0.70**	**0.58**	**313.55**	**313.87**

Table II. Summary of Spearman's correlation, coefficient of determination (R^2), and error metrics (MAE- Mean Absolut Error, RMSE- Root Mean Squared Error) for comparisons between *in situ* (Tag) and modelled sea water temperature (TºC).

ID	*Spearman*	*R2*	*MAE(ºC)*	*RMSE(ºC)*
BLU_05	**1.00**	**0.99**	**2.63**	**2.69**
BLU_06	**0.99**	**0.97**	**2.67**	**2.72**
BLU_07	**1.00**	**0.97**	**2.34**	**2.40**
PIN_02	**0.98**	**0.93**	**0.86**	**1.04**
JAM_02	**1.00**	**0.99**	**1.99**	**2.02**
JAM_03	**1.00**	**0.99**	**2.35**	**2.38**
JAM_04	**0.99**	**0.99**	**2.07**	**2.13**

Annex V: PYRO Calculation tool

To verify the accuracy of dissolved oxygen (DO) measurements obtained from the 2025 LITE tag deployments, DO concentrations were recalculated using the PyroScience Oxygen Calculation Tool (PYRO). This tool computes DO from the raw optical sensor output (*dphi*, °), Input data included raw parameters: dphi (°), temperature (°C from the KELLER 4LD sensor), pressure (mbar), and salinity (g/L) and calibration pressure parameters reflecting the environmental conditions during calibration (temperature, humidity, atmospheric pressure). The inclusion of *dphi* in the upgraded 2025 LITE tag version enabled this new validation approach. Although the underlying equation was not provided, PyroScience supplied an Excel spreadsheet that automatically performs DO calculations based on these inputs.

Recalculated DO concentrations were, on average, higher than the original LITE tag values: 47.17 ± 3.33 µmol/L for JAM_08, 37.01 ± 3.92 µmol/L for JAM_09, and 47.50 ± 3.49 µmol/L for JAM_10. Interpolated PYRO-derived values were compared to *in situ* tag data using Spearman's correlation and mean offset (MAANTA – PYRO). Across all individuals, DO values were highly correlated ($\rho \geq 0.996$), confirming strong sensor consistency, though statistically significant differences were detected ($p < 0.05$) (Table I).

Table I. Recalculated DO Concentrations: Correlation and Mean Difference Across Individuals

ID	***Correlation (Spearman´s)***	***Mean* ± SD *(µmol/L)***
JAM_08	**0.998**	**47.17 ± 3.33**
JAM_09	**0.996**	**37.01 ± 3.92**
JAM_10	**0.998**	**47.5 ± 3.49**